UNIVERSITY OF NAPLES "FEDERICO II"

Polytechnic and Basic Science School

Ph.D. School in Chemical Sciences

Isolation and chemical and biological characterization of phytotoxins produced by phytopathogenic fungi of agrarian crops

Paola Nocera

Supervisor:
Prof. Antonio Evidente

Examiner:
Prof. Marina della Greca

XXXII Cycle 2017-2020

Coordinator: prof. Angela Lombardi

ABSTRACT

Phytopathogenic fungi are the first determinants in infectious diseases of crop plants, playing an important role not only in causing devastating epidemies but also through the persistent and significant annual crop losses with consequent heavy economic problems. Considering the social and economic impact of the plant diseases, many efforts have been made to avoid losses in agrarian production.

Thus, the study of phytotoxins and the knowledge of plant pathogenesis processes can help to find the best and rapid remedial to control plant diseases. To protect crops from pathogens, phytotoxins could be a useful tool, to develop specific and rapid diagnostic methods, to select plants naturally resistant to the pathogen identifying the genes of innate resistance. They could be used to formulate new bio-pesticides and to develop new drugs to be applied in medicine.

The aim of this PhD project has been the investigation of phytotoxins isolated from agrarian crops pathogens. Phytotoxic fungal culture filtrates were obtained from *Ascochyta lentis* var. *lathyri* and *Ascochyta lentis*, responsible for Ascochyta blight on grasspea and lentil respectively, *Colletotrichum lupini*, the etiological agent of antrachnose on lupin, and *Neofusicoccum batangarum* the causal agent of "scabby cankers" on cactus pear.

Phytotoxic cultures have been extracted and, the corresponding phytotoxic extracts have been purified to obtain phytotoxic metabolites by bio-guided chromatographic processes.

Two new phytotoxic phenols, named lathyroxins A and B, were isolated from the culture filtrates of *A. lentis* var. *lathyri*. They were characterized by spectroscopic methods and the absolute configuration was assigned by recording their electronic circular dichroism (ECD) spectra. Other three well-known fungal metabolites, named, *p*-hydroxybenzaldehyde, *p*-methoxyphenol, and

tyrosol, were identified. Lathyroxins A and B showed interesting phytotoxic properties on host and non-host plants.

From the culture filtrates of *A. lentis* were isolated three new anthraquinone derivatives, named lentiquinones A, B, C, together with the known lentisone. From the mycelium, four known analogues were also identified as pachybasin, ω-hydroxypachybasin, 1,7-dihydroxy-3-methylanthracene-9,10-dione, and phomarin. Lentiquinones A–C were characterized by spectroscopic methods. The relative configurations of lentiquinones C and D were deduced by X-ray diffraction analysis. Their absolute configuration was determined by electronic circular dichroism (ECD) in solution and solid-state, and TDDFT calculations. When tested by using different bioassays, the novel compounds showed interesting activities. The new compounds, together with lentisone, proved to have also antibiotic properties.

From the culture filtrates of *C. lupini* a 3-substituted indolinone, named lupindolinone, and a 5,6-disubstituted tetrahydro-α-pyrone, named lupinlactone, were isolated together with the known (3*R*)-mevalolactone and tyrosol. Lupindolinone and lupinlactone were characterized by spectroscopic methods (essentially NMR and HRESIMS). The absolute configuration of lupinlactone was assigned applying the advanced Mosher's method. The metabolites were assayed on host and non-host plants and proved to have some activities at the used concentration.

Five phytotoxic secondary metabolites were isolated from the culture filtrates of *Neofusicoccum batangarum*. The phytotoxins were identified as (-)-(*R*)-mellein, (±)-botryoisocoumarin A, (-)-(3*R*,4*R*)- and (-)-(3*R*,4*S*)-hydroxymellein, (-)-terpestacin, and (+)-neoisocoumarin, by comparing their spectroscopic (essentially NMR and ESIMS) and specific optical rotation with those reported in literature. The absolute configuration to (+)-neoisocoumarin was assigned

applying the advanced Mosher's method. All five metabolites showed to have phytotoxic activity on host (cactus pear) and non-host (tomato) plants.

Index

1 INTRODUCTION

The first human activity required to obtain more food with better quality was agriculture. Despite the significant progress made by the introduction of new technologies, the need to produce more food has grown and is growing with the gradual increase in population that will reach almost 10 billion by 2050 (Tilman *et al.*, 2011; FAO, 2017; Evidente, Cimmino and Masi, 2019).

Since the beginnings of agriculture about 10000 years ago, harmful organisms, collectively called pests, as animal pests (insects, mites, nematodes, rodents, birds), plant pathogens (viruses, bacteria, fungi) and weeds (competitive plants), have represented the biggest problem for crop production grown for human use and consumption.

Crop losses could be ascribed both to the abiotic factors, especially high/low temperatures, the presence or the absence of water in the growing season, high/low irradiance and nutrients, and to the biotic stressors that could reduce the crop production. The latter may be controlled using biological (cultivar choice, crop rotation, antagonists, predators, etc.) physical (cultivation, mechanical weeding, etc.), and/or chemical methods (pesticides) (Fig. 1). Different techniques have been developed to prevent and to control crop losses caused by pests in the field (pre-harvest losses) and during the storage (post-harvest losses).

Following their impacts, pests can be classified as stand reducers (damping-off pathogens), photosynthetic rate reducers (fungi, bacteria, viruses), leaf senescence accelerators, light stealers (weeds), assimilate sappers (nematodes, sucking arthropods), and tissue consumers (chewing animals, necrotrophic pathogens) (Boote *et al.*, 1983; Oerke, 2006).

The major cause of severe losses in agrarian production and food safety are the microbial pathogens, weeds and animal pests and their main control was done, until now, by synthetic and chemical pesticides. On the other hand, these

compounds caused resistance in the host plants and remain for long-term in the agricultural products (Oerke, 2006; Cimmino, Masi, Evidente, Superchi, *et al.*, 2015). Thus, in the last decades, many efforts have been made to apply an integrated approach of pest-crop management (Oerke, 2006) to reduce or eliminate chemical pesticides. In fact, the public administrators are asking for healthier and safer foods with less risk for human and animal health, so the use of natural compounds-based pesticides could be a good and alternative strategy to achieve this result (Rosegrant and Cline, 2003; Godfray *et al.*, 2010; Cimmino, Masi, Evidente, Superchi, *et al.*, 2015).

Hence, the awareness to reduce the use of chemical pesticides (Tscharntke *et al*., 2012) stimulated more studies on the knowledge about microbial plant diseases and on the negative effects of other pests as weeds, parasitic plants and insects and to propose new eco-friendly pesticides (Evidente *et al.*, 2011; Evidente, Andolfi and Cimmino, 2011; Fernández-Aparicio *et al.*, 2013; Puopolo *et al.*, 2014; Cimmino, Masi, Evidente, Superchi, *et al.*, 2015; Cimmino, Masi, Evidente and Evidente, 2015; Sarrocco *et al.*, 2015; Ganassi *et al.*, 2016; Barilli *et al.*, 2017; Aznar-Fernández *et al.*, 2019).

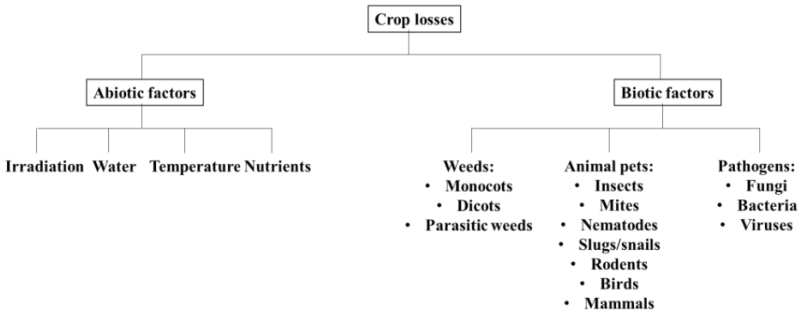

Figure 1. Abiotic and biotic factors causing crop losses

1.1 Phytotoxins produced by phytopathogenic fungi

Fungi and bacteria are the most dangerous microorganisms among biotic stressors. Their distribution and diversity cause a total damage to plants in field and/or in storage. Most of these parasites have the ability to produce phytotoxic compounds (called phytotoxins) that can cause disease symptoms (Strobel, 1974).

Phytopathogenic fungi are the first actors in infectious diseases of crop plants, playing an important role not only in causing devastating epidemics but also through the persistent and significant annual crop yield losses that fungal plant pathogens cause to the economy. The production of low molecular weight phytotoxins is involved in the processes of infection and establishment of a parasitic fungal-plant interaction, playing a key role in infection and virulence processes (Friesen *et al.*, 2008; Möbius and Hertweck, 2009).

During the second half of the 19th century was experimentally demonstrated that phytotoxins, produced by phytopathogenic fungi, are involved in plant diseases. Initially, this assumption was made for infectious plant diseases whose symptoms could not be directly related to the pathogen on the host tissues (Graniti, 1991).

Typically, fungal secondary metabolites alone reproduce some or all the symptoms of the disease caused by the pathogen. Generally, phytotoxins can interact with a large range of cellular targets, altering gene expression or breaking membrane integrity; several phytotoxins inhibit the activity of plant enzymes, as well as disrupting the biosynthesis of crucial metabolites (Oliver and Solomon, 2008; Möbius and Hertweck, 2009).

How toxins should be defined in plant pathology has been discussed several times as well as which classes of active substances they include. The term phytotoxins identify the secondary metabolites produced by microbial pathogens, that interfere with the physiological mechanisms of infected plants.

However, more important than defining the term is to point out what awards on a substance the character of a toxin. Phytotoxins are produced by many plant pathogenic fungi both in culture and in their hosts. These compounds, especially if they are produced during the early stages of plant disease development, have a function in pathogenesis and reproduce some or even all the symptoms of the disease caused by the producer organisms. Phytotoxins, unlike microbial toxins excreted by the animal or human pathogens, are small molecules and have a variety of structures, quite unusual. These compounds can diffuse from the site of infection into the surrounding tissues and/or translocate within the plant *via* the apoplasts (Graniti, 1991).

From the cultures of many bacterial and fungal pathogens have been extracted many toxins, as mixtures of related or unrelated substances, and for some of them, structures have been completely characterized. The virulence and the pathogenicity of plant pathogens may depend on their ability to produce one or more toxins and to use them as chemical weapons (Misaghi, 1982; Durbin, 1983; Mitchell, 1984; Graniti, 1991).

These biologically active metabolites are broad-spectrum toxins which can affect many economically important crops, so their total impact on agriculture could be very serious (Ayres, 1981; Strobel, 1982; Durbin, 1983; Graniti, 1991; Evidente, Cimmino and Masi, 2019).

Thus, the study of secondary metabolites, like phytotoxins and the knowledge on plant pathogenesis process, can help to find the best and rapid remedial tool to control plant diseases. To protect crops from pathogens, phytotoxins could be a prime tool, preventing the use of chemical pesticides. In fact, the phytotoxins can be used: (a) to develop specific and rapid diagnostic methods to identify the disease and to develop simple kits directly used in the field (Sorbo, Evidente and Scala, 1994; Evidente, Andolfi, *et al.*, 1997; Evidente, Lanzetta, *et al.*, 1997; Andolfi *et al.*, 2009); (b) to select plants naturally resistant to the pathogen and

identify the genes of innate resistance (Bani *et al*., 2018); (c) to formulate new bio-pesticides (herbicides, fungicides, bactericides, insecticides, etc.) (Evidente and Motta, 2001; Schrader *et al.*, 2010; Evidente *et al.*, 2011; Fernández-Aparicio *et al.*, 2013; Puopolo *et al.*, 2014; Cimmino, Masi, Evidente, Superchi, *et al.*, 2015; Cimmino, Masi, Evidente and Evidente, 2015; Sarrocco *et al.*, 2015; Ganassi *et al.*, 2016; Barilli *et al.*, 2017; Masi *et al.*, 2018; Aznar-Fernández *et al.*, 2019); (d) to develop new drugs to be applied in medicine because of their activity and specificity related to a new mechanism of action (antiviral, antimalarial, anticancer, etc.) (Bajsa *et al.*, 2007; Balde *et al.*, 2010; Cimmino *et al.*, 2013; Evidente *et al.*, 2014; Cimmino, Evidente, *et al.*, 2015; Masi *et al.*, 2018; Evidente, Cimmino and Masi, 2019).

Insects, nematodes, bacteria, and fungi have been studied to be applied as natural enemies with safety and simplicity. Initially, they have attracted attention due to the hazards they cause to the agricultural productivity of economic interest and the environmental damage for which they are responsible but successively they proved to be a good source of potent phytotoxins (Abbas and Duke, 1995).

Usually, these compounds play an important role in the pathogenesis reproducing some or all the symptoms of the disease. Phytotoxins are, in many cases, low molecular weight compounds belonging to a variety of classes of natural products, they can diffuse from the site of the infection to surrounding tissues and be translocated through the plant, so the virulence of the plant pathogen may depend on its capability to synthesize one or more toxins. At beginning phytotoxins are isolated from infected plant tissues and germinating conidia of fungi, but this approach cannot be prosecuted because of the low content of the target compounds. In order to obtain phytotoxins in a good amount to study their chemical and biological properties, fungi are usually, grown *in vitro*. The production of phytotoxins depends on several factors as the

composition of medium, its pH, the duration and conditions of culturing (i.e. light, temperature, culture medium), and most of these factors are not identified in advance as being able to affect the process (Berestetskiy, 2008).

Moreover, microorganism strains are genetically unstable and when they are stored and re-inoculated might change their ability to produce toxins (Kale and Bennett, 1992).

1.1.1 Classification of fungal toxins

The production of phytotoxins by fungal pathogens has been examined by different research groups in the last decade, dividing phytotoxins into two main groups: host-specific and non-host specific (Duke, 1986; Cutler, 1988; Saxena and Pandey, 2001).

Host-specific phytotoxins: This is a class of extracellular fungal metabolites produced by plant-specific pathogens, only toxic to certain cultivars. Maculosin (Fig. 2), for example, is a cyclic dipeptide produced by *Alternaria alternata*, host-specific to spotted knapweed (*Cantaeurea maculosa*). Similarly, from *Bipolaris cyanodontis* Shoemaker, a fungal pathogen of Bermuda grass (*Cynodon dactylon*) was isolated and named bipolaroxin (Fig. 2), a host-selective phytotoxin which works at low concentrations. When it was used at concentrations 20 times greater than that required to affect Bermuda grass, bipolaroxin caused also phytotoxicity to maize, sugarcane, and wild oats (Sugawara and Strobel, 1986).

It is important to underline that in many cases crop species share common weed species, so host-specific phytotoxins will be not so useful and, commercially, they would be too expensive to use, when compared to non-specific phytotoxins (Saxena and Pandey, 2001).

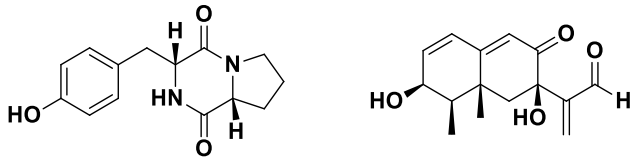

maculosin **bipolaroxin**

Figure 2. Host-specific phytotoxins.

Non-host-specific phytotoxins: This class of phytotoxins has a broader range of activity and applicability on weeds. Cornexistin and irpexil (Fig. 3), isolated respectively from *Paecilomyces variotii* and *Irpex pachydon* are two fungal non-host specific phytotoxins that are used as templates for designing eco-friendly herbicides. Cornexistin is active against both monocotyledonous and dicotyledonous plants, with selective protection to corn (Nakajima *et al*., 1991). From *Helminthosporium* sp., the pathogen of johnsongrass have been isolated two non-host specific phytotoxins, prehelminthosporal and dihydro-prehelminthosporal (Fig. 3). These two compounds have been tested against different plant species as sorghum (*Sorghum bicolor*) and johnsongrass (*Sorghum halpense*). Prehelminthosporal was found to be more active than dihydro-prehelminthosporal, and its toxicity had a range of over 12.5-25 µg/5 µL droplet when applied on leaves (Pena-Rodriguez *et al*., 1988).

Thus, prehelminthosporal, because of its low toxicity, might be a good candidate to develop natural-based herbicides (Cutler *et al*., 1982).

Another example of broad-spectrum phytotoxin is viridiol (Fig. 3), a metabolite produced by the fungus *Gliocladium virens*, toxic only on dicotyledonous plants (Howell and Stipanovic, 1984).

Tentoxin (Fig. 3), is a cyclic tetrapeptide produced by *Alternaria alternata*, that causes phytotoxic damage to both monocotyledonous and dicotyledonous weed species. This secondary metabolite acts inhibiting the CF1 ATPase activity (Steele *et al*., 1976).

Different species of *Alternaria* spp. and *Phoma macdonaldii* Boerma produce zinniol (Fig. 3), the phototoxic metabolite causing necrosis in tissues, probably through calcium regulation (Sugawara and Strobel, 1986; Thuleau *et al.*, 1988).

The potent phytotoxin, 1233A (Fig. 3) is produced by *Cepahlosporium* sp., *Scopulariopsis candidus*, and *Fusarium* sp.; it is the inhibitor of 3-hydroxy-3-methylglutaryl co-enzyme A 14 synthetase (Greenspan *et al*., 1987).

Several phytotoxins: pyrenolide A, ascochytine, and hyalopyrone (Fig. 3) were isolated from *Ascochyta hyalospora* the causal agent of leaf spot on lambsquaters. They resulted to be active on nine weed species, including, *Sida spinosa* L. (prickly sida), *Ipomea* sp. (morning glory), *Chenopodium album* (lambsquarters), and *Sorghum halepense*. Moreover, putaminoxin and pinolidoxin, two phytotoxic nonenolides, produced by the phytopathogenic fungi *Phoma putaminum* and *Didymella pinodes* were isolated and identified as potential bio-herbicide (Evidente *et al*., 1998a).

The virulent plant pathogen *Fusarium oxysporum* Schlechtend Fr. and the non-pathogenic *Fusarium* species produce the phytotoxic metabolite, fusaric acid (Fig. 3) that has shown herbicidal activity against several weed species, including jimsonweed and duckweed (Vesonder *et al*., 1992).

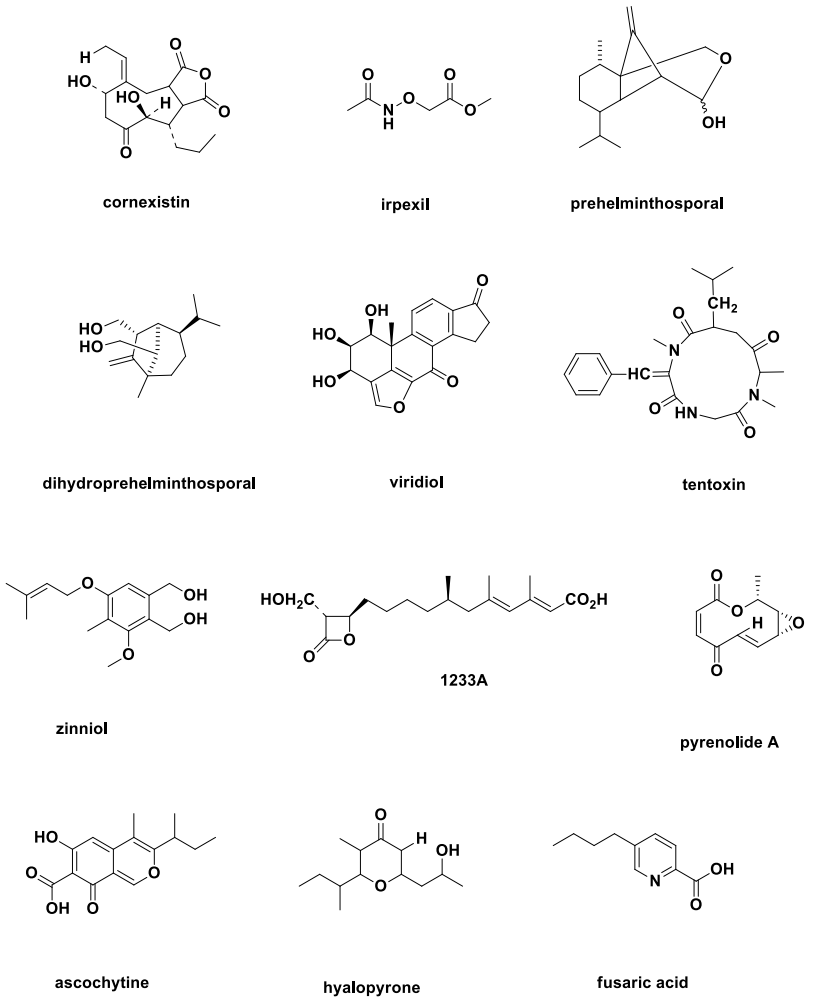

Figure 3. Non-host-specific phytotoxins

1.1.2 Biological activities of fungal toxins

Aside from their clear role in the development of symptoms of some plant diseases, phytotoxins also possess some unusual chemical and biological proprieties (Berestetskii and Borovkov, 1979; Berestetskii and Borovkov, 1981).

Screening of plant genotypes: In order to obtain plants resistant to disease, phytotoxins might replace live pathogens. This approach although simplified is successful in many cases, even though not perfect (Švábová an d Lebeda, 2005). An extremely powerful means to select resistant cultivars seems to be the use of host-specific phytotoxins; this tool is not appropriate for large-scale screening, because these toxins attack plants with a specific and relatively rare genotype. However, it can be used for screening plants that have the gene that determines the host-specific sensitivity. For example, it has been demonstrated that the locus of sensitivity (asc/asc) to AAL-toxin produced by *Alternaria alternata* f. sp. *lycopersici*, specific for certain tomato cultivars, is detected in plants belonging to the genera *Nicotiana*, although the plants in question are not affected by the pathogen (Mesbah *et al.*, 2000; Brandwagt *et al.*, 2001).

Toxin inactivation: Nowadays one of the most important problem for agriculture is to eliminate toxin-forming fungi, particularly those that belong to the genus *Fusarium*. To predict the onset of the disease in the field or prevent spoilage of agricultural products throughout storage is important to know factors, such as temperature and moisture content, that affect the fungal growth and toxin forming activity. A prophylactic measure against toxin-forming fungi might be the use of fungicides, but these latter will eventually stimulate toxin formation by the fungi if the plants have already been infected or if the agricultural products have been contaminated (Magan *et al*., 2002).

The best means of fighting toxin-forming fungi, in terms of efficiency and ecological safety might be constituted by breeding of resistant cultivars. However, it is not practical to use conventional plant breeding techniques to

accomplish this goal. For this reason, there are made every effort to obtain transgenic plants that would be capable of enzymatically degrading the toxins using, for example, the enzymes that cleave the active groups of mycotoxins (Duvick, 2001; Mitterbauer and Adam, 2002).

All the organisms resistant to a phytotoxin might be used as sources of genes that inactivate this phytotoxin; for example, from the plant *Arabidopsis thaliana* was found that the enzyme UDP-glucosyl transferase was able to add glucose to the hydroxyl at C-3 of deoxysqualenol, which results in the inactivation of this phytotoxin (Poppenberger *et al*., 2003).

Development of rapid diagnostic methods: The identification of the organisms responsible for specific crop diseases directly in fields is the main goal of plant pathology, in order to make the best decision about the appropriate control measures. Conventionally, the methods to identify fungal plant pathogens, are related to the interpretation of visual symptoms and/or the isolation, the growth and the laboratory identification of the pathogen. The results of this process, in terms of accuracy and reliability, require a lot of time and depend on the abilities of the staff who make the diagnosis. In this *scenario,* newer methods that apply the diagnosis of plant pathogens, through immunological methods, DNA/RNA probe technology and polymerase chain reaction (PCR) amplification of nucleic acid sequences, are incoming. Despite conventional diagnostic methods, these techniques have several potential advantages, in fact, they are faster and more accurate, and can be used by staff with less experience in plant pathology. Immunological techniques use antibodies to recognize specific antigens present on the surface or secreted by the pathogen. The most common immunological method is the enzyme-linked immunosorbent assay (ELISA), a technology developed in the 1970s (Clark and Adams, 1977). This method produces relatively cheap and simple assays and it can quantify the target pathogen and detect it. Thus, using the ELISA test (Enzyme-Linked Immunoabsorbent Assay),

when the pathogen, defined antigen, is bound to the specific antibody, it is visible using a "tag" enzyme generating a colored product. This test is especially useful to determine antigens in complex mixtures, such as soil or plant extracts (Miller and Martin, 1988).

From the culture filtrates of a *Pseudomonas syringae* pv. *actinidiae* strain, the causal agent of bacterial canker of kiwifruit in Italy, were isolated and analyzed basic, hydrophilic, low molecular weight and hydrophilic, and high-molecular weight compounds belonging to exopolysaccharides (EPSs). EPSs, which are natural antigens, were partially identified and used to develop antibodies following the ELISA assay. The antibodies were used to obtain a rapid and specific method to detect *Pseudomonas syringae* pv. *actinidiae* EPSs isolated from culture and infected plant samples, which represents a tool for rapid immunochemical detection of kiwifruit bacterial canker (Cimmino *et al*., 2017b).

Over the last ten years, the development of new methods for the detection and identification of plant pathogens based on DNA/RNA probe technology and PCR amplification of nucleic acid sequences (Torrance, 1992; Ward, 1994; Oliver, Dewey and Schots, 1994; Martin, James and Lévesque, 2000) has allowed the distinction between different fungal species and within a single species (Ward, 1995; Ward and Adams, 1998). New opportunities to study and understand more about the biology of plant pathogenic fungi, the pathogen population structure, and dynamics, the host-pathogen interactions, are achieved by the ability to design diagnostic methods to target specific genes or sequences. Thank to PCR and other DNA-based methods it is possible to detect, for example, from a single fungal spore, the DNA in a few minutes (Lee, 1990).

These technologies are until now, laboratory-based, but the aim is to develop and obtain detection kits to use into the field in order to directly identify the fungal diseases (Atkins and Clark, 2004).

Formulation of bio-pesticides: Over the past several decades, the possibility to use naturally occurring microorganisms with the ability to control or suppress a pest population has received a modest research support, but, the recent guidelines imposed by governments about the deregistration of chemical pesticides and the public's concern of pesticide residues in food and in public spaces has motivated great interest in biological means of pest control (Whipps and Lumsden, 2001).

The term biopesticide is referred to the use of microbial agents for pest control, crop protection and plant grown regulation (Marrone, 2019). These compounds are the result of coevolution of the producing organism and its biotic environment. Thus, many of them are defense compounds against other organisms. They often have a shorter environmental half-life than synthetic compounds, reducing potential environmental impact. In fact, biopesticides generally affect only the target pests or plant pathogens and do not show risk to birds, fish, beneficial insects, pollinators, mammals and other non-target organisms. They also show a minimal risk to workers and, being biodegradable products, do not pollute air and water. Most of the chemical pesticides commonly used have a single site of action, attacking one vulnerable metabolic pathway or process of the pest. Therefore, pests, after repeated use of a chemical pesticide, can develop resistance to that product and when this happen, pesticides do not work anymore. On the contrary, biopesticides typically have multiple modes of action, so pests are less likely to evolve resistance to them (Marrone, 2019).

Moreover, biopesticides, showing generally low risk to consumers, are exempt from residue tolerances rules (the amount of chemical allowed on the crop at time of harvest) and, can be used right up to harvest (Rimando and Duke, 2006; Marrone, 2019).

The use of biopesticide is increased, from 1.4% in 1995 (Gaugler, 1997) to 2.9% in 2001 while the sales of synthetic pesticides are decreased. In a few years, the chemical pesticide industry will be faced with a scheduled removal of many synthetic pesticides from the market. The European Union had, for example, scheduled a 56% reduction of synthetic pesticides by 2008 (Montesinos, 2003) while in the US, the Food Quality Protection Act had implemented in 1996 required a review by 2006 of all insecticides containing carbamate and organophosphate to compliance the new standards (Ijaz *et al*., 2019; Singh *et al*., 2019; Hynes and Boyetchko, 2006).

Several biochemical products are still on the market. Rhamnolipids, for example, that are produced by *Pseudomonas aeruginosa*, that show broad-spectrum fungicides activity being highly effective against several economically important fungi such as *Cercospora kikuchii*, *Cladosporium cucumerinum*, *Colletotrichum orbiculare*, *Cylindrocarpon destructans*, *Magnaporthe grisea*, *Phytophthora capsici*, *P. cryptogea*, *Plasmopara lactucae-radicis*, *Pythium aphanidermatum* and *Rhizoctonia solani*. Rhamnolipids have surfactant properties, killing zoospores by rupturing the plasma membrane (De Jonghe *et al*., 2005).

Development of new drugs: Natural products have always been the basis of treatments of human diseases (Lahlou, 2007; Patwardhan, Vaidya and Chorghade, 2004). Historically, the first drugs were obtained from natural products (Lahlou, 2007) and before the 20th century, the only medications available to treat human and domestic animal illnesses were represented by crude and semi-pure extracts of plants, animals, microbes, and minerals. Natural products have always played a key role in pharma research, in fact, about 40% of all medicines are natural products or their derivatives (John, 2009). These compounds are still an important source of new drugs, especially in the anticancer, antihypertensive, anti-infectives, immunosuppression, and

neurological disease therapeutic areas, and some of them are progressing into clinical trials or onto the market (Butler, 2004).

The interest in drugs derived from a natural source can be attributed to different factors, as the unmet therapeutic needs, the incredible diversity of both chemical structures and biological activities of naturally occurring secondary metabolites (Clark, 1996).

For example, fungi-derived natural products are an excellent source of pharmaceuticals. The importance of investigating fungal sources for new medicines is well represented by the antibacterial activity of penicillins, the cholesterol-lowering of lovastatin, the antifungal activity of echinocandin B, and the immunosuppressive activity of cyclosporin A.

With the discovery of natural penicillins from the fungus *Penicillium*, the course of medicinal history was significantly changed, and was introduced the antibiotic era (Bérdy, 1980). The discovery of antibiotics not only provided of important drugs, but also allowed the explorations into the mechanisms by which these natural products exert their action have led to an understanding of the biology of the target pathogens that would not likely have been possible without these important biochemical probes.

A therapeutic area where natural derivates have had a large impact on longevity and quality of life is the chemotherapy of cancer (Clark, 1996).

Ophiobolins, for example, are produced by phytopathogenic fungi mainly belonging to the genus *Bipolaris* (Au *et al.*, 2000). Ophiobolin A was the first member of the group to be isolated and characterized in the middle of 1960s (Nozoe *et al.*, 1965; Canonica *et al.*, 1966) and after that other 25 biogenic analogues were identified (Zhang *et al.*, 2012). Ophiobolins are cytotoxic compounds of cancer cells (Ahn *et al.*, 1998). For example, ophiobolin O inhibit the growth of human breast cancer MCF-7 cells arresting the G0/G1 cell cycle and reducing the viability of these cells in a time- and dose-dependent

manner activating apoptotic processes, modifying JNK (c-Jun NH_2-terminal kinase), p38 MAPK (mitogen-activated protein kinase) and ERK (extracellular signal-regulated kinase) kinase activity and reducing Bcl-2 phosphorylation (Ser70) (Yang *et al*., 2012). Marked changes in the dynamic organization of the F-actin cytoskeleton were induced by ophiobolin A that also damage the proliferation and migration of glioma cells, inhibiting BKCa ion channel activity (Bury *et al*., 2013). This metabolite induces the death of glioblastoma cell through paraptosis, a form of cell death characterized by a process of vacuolization that begins with the physical enlargement of mitochondria and the endoplasmic reticulum (ER) (Sperandio, de Belle and Bredesen, 2000; Kornienko *et al.*, 2013; Evidente *et al.*, 2014).

In this scenario, the importance of natural products in the future of drug discovery is very clear and the active natural products will continue to be lead compounds for drug development and biochemical processes. Coupling the technological capabilities to explore the inner part of cells that molecular biology offers with the creativity and innovation of nature, the future of natural product drug discovery is more promising than even before (Clark, 1996).

1.2 Agrarian crops: legumes

Among crops, legumes (*Fabaceae* or *Leguminosae*) are broadly defined by their unusual flower structure, podded fruit, and the ability of 88% of the species examined to form nodules with rhizobia (De Faria *et al*., 1989). The 18,000 species gathered in 650 genera include important grain, and pasture species (Polhill, 1981).

Grain and forage legumes are grown on between 12% to 15% of the earth's arable surface and account for 27% of the world's primary crop production, with grain legumes alone contributing 33% of the dietary protein nitrogen (N) need of humans. They provide the largest source of vegetable protein in human diets and forages and contribute to agriculture, environment, and human health (Graham

and Vance, 2003; Dita *et al.*, 2006). They are, in fact, recommended to maintain good health and prevent chronic diseases, such as diabetes or cardiovascular diseases. Furthermore, they can assist in weight management and are also crucial components of vegetarian diets. The primary legumes present in a diet, are represented by bean (*Phaseolus vulgaris* L.), pea (*Pisum sativum*), chickpea (*Cicer arietinum*), broad bean (*Vicia faba*), pigeon pea (*Cajanus cajan*), cowpea (*Vigna unguiculata*), and lentil (*Lens culinaris*) (Socolow, 1999). Legumes, especially, soybean (*Glycine max* L. Merr.) and peanut (*Arachis hypogeae*) provide more than 35% of the world's processed vegetable oil, and soybean and peanut are also rich sources of dietary protein for the chicken and pork industries. The potential of legume crops is evident, for example, in the huge increase in soybean production in Brazil, with national mean yields more than duplicated from 1968 to 2002 (Hungria, 1997).

The *Fabaceae*, together with the *Graminaceae* constitute one of the most important group of cultivated plants and both have been fundamental for the evolution of modern agriculture. These crops are second in importance, for the human and animal food needs, only to herbaceous plants. The main leguminous crops include chickpeas (*Cicer arietinum* L.), common beans (*Phaeseolus* spp.), lentils (*Lens culinaris* Medik.), Broad beans (*Vicia faba* L.), and peas (*Pisum sativum* L.) (Rubiales and Mcphee, 2015).

Since ancient times, they have contributed to support the productivity of crop systems in the Mediterranean, supplying nitrogen to the soil and helping to control diseases, pests, and weeds (Mudryj *et al*., 2014). Since 8000 BP, lentils (*Lens esculenta*) have reported as domestic in current Iran while *Hymenaea* has been noted as a food source in Amazonian prehistory (Roosevelt *et al*., 1996). Staple crops of bean (*Phaseolus vulgaris*) and soybean (*Glycine max*), respectively in the Americas and Asia, were domesticated more than 3000 years ago (Hymowitz, 1987; Kaplan and Lynch, 1999).

Use of legumes in pastures and for soil improvement dates back to the Romans, with Varro who noted: “Legumes should be planted in light soils, not so much for their own crops as for the good they do to subsequent crops” (Fred *et al*., 2002). In some parts of the Mediterranean basin legumes are primary components of grasslands as they have been for thousands of years (Cocks and Bennett, 1999). *Trifolium alexandrinum* L. (berseem or Egyptian clover) for example, was cultivated, more than 5000 years ago, as a fodder legume in the region of Nile delta but still now is a prevalent crop of this area, with others, due its ability to improve soil yield, particularly after planting lupine and other self-healing herbaceous legumes (Howieson *et al*., 2000).

Legumes have been used, since ancient times, as a primary source of nitrogen for agricultural and economic reasons. After carbon and water, nitrogen is often, the most important limiting nutrient for plant growth (Van Kammen, 1997) and crop productivity, (Bohlool *et al.*, 1992; Peoples, Herridge and Ladha, 1995) so legumes are fundamental for sustainable production of crops. They also have a high impact on agriculture as natural fertilizers for their ability to fix nitrogen, reducing the need for chemical fertilizers while enhancing overall crop productivity. In farming systems, legumes are often used as an inter-crop (e.g., combined with cereals) or in crop rotation resulting in a decrease in pests, diseases and weed populations, while enhancing the overall farm productivity and income of smallholder farmers. Based on these attributes, it is tempting to claim that legumes are one of the most promising components of the Climate Smart Agriculture concept (Palombi and Sessa, 2013).

Legumes, in addition to traditional food and forage uses, might be turned into flour or used in liquid form to produce kinds of milk, yogurt, and infant formula (García *et al*., 1998). For example, pop beans (Popenoe, 1989), licorice (*Glycyrrhiza glabra*) (Kindscher, 1992), and soybean candy (Genta *et al*., 2002) represent innovative uses for specific legumes. They have been also used to

prepare biodegradable plastics (Paetau *et al*., 1994), oils, gums, dyes, and inks (Morris, 1997).

From *Cyamopsis* spp. and *Sesbania* spp. derives galactomannan gums that are used in sizing textiles and paper, as a thickener, and in pill formulation. Many legumes have been traditionally used in folk medicine (Duke, 1992; Kindscher, 1992).

For example, isoflavones from soybeans and other legumes have been suggested to reduce the risks of cancer and to lower serum cholesterol (Kennedy, 1995). Moreover, phytoestrogens from soybean have been suggested as possible alternatives to hormone replacement therapy for postmenopausal women (Molteni *et al*., 1995).

The year 2016 was declared "the international year of legumes" to underline the importance of legume cultivation worldwide. The Food and Agriculture Organization of the United Nations (F.A.O), have coordinated the initiatives connected to the event. At the opening event, the greatest exponents of O.N.U. and F.A.O. have pointed attention to several important global motivations for which legumes are so prominent:

- nutrition and food security welfare;
- environmental sustainability and high adaptability to different climatic conditions, due to the high biodiversity;
- improvement of soil biodiversity;
- healthy feeding of farmed animals by the successful re-use of crop residues;
- prevention of various diseases such as cardiovascular, gastrointestinal, diabetes, anemia, and cancer diseases, high intake of low-cost proteins and other healthy nutrients for human nutrition;

- increase legumes production and trade and encourage new and more intelligent uses throughout the food chain, higher remuneration to better support farmers' incomes;
- reduced dependence on synthetic fertilizers with a natural supply of nitrogen to the soil.

O.N.U and F.A.O are aimed above all to increase the use of agrarian crops in countries, where meat, dairy products, and fish are expensive and therefore difficult to be reached by everyone. These populations depend on plant foods to cover their protein needs and legumes are an important source of accessible proteins, especially for small farmers who consume part of their agricultural products (Oppenheimer, 2001).

However, climate change and the growing attention to a healthier, more rational and sustainable diet, have recently pointed attention to legumes even in countries with an advanced economy. In a world in which the amount of water tends to be more and more scarce, it is important to cultivate crops able to resist to drastic conditions, as many types of legumes that are drought-resistant: pigeon peas (*Cajanus cajan* L. Huth), bambara beans (*Vigna subterranea* L. Verdc.) and lentils (*Lens culinaris* Medik.). These legumes can be grown in arid climates that have limited and often irregular rainfall. Furthermore, legumes represent, in the case of many countries including Italy, an important aspect of the gastronomic tradition. Legumes are recognized in 2010 by the U.N.E.S.C.O. "Intangible cultural heritage of humanity", being an important part of the Mediterranean diet (Serra-Majem and Medina, 2015).

Among legumes, there is a high request for soybean, pea and fava beans. However, in some cases, their production is not profitable for farmers due to the several pests affecting these crops (Bhatnagar-Mathur *et al*., 2012) and phytopathogenic fungi (Araújo *et al*., 2015).

Especially in the tropics and subtropical regions, diseases and pests are major constraints to legume production. In common bean, for example, important pathogens include viruses, fungi-causing root rots, anthracnose, angular leaf spot, bean rust, white mold, and web blight, and the bacteria responsible for common bacterial blight and halo blight (Coyne *et al*., 2003). A number of these pathogens are seed transmitted; others can be carried by insects. Limiting crop losses requires integrated approaches that might include certified seed programs, biological control of root disease, chemical application, and resistance breeding (Beaver *et al.*, 2003; Coyne *et al.*, 2003).

Molecular markers have permitted rapid progress in disease resistance breeding in beans, (Kelly *et al*., 2003) but many of the measures suggested above are beyond the resources of the subsistence farmer, which is another reason why legume yields in third-world countries are low (Graham and Vance, 2003).

1.2.1 Phytotoxins produced by phytopathogenic fungi on legumes

Legumes are among the most important crops worldwide due to their impact on agriculture, environment, nutrition of humans and animals and health (Graham and Vance, 2003).

They constitute a significant source of nitrogen and play an important role in the structure of ecosystems and in sustainable agriculture, worldwide. Nevertheless, biotic (fungi, bacteria, nematodes, viruses, parasitic plants, insects) and abiotic (drought, freezing, salinity, waterlogging) stressors are severely affecting the yield of these crops. Fungal diseases are the major biotic stresses affecting legumes, although insects, nematodes, viruses, bacteria, and parasitic weeds can also drastically decrease legume production (Dita *et al.*, 2006).

There are different reasons because fungi are a problem as invasive species. Fungi are, in fact, organisms that obtain their nutrition through absorption of nutrients from other organisms, often plants, but also insects and humans, acting as parasites, symbionts, or saprobes and in many cases, they might be detected

only when are sporulating, often after the plant starts dying. At present, it is estimated that about 1.5 million species of fungi exist and, of the total number of fungi thought to exist, only 7–20% or about 150,000 fungal species have been described and illustrated (Hawksworth and Rossman, 1997; Hawksworth, 2001). Although rapid progress is being made with the use of molecular tools, the identification of fungi has only recently moved from being based on microscopic characteristics to molecular diagnostics that are the result of phylogenetic studies (Rossman, 2008).

Several phytotoxins produced by phytopathogenic fungi of legumes have been studied. Their structure-activity relationships, mode of action and their roles in the pathogenesis have been also investigated.

1.2.1.1 Some *Ascochyta* phytotoxins

The *Ascochyta* genus includes a wide number of species that have high phytopathological importance, being responsible for severe diseases of important crops. This genus is responsible for foliar and pod diseases on legumes, the ascochyta blight is the major necrotrophic fungal diseases produced by this genus on various grain legumes, while chocolate spot is typical on faba bean and anthracnose on lupin and lentil (Tivoli *et al*., 2006).

Considering that the presence of fungal metabolites in food and feed causes problems for human and animal health, it seems to be important the investigation of the production of toxic metabolites by several *Ascochyta* species, and their occurrence in infected crops (Vurro *et al*., 1992).

Pea diseases are caused by several fungal pathogens as *Ascochyta pisi* var. *pisi*, the causal agent of anthracnose on pea but also on the bean. The main phytotoxin produced by this fungus when grown on wheat kernels was a derivative of salicylic aldehyde, named ascosalitoxin (Fig. 4a). This metabolite, tested at 2 and 0.1 μg/μL, respectively, displayed phytotoxic activity on pea and bean leaves and pods, and on tomato seedlings. Assayed on brine shrimps at 0.2

μg/μL and on *Geotrichum candidum* at 100 μg/disk, the toxin showed no toxicity (Evidente *et al*., 1993a).

From the culture organic extracts of *Ascochyta pinodes* Jones, the causal agent of the anthracnose of pea (*Pisum sativum* L.), characterized by severe lesions and necrosis of leaves and pods, was isolated a phytotoxic nonenolide named pinolidoxin (Fig. 4a). Despite its absolute configuration (AC) was not assigned, it showed high phytotoxic activity when tested by leaf-puncture assay, against pea and bean leaves and pods but weak zootoxicty on brine shrimps (*Artemia salina* L.) (Evidente *et al*., 1993b).

It is important to underline that the phytotoxic activity of pinolidoxin is not host-specific, but this is not unexpected because until now only very few selective phytotoxins have been isolated (Cimmino, Masi, Evidente and Evidente, 2015; Masi *et al.*, 2018). Further chemical investigation on the same organic extract allowed the isolation of three new pinolidoxin analogs characterized as 7-*epi*-, 5,6-dihydro-, 5,6-epoxy-pynolidoxin. Nevertheless, only the first two compounds resulted to be phytotoxic, causing necrotic lesions on the host plant while, the third one showed only weak zootoxicity (Evidente *et al*., 1993b).

Putaminoxin (Fig. 4a), another nonenolide related to pinolidoxin, was isolated from *Phoma putamus* as the main phytotoxin. This fungus was suggested as mycoherbicide against *Erigeron annuus*, a very noxious weed of field and pasture in North America and Europe. Putaminoxin, tested on leaves of *E. annus*, showed higher activity than when tested on an array of weed and cultivated plants (Evidente *et al*., 1995).

From the organic extract of the same fungal culture filtrates, were also isolated some putaminoxin analogs as, 9-butyl, its 9-epimer, 5-*O*-formyl, and a close diketone, named putaminoxins B, D, E, and C respectively (Evidente, Lanzetta, *et al.*, 1997; Evidente, Capasso, Andolfi, *et al.*, 1998a).

When tested using the same assays, only putaminoxin C showed phytotoxic activity. Successively, pinolidoxin, putaminoxin and their natural analogs were used to carry out the study of a structure-activity relationship. Only putaminoxin and pinolodoxin showed the strongest phytotoxicity and their activity plausibly was related to the presence of both the hydroxy groups and the unmodified propyl side chain and to the integrity of the nonenolide ring (Evidente *et al*., 1998a). This result was confirmed by the capability to inhibit the phenylalanine ammonia-lyase, an enzyme fundamental in the production of plant defense phytoalexins as flavones, isoflavones, and salicylic acid (Vurro and Ellis, 1997). A more aggressive strain of *A. pinodes*, reclassified as *Dymidella pinodes* was recently isolated in Spain. It produced pinolidoxin, as the main phytotoxin, but also a new nonenolide named pinolide (Fig. 4a) together with the known herbarumin II and 2-*epi*-herbarumin II (Fig. 4a). During this study it was observed that stereochemistry of the hydroxy group at C-7 might have an important role in the induction of phytotoxic activity while the stereochemistry of the hydroxy group at C-2 appeared to be less important (Cimmino *et al*., 2012a).

The possibility to practically use pinolidoxin in agriculture prompted its partial (de Napoli *et al*., 2000) and total stereoselective synthesis as well as that of herbarumin I and II (Fürstner *et al.*, 2002; García-Fortanet *et al.*, 2005). After different studies, appeared that not only pinolidoxin, but also some natural 10-macrolide analogs have a promising potential for application in agriculture as biopesticides (Cimmino *et al*., 2015a). *Ascochyta fabae* and *Ascochyta pisi*, two pathogens and etiological agents of 'brown spots" disease on broad bean and necrotic lesions on pea leaves, produced, as the main phytotoxin, the ascochitine, a tetrasubstituted benzopyran (Fig. 4a) (Iwai and Mishima, 1965). This metabolite showed antibiotic activity and a wide range of organisms affected, from bacteria to higher plants, interfering with cell permeability (Oku

and Nakanishi, 1966). Ascochitine, according to some biosynthetic studies, has demonstrated to be generated from a single hexaketide chain, possessing three C1 units introduced by *S*-adenosylmethionine (Colombo *et al*., 1979). Cytochalasins A and B (Fig. 4a) were isolated from a strain of *A. lathyri* (Vurro *et al*., 1992).

These metabolites are cytochalasans, a class of fungal bioactive metabolites, well known for their potential practical application in agriculture and medicine (Cimmino *et al.*, 2014; Cimmino, Masi, Evidente, Superchi, *et al.*, 2015).

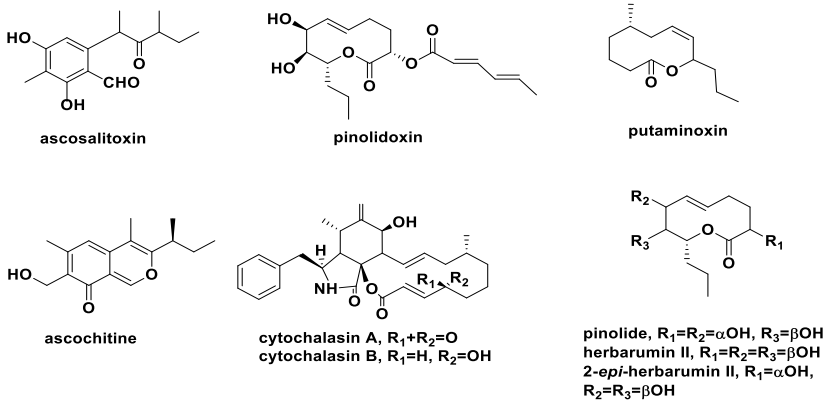

Figure 4a. Some *Ascochyta* phytotoxins.

Lentisone is a new phytotoxic anthraquinone, (Fig. 4b) recently isolated, from the organic extract of an aggressive isolate of *Ascochyta lentis* obtained from lentil (*L. culinaris*). It was identified together with the known pachybasin, pseurotin A and tyrosol (Fig. 4b). Lentisone resulted to be the most toxic compound not only on lentil but also on other legumes such as chickpea, pea,

and faba bean, followed by tyrosol and pseurotin A. Moreover, its activity resulted to be light-dependent (Andolfi *et al*., 2013).

Ascochyta rabiei (Pass.) Labrousse, is the fungal agent responsible for a severe disease of chickpea (*Cicerum arietinum* L.), which caused heavy crop losses in areas around the Mediterranean basin and Pakistan. Infections of chickpea pods are very frequent, and *A. rabiei* can colonize extensively the seeds in the field. This fungus resulted to be able to produce three new substituted α-pyrones, named solanapryones A-C (Fig. 4b). When tested on different varieties of host plants, solanapyrones A resulted to be three-time more active than solanapyrones C (Alam *et al.*, 1989; Höhl *et al.*, 1991). The mechanism of action of these phytotoxins is not established, although the symptoms caused by the toxins (epinasty, chlorosis and necrosis), are consistent with the chickpea disease (Evidente and Motta, 2001).

Successively, from the same fungus were isolated also other two closely related metabolites, named solanapyrones D and E (Fig. 4b) (Oikawa *et al*., 1998).

Ascochyta caulina (P. Karst.) v.d. Aa and v. Kest., has been proposed as a mycoherbicide against *Chenopodium album* (Kempenaar, 1995), a common world-wide weed of many arable crops such as sugar beet and maize (Holm *et al*., 1977). From the culture filtrate of *A. caulina*, that showed high phytotoxic activity on host and non-host plants, when tested on leaves and cuttings, was isolated a new metabolite named ascaulitoxin (Fig. 4b). When assayed on fat hen at 30 µg/droplet in the leaf-puncture assay, it caused the appearance of clear necrotic spots surrounded by chlorosis. The development of symptom varied between two and five days. At 10^{-4} M the toxin caused 57 and 39% reduction of root elongation of fat hen and tomato seedlings, respectively. On the contrary, assayed up to 100 µg/disk on some fungi and bacteria it showed no antimicrobial activity (Evidente *et al.*, 1998c).

Considering the interesting phytotoxicity of ascaulitoxin on *C. album* and considering that toxins could be used indirectly as a biomarker, it might be suggested the use of *A. caulina* as mycoherbicide. In fact, further studies might permit the evaluation of the possible direct use of the metabolite as a natural herbicide, either in combination with other toxic metabolites, as well as with other control methods in the integrated weed management approach (Evidente and Motta, 2001).

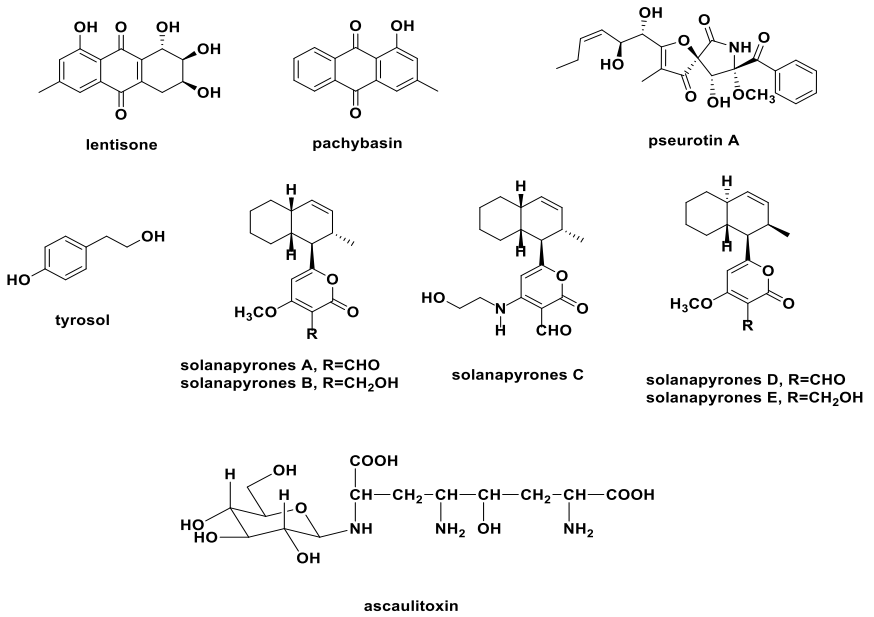

Figure 4b. Some other *Ascochyta* phytotoxins.

1.2.1.2 Some *Drechslera* phytotoxins

Fungi belonging to *Drechslera* genus produce brown spot lesions on different agrarian crops. The phytotoxic activity of this genus is related to the production of many sesquiterpenes, named ophiobolins. Ophiobolin A (Fig. 5) also called cochliobolin, was the first and most representative member of this group (Nozoe *et al.*, 1965; Canonica *et al.*, 1966).

After ophiobolin A, other secondary phytotoxic metabolites, belonging to the class of ophiobolins, have been isolated as produced by fungal pathogens of some cereals, legumes, and weeds. In fact, from *Drechslera sorghicola* were isolated ophiobolin A together with 3-anhydroophiobolin A and their 6-epimers (Fig. 5). When tested by leaf spot assay on several plants, ophiobolin A and its 6-epimer resulted to be more phytotoxic than their anhydrous derivatives (Pena-Rodriguez and Chilton, 1989). Until 2000, many other ophiobolins analogs, have been isolated and identified from different fungi. Their biological properties, their role in plants, animals and microorganisms, and their mode of action, when possible have been reported. About ophiobolin A has been discussed its use as a calmodulin antagonist (Au *et al.*, 2000).

Successively, studies on *Drechslera gigantea*, as mycoherbicide against *Digitaria sanguinalis*, led to the isolation of ophiobolin A together with 3-anhydrous and 6-*epi*-ophiobolin A, and ophiobolin I (Fig. 5) (Evidente *et al.*, 2006a).

From the same culture filtrates were also isolated a new ophiobolin, named ophiobolin E (Fig. 5), together with ophiobolins B and J (Fig. 5) and its 8-epimer that was isolated for the first time (Fig. 5). When assayed by the leaf-puncture assay on four different weeds, only ophiobolins B and J resulted to be toxic, with ophiobolin B highly toxic on *Bromus* sp. and *Hordeum marinum* leaves (Evidente *et al.*, 2006b). The possibility to have a good amount of ophiobolin A allowed wider range of studies. Thus, ophiobolin A showed to

have strong anticancer activity against different human cancer cells (Bury *et al.*, 2013; Locato *et al.*, 2015). Other ophiobolins (K-W) and analogs were also isolated from different fungal genera including those of marine origins *(Tian et al.*, 2017).

Drechslera avenae is the causal agent of leaf blotch of oats and from its liquid culture was isolated a new macrolide named (-)-dihydropyrenophorin (Fig. 5). Its phytotoxic activity depended on the plant species used and from its concentration (Sugawara and Strobel, 1986).

From *Drechslera tritici-repentis* the causal agent of reddish-brown spots on wheat (*Triticum vulgare*) were isolated two spirocyclic γ-lactams named triticones A and B (Fig. 5). When assayed on wheat they showed phytotoxicity on both leaf and protoplasts (Sugawara *et al*., 1988).

De-*O*-methyldiaporthin (Fig. 5) is a new isocoumarin, isolated from the liquid culute of *Drechslera siccans* a fungus pathogenic on oats (*Aoena sativa*), perennial ryegrass (*Lolium perenne*) and Italian ryegrass (*Lolium multiflorum*). When tested on host plants no symptoms appeared but when tested on corn (*Zea mays*), crabgrass (*Digitaria ischaemum*), and soybean (*Glycine max*) necrotic lesions were observed (Hallock *et al.*, 1993).

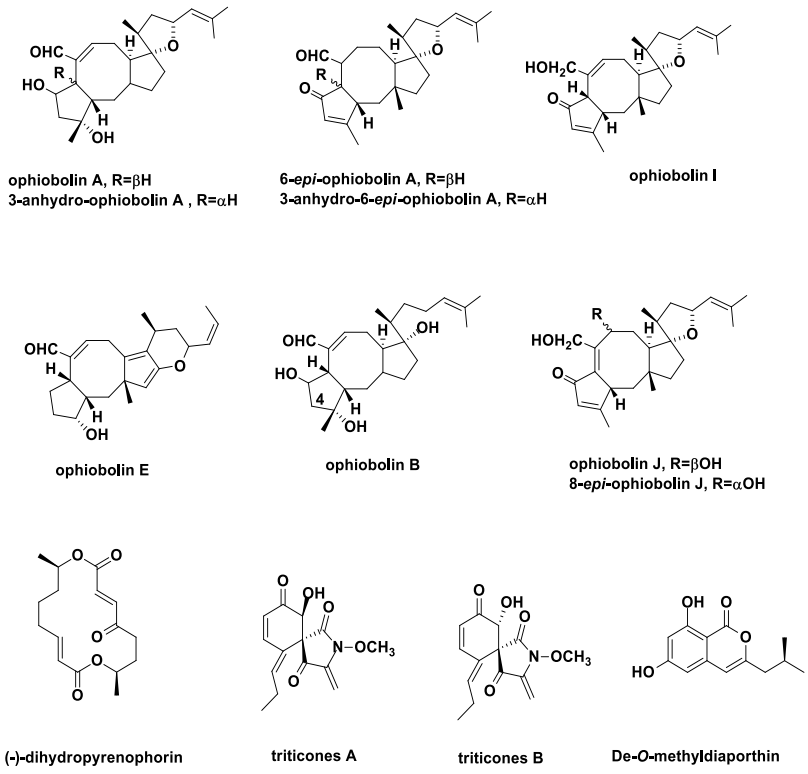

Figure 5. *Drechslera* phytotoxins.

2 OBJECTIVES

The quality and quantity of crop production are strongly reduced by severe plant diseases caused by old and new pathogens. In this scenario, novel methods are ever more required to efficiently control plant diseases and to limit the use of chemical fungicides for sustainable agriculture.

The aim of the present thesis has been the isolation and the chemical and biological characterization of phytotoxins produced by fungal pathogens of important agrarian crops and their possible use as tools for crop protection.

Firstly, toxic fungal culture filtrates were obtained from selected pathogens and, successively, their production of phytotoxic secondary metabolites was investigated, as below reported:

- Production, extraction and purification of phytotoxic secondary metabolites from culture filtrates of *Ascochyta lentis* var. *lathyri*, *Ascochyta lentis*, *Colletotrichum lupini*, and *Neofusicoccum batangarum*.
- Identification of the already known metabolites.
- Chemical characterization of new phytotoxic metabolites.
- Assignment of their relative and absolute configurations.
- Biological characterization.

3 MATERIALS AND METHODS

3.1 Fungal strains

3.1.1 *Ascochyta lentis* var. *lathyri* [1]

The strain of *Ascochyta lentis* var. *lathyri* was isolated from diseased *Lathyrus sativus* (grass pea) plants in Italy (Infantino *et al*., 2016). Firstly, symptomatic grass pea tissues were disinfested using NaOCl (2% active Cl_2) for 2 min, rinsed three times with sterile water and then placed on potato dextrose agar (PDA) amended with 100 ppm each of streptomycin sulphate and ampicillin. The isolation from seeds required several grasspea seed lots. 100 seeds *per* lot were disinfested with NaOCl for 5 min, rinsed three times with sterile water, and similarly, placed on PDA with antibiotic and incubated for 7 days at 23°C under near ultraviolet light (Philips TLD 18W/08 Blacklight Blue Fluorescent Lamp, peak 360 nm) with a 12h photoperiod. Single conidia, after isolation from developing colonies, were transferred to fresh PDA plates (Peever *et al*., 1999). Isolates were stored in the fungal collection of the Istituto di Scienze delle Produzioni Alimentari, CNR, Italy, with the code ITEM 17453. It was routinely grown and maintained in plates and slants containing potato-dextrose agar (PDA, Sigma −Aldrich, Chemie Gmbh, Buchs Switzerland).

3.1.2 *Ascochyta lentis* [2]

The strain of *Ascochyta lentis* was isolated from diseased *Lens culinaris* L. plants and kindly supplied by Dr. W. Kaiser (USDA-ARS, Western Regional

[1] The work presented in these paragraphs has been published as: Masi, M., Nocera, P., Boari, A., Cimmino, A., Zonno, M. C., Infantino, A., Vurro, M., Evidente, A. (2018). Lathyroxins a and B, phytotoxic monosubstituted phenols isolated from *Ascochyta lentis* var. *lathyri*, a fungal pathogen of grass pea (*Lathyrus sativus*). *J.Nat.Prod*., 81: 1093-1097.

[2] The work presented in these paragraphs has been published as: Masi, M., Nocera, P., Zonno, M. C., Tuzi, A., Pescitelli, G., Cimmino, A., Boari, A., Infantino, A., Vurro, M., Evidente, A. (2018). Lentiquinones A, B, and C, phytotoxic anthraquinone derivatives isolated from *Ascochyta lentis*, a pathogen of lentil. *J.Nat.Prod*., 81: 2700-2709.

Plant Introduction Station, Washington State University) for the genetic studies. It was stored in the ATCC Collection as #ATCC96419, Mating type 1, and in the ISPA fungal collection as #ITEM 17454. The isolate was routinely grown and maintained in plates and slants containing potato-dextrose-agar (PDA).

3.1.3 *Colletotrichum lupini* [3]

The *Colletotrichum lupini* isolate RB221 (also known as IMI 504893, CABI Culture Collection; UBOCC-A-117274, Culture Collection of the University of Western Brittany), was originally collected in August 2014 in the area of Moisdon-la-Rivière, Pays de la Loire, France, from symptomatic stems of *Lupinus albus*. The strain was selected because highly aggressive and a member of the most representative genetic group (Dubrulle *et al*., 2019). The genome of *C. lupini* RB221 has also been fully sequenced, opening new perspectives in linking biosynthetic genes to newly identified secondary metabolites.

3.1.4 *Neofusicoccum batangarum* [4]

Strains of *N. batangarum* were collected from the infected host plant tissues from 2013 to 2018 in the islands of Favignana, Lampedusa, Linosa and Ustica and maintained on potato-dextrose-agar (PDA, Fluka, Sigma-Aldrich Chemic GmbH, Buchs, Switzerland) and stored at 4 °C in the strain collection of Dipartimento di Agricoltura, Alimentazione e Ambiente, Università di Catania, Catania, Italy.

[3] The work presented in these paragraphs will be published as: Masi, M., Nocera, P., Boari, A., Zonno, M. C., Pescitelli, G., Sarrocco, S., Baroncelli, R., Vannacci, G., Vurro. M., Evidente, A. (2020). Secondary metabolites produced by *Colletotrichum lupini*, the causal agent of anthachnose of lupin (*Lupinus* spp.). *Mycologia*, IN PRESS

[4] The work presented in these paragraphs has been published as: Masi, M., Aloi, F., Nocera, P., Cacciola, S. O., Surico, G., Evidente, A. (2020). Phytotoxic metabolites isolated from *Neufusicoccum batangarum*, the causal agent of the scabby canker of cactus pear (*Opuntia ficus-indica* L.). *Toxins*, doi:10.3390/toxins12020126

3.2 General procedures

Optical rotation was measured on a Jasco P-1010 digital polarimeter (Jasco, Tokyo, Japan); IR spectra were recorded using a Thermo Nicolet 5700 FT-IR Perkin Elmer spectrometer (Waltham, MA, USA) depositing the samples on a glass film. UV spectra were measured on a Jasco V-530 spectrophotometer. ECD spectra were recorded on a Jasco J-815 spectropolarimeter calibrated for intensity with ammonium [D_{10}] camphorsulfonate ($[\theta]_{290.5}$=7910 deg cm^2 $dmol^{-1}$); scanning speed 50 nm min^{-1}, step size 0.1 nm, bandwidth 1 nm, response time 1 second, with an accumulation of 8 or 32 scans. The Hellma cells were made of quartz Suprasil and the path length was 0.2 cm. The solid-state ECD spectra were measured following the KCl pellet technique described by Pescitelli *et al.,* 2009. Bruker and Varian (Palo Alto, CA, USA) instruments (400 and 500 MHz respectively) were used to recorded ^{1}H, ^{13}C and 2D NMR spectra using suitable deuterated solvents and, the same solvents were used also as internal standards. DEPT spectra were used to determined carbon multiplicities (Berger and Braun, 2004). DEPT, Correlated Spectroscopy (COSY-45), Heteronuclear Single Quantum Coherence (HSQC) and Heteronuclear Multiple Bond Correlation (HMBC) experiments (Berger and Braun, 2004) were performed using Bruker and Varian microprograms.

High resolution electrospray ionization mass spectrometry (HRESIMS), electrospray ionization mass spectrometry (ESIMS) and liquid chromatography mass spectrometry (LC/MS) analyses were performed using the LC/MS Time-of-flight (TOF) system AGILENT (Agilent Technologies, Milan, Italy) 6230B, HPLC 1260 Infinity. The HPLC separations were performed with a Phenomenex (Bologna, Italy) LUNA column (C18 (2) 5µm 150x4.6 mm). Column chromatography was performed using silica gel (Kieselgel 60, 0.063-0.200 mm, Merck). Analytical, preparative, and reverse-phase thin-layer chromatography (TLCs) were carried out on silica gel (Kieselgel 60, F_{254}, 0.25 and 0.5 mm and

RP-18 F_{254}s, respectively) plates (Merck, Darmstadt, Germany). The spots were visualized by exposure to UV radiation, or by spraying first with 10% H_2SO_4 in MeOH, and then with 5% phosphomolybdic acid in EtOH, followed by heating at 110°C for 10 min. Column chromatography was performed using silica gel (Kieselgel 60, 0.063-0.200 mm, Merck).

4 EXPERIMENTAL

4.1 Production, extraction, and purification of secondary metabolites from *Ascochyta lentis* var. *lathyri* culture filtrates [1].

Ascochyta lentis var. *lathyri* was grown for 4 weeks at 25 °C in the dark using a 1L Roux flasks which contained 200 mL of a defined mineral medium. After filtration, the culture filtrate (7L), was lyophilized and stored at −20°C until use. Distilled water at 1/10 of its initial volume was used to redissolve the culture filtrate which was then acidified to pH 2 with HCOOH and exhaustively extracted with EtOAc. The residue of the organic extract (2.3 g) was firstly dried with Na_2SO_4 and then evaporated under reduced pressure. This latter was chromatographed on silica gel eluted with $CHCl_3$-*i*-PrOH (9:1), obtaining eight groups of homogeneous fractions (Scheme 1). The residue of fourth fraction (64.1 mg) was further purified by preparative TLC eluted with $CHCl_3$-MeOH (95:5), yielding an amorphous and homogeneous solid identified, as below reported, as *p*-hydroxybenzaldehyde (**3**, 1.9 mg, 0.3 mg/L, R_f 0.5, Fig. 6). The residue of fifth fraction (313.5 mg) was purified by silica gel column chromatography eluted with CH_2Cl_2-MeOH (9:1), yielding 11 homogeneous fractions. The residue of fourth fraction (14.1 mg) was subsequently purified by two successive TLC steps, using first Me_2CO-H_2O (1:1) and then *n*-hexane-Me_2CO (6:4), obtaining an amorphous solid, which, being new, was named lathyroxin A (**1**, 4.8 mg, 0.7 mg/L, R_f 0.7, Fig. 6). The residue of fifth fraction (14.1 mg) was purified by reverse-phase TLC, eluted with Me_2CO-H_2O (1:1), obtaining an amorphous solid identified, as below reported, as tyrosol (**5**, 3.2 mg, 0.5 mg/L, R_f 0.6, Fig. 6). The residue of sixth fraction (33.0 mg) of the same column, purified by two successive TLC steps using *n*-hexane-Me_2CO (1:1) and Me_2CO-H_2O (4:6), respectively, yielded an amorphous solid which, being new, was named lathyroxin B (**2**, 20.1 mg, 2.9 mg/L, R_f 0.7, Fig. 6). Finally, the residue of seventh fraction (273.4 mg) of the first column was purified by silica

gel column chromatography eluted with $CHCl_3$-*i*-PrOH (85:15), giving seven fractions. The residue of fourth fraction (43.3 mg) of this latter was purified by reverse-phase TLC using MeCN-H_2O (4:6), obtaining an amorphous solid identified, as below reported, as *p*-methoxyphenol (**4**, 2.7 mg, 0.4 mg/L, R_f 0.7, Fig. 6).

4.1.1 Lathyroxin A (1)

Lathyroxin A, obtained as an amorphous solid, had: IR ν_{max} 3358, 1613, 1516, 1549 cm^{-1} (Fig. 13); UV λ_{max} (log ε) 278 (3.17), 223 (3.65) nm (Fig. 12); ^1H and ^{13}C NMR (Fig. 7 and 8) are reported in Table 1; HRESIMS (+) *m/z* 447 $[2M+Na]^+$ and 235.0931 $[M+Na]^+$ (calcd for $C_{11}H_{16}O_4Na$ 235.0946) (Fig. 11).

4.1.2 Lathyroxin B (2)

Lathyroxin B, obtained as an amorphous solid, had: IR ν_{max} 3364, 1613, 1569, 1458 cm^{-1} (Fig. 20); UV λ_{max} (log ε) 278 (3.07), 224 (356) nm (Fig. 19); ^1H and ^{13}C NMR (Fig. 14 and 15), are reported in Table 1; HRESIMS (+) *m/z* 359 $[2M+Na]^+$, 191.0663 $[M+Na]^+$ (calcd for $C_9H_{12}O_3Na$ 191.0684) and 107 [HO −Ph $-CH_2]^+$ (Fig. 18).

4.1.3 *p*-Hydroxybenzaldehyde (3)

p-Hydroxybenzaldehyde, obtained as an amorphous and homogeneous solid, had: ^1H NMR (500 MHz in DMSO-d_6) δ 9.90 (s, CHO), 7.83 (d, *J* = 7.9 Hz, H-2 and H-6), 6.98 (d, *J*=7.9 Hz, H-3 and H-5), 4.70 (s, OH). These data agree with those previously reported (Ren-Yi *et al*., 2015); ESIMS (+) *m/z* 145 $[M+Na]^+$.

4.1.4 *p*-Methoxyphenol (4)

p-Methoxyphenol, obtained as an amorphous solid, had: ^1H NMR (500 MHz, in $CDCl_3$) δ 7.05 (d, *J*=8.5 Hz, H-3 and H-5), 6.80 (d, *J*=8.5 Hz, H-2 and H-6), 4.69 (s, OH), 3.64 (s, OCH_3). These data agree with those previously reported (Liu and Ackermann, 2013); HRESIMS (+) *m/z* 269.07452 $[2M+Na]^+$ (calcd for $C_{14}H_{14}O_4Na^+$, 269.07843) and 107.04869 $[M-H_2O]^+$ (calcd for $C_7H_7O^+$, 107.04969).

4.1.5 Tyrosol (5)

Tyrosol, obtained as an amorphous solid, had: ^{1}H NMR (500 MHz, in $CDCl_3$) δ 7.12 (d, *J*=6.5 Hz, H-2 and H-6), 6.81 (d, *J*=6.5 Hz, H-3 and H-5), 4.87 (s, OH), 3.85 (t, *J*=6.5 Hz, H-8 and OH), 2.82 (t, *J*=6.5 Hz, H-7); ESIMS (+) *m/z* 299 $[2M+Na]^+$, 161 $[M+Na]^+$. These data agree with those previously reported (Kimura and Tamura, 1973; Capasso *et al.*, 1992; Cimmino *et al*., 2017c)

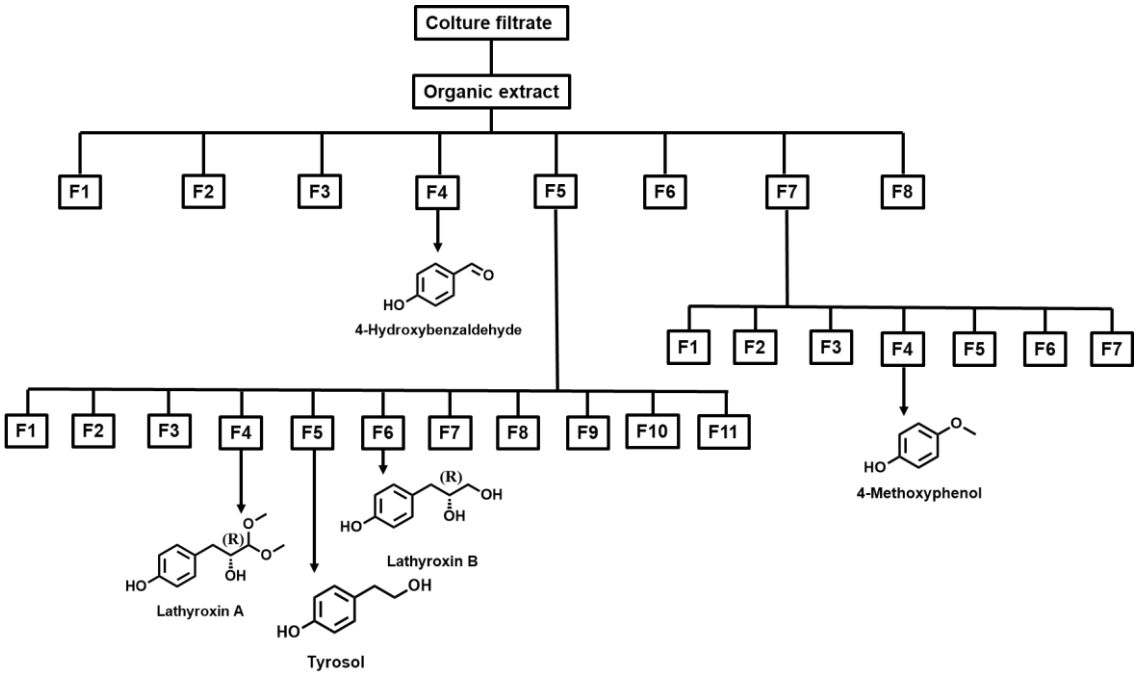

Scheme 1. Extraction and purification of *Ascochyta lentis* var. *lathyri* culture filtrates.

4.2 Production, extraction and purification of secondary metabolites from *Ascochyta lentis* culture filtrates [2].

The fungus was grown using a 1L Roux flasks which contained 200 mL of a defined mineral medium for 4 weeks at 25 °C in the dark. After filtration, the culture filtrate (7.2L), was lyophilized and stored at −20 °C until use. Distilled water at 1/10 of its initial volume was used to redissolved the culture filtrate that was exhaustively extracted with EtOAc. The combined organic extracts were dried with Na_2SO_4 and evaporated under reduced pressure. The organic residue (290 mg) was chromatographed on silica gel and eluted with $CHCl_3$-*i*-PrOH (85:15), obtaining 18 groups of homogeneous fractions (Scheme 2). The residue of ninth fraction (21.3 mg) was further purified by preparative TLC eluted with *n*-hexane-acetone (6:4), yielding nine fractions. The residue of fourth fraction of the latter purification was further purified by reverse phase TLC eluted with MeOH-H_2O (7:3), to afford a pure metabolite in the form of an amorphous solid, which, being new, was named lentiquinone A (**7**, 2.4 mg, 0.3 mg/L, R_f 0.3, Fig. 22). The residue of thirteenth fraction (20.2 mg) of the first column was purified by preparative TLC eluted with $CHCl_3$-*i*-PrOH (85:15), yielding an amorphous solid that was further purified by analytical TLC eluted with $CHCl_3$-MeOH (85:15), to give two crystalline solids which, being new, were named lentiquinone B (**8**, 4.3 mg, 0.6 mg/L, R_f 0.4, Fig. 22) and C (**9**, 2.9 mg, 0.4 mg/L, R_f 0.35, Fig. 22). The residue of twelfth fraction (15.4 mg) was purified by analytical TLC, using $CHCl_3$-*i*-PrOH (9:1), giving an amorphous solid, which was purified by reverse phase TLC eluted with MeOH-H_2O (8:2), to yield an amorphous solid, identified, as below reported, as lentisone (**10**, 1.2 mg, 0.2 mg/L, R_f 0.6, Fig. 22).

4.2.1 Lentiquinone A (7)

Lentiquinone A, obtained as an amorphous solid, had: IR ν_{max} 3362, 1660, 1640 cm^{-1} (Fig.30); UV λ_{max} (log ε) 419 (3.08), 278 (3.40), 250 (3.39), 220 (3.39) nm

(Fig. 29); ^{1}H and ^{13}C NMR (Fig. 23 and 24), are reported in Table 3; HRESIMS (+) *m/z* 571 $[2M+Na]^+$, 297 $[M+Na]^+$, 275.0559 $[M+H]^+$ (calcd for $C_{14}H_{11}O_6$ 275.0550) (Fig. 28).

4.2.2 Lentiquinone B (8)

Lentiquinone B, obtained as a crystalline solid, had: $[\alpha]^{25}_{D}$ +87.4 (c=0.5 MeOH); IR ν_{max} 3311, 1662, 1456 cm^{-1} (Fig. 38); UV λ_{max} (log ε) 338 (2.58), 285 (3.24), 254 (3.21), 220 (3.23) nm (Fig. 37); ECD (MeCN) λ_{max} (Δε) 366 (−0.93), 336 (0), 294 (+1.15), 263 (0), 251 (−0.77), 236 (0), 226 (+1.23), 218 (0), 201 (−11.9) nm (Fig. 52); ^{1}H and ^{13}C NMR (Fig. 31 and 32) are reported in Table 3; HRESIMS (+) *m/z* 607 $[2M+Na]^+$, 293.1013 $[M+H]^+$ (calcd for $C_{15}H_{17}O_6$ 293.1020) (Fig. 36).

4.2.3 Lentiquinone C (9)

Lentiquinone C, obtained as a crystalline solid, had: $[\alpha]_{D}^{25}$ +71.4 (c=0.5 MeOH); IR ν_{max} 3315, 1662, 1450 cm^{-1} (Fig. 46); UV λ_{max} (log ε) 345 (2.56), 284 (3.25), 252 (3.24), 218 (3.29) nm (Fig. 45); ECD (MeCN) λ_{max} (Δε) 366 (−1.25), 340 (0), 287 (+2.88), 258 (+3.17), 227 (+1.53), 222 (0), 202 (−18.8) nm (Fig. 53); ECD (KBr) λ_{max} (mdeg) 388 (−0.72), 353 (0), 311 (+0.75), 280 (0), 237 (−1.0), 203 (−3.5) nm (Fig. 54); ^{1}H and ^{13}C NMR (Fig. 39 and 40), are reported in Table 3; HRESIMS (+) *m/z* 607 $[2M+Na]^+$, 293.1028 $[M+H]^+$, (calcd for $C_{15}H_{17}O_6$ 293.1020) (Fig. 44).

4.2.4 Lentisone (10)

Lentisone, obtained as an amorphous solid, had: ^{1}H NMR (500 MHz, in MeOD), δ 7.45 (brs, H-7), 7.09 (brs, H-5), 4.89 (d, *J*=3.0 Hz, H-1), 4.11 (ddd, *J*=9.4, 5.7, 2.1 Hz, H-3), 3.99 (dd, *J*=3.0, 2.1, H-2), 2.94 (dd, *J*=19.5, 5.7, H-4A), 2.53 (dd, *J*=19.5, 9.4 Hz, H-4B), 2.43 s (Me-6); ESIMS (+) *m/z* 291 $[M+H]^+$. These data agree with those previously reported (Andolfi *et al.*, 2013).

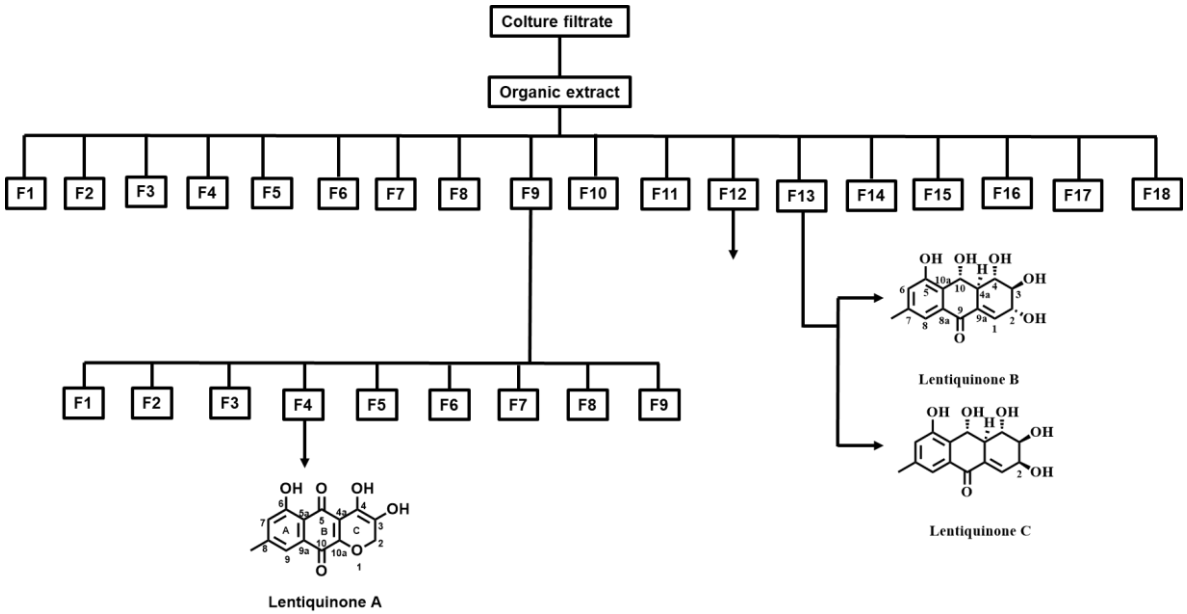

Scheme 2. Extraction and purification of *Ascochyta lentis* culture filtrate.

4.3 Crystal structure determination of lentiquinone B and C [2]

For the crystal structure determination of lentiquinones B and C (**8** and **9**), single crystals of them were obtained by water solution in MeOH followed by slow evaporation of the aqueous alcohol mixture. The selected suitable crystal was mounted on a Bruker-Nonius KappaCCD diffractometer in a flowing of N_2 at 173K. The instrument was equipped with an Oxford Cryostream apparatus (graphite monochromated Mo Kα radiation λ=0.71073 Å, CCD rotation images, thick slices, φ and ω scans to fill the asymmetric unit). It was also applied a semiempirical absorption correction (multiscan, SADABS). Both the two lentiquinones were directly solved by the SIR97 program (Altomare *et al*., 1999) and anisotropically refined by the full matrix least-squares method on F2 against all independent measured reflections using the SHELXL-2016/6 program (Sheldrick, 2008). For the lentiquinone B (**8**) was found, in its asymmetric unit, one solvent crystallization water molecule. The hydroxy H present in lentiquinone B (**8**) and C (**9**) and that present in the water were in difference Fourier maps and freely refined with U_{iso}(H) equal to 1.2U_{eq} of the carrier atom. While the other H atoms were placed in calculated positions and refined accordingly to a riding model (C−H distances in the range 0.95-1.00 Å and U_{iso}(H) equal to 1.2U_{eq} of the carrier atom). For lentiquinone B (**8**) was established the relative configuration of 2*R**,3*S**,4*S**,4a*S**,10*R** while for lentiquinone C (**9**) was 2*S**,3*S**,4*S**,4a*S**,10*R**. According to the literature methods recently reported to assign the absolute configuration in light-atom structures when Mo Kα radiation is used, the X-ray diffraction data for both the metabolites were collected and analyzed (Escudero-Adán *et al*., 2014). It was not possible to obtain the calculated absolute structure factors, using the programs SHELXL- 2016/6 and PLATON-v30118, necessary to define the absolute configuration for both the metabolites (Parsons, Flack and Wagner, 2013; Parsons, 2017).

4.3.1 Crystallographic data of lentiquinone B (8)

Crystallographic data of lentiquinone B showed: $C_{15}H_{16}O_6 \cdot H_2O$, M=310.29, orthorhombic, $P2_12_12_1$, a=5.0230(13) Å, b=6.942(3) Å, c=40.656(6) Å, α=β=γ=90°, V=1417.7(7) Å^3, T=173(2) K, Z=4, D_{calcd}=1.454 Mg/m^3, crystal size 0.50×0.25×0.10 mm^3, F(000)=656, absorption coefficient 0.116 mm^{-1}, reflections collected 29666, independent reflections 4820 [R_{int}=0.0328], final R indices [I>2σ(I)] R_1=0.0509, wR_2=0.1195, R indices (all data) R_1=0.0571, wR_2=0.1221. Flack x determined using 1563 quotients: 0.0(2). Parsons z: 0.0(2), Hooft y: 0.0(2), Bijvoet pairs 1941.

4.3.2 Crystallographic data of lentiquinone C (9)

Crystallographic data of lentiquinone C showed: $C_{15}H_{16}O_6$, M=292.28, monoclinic, $P2_1$, a=5.5150(11) Å, b=20.433(3) Å, c=5.8530(7) Å, α=90°, β=100.075(15)°, γ=90°, V=649.39(18) Å^3, T=173(2) K, Z=4, D_{calcd}=1.495 Mg/m^3, crystal size 0.35×0.35×0.25 mm^3, F(000)=308, absorption coefficient 0.116 mm^{-1}, reflections collected 31356, independent reflections 5691 [R_{int}=0.0255], final R indices [I>2σ(I)] R_1=0.0341, wR_2=0.0906, R indices (all data) R_1=0.0380, wR_2=0.0932. Flack x determined using 2455 quotients: 0.14(12). Parsons z: 0.17(12), Hooft y: 0.20(11), Bijvoet pairs 2773.

These data have been deposited in the Cambridge Crystallographic Data Centre with deposition numbers CCDC 1832451 and 1832452 respectively and can be obtained free of charge from the Cambridge Crystallographic Data Centre via www.ccdc.cam.ac.uk/.

4.3.3 Computational section.

MMFF and preliminary DFT calculations were run with Spartan'16 (Wavenfunction, Irvine, CA, USA, 2016) with standard parameters and convergence criteria; DFT and TDDFT calculations were run with Gaussian'16 with default grids and convergence criteria (Frisch *et al*., 2016). Conformational searches were run with the Monte Carlo algorithm implemented in Spartan'16

using Merck molecular force field (MMFF). Thus, all the obtained structures were first optimized with the DFT method at the ωB97X-D/6-31G(d) level in vacuo, and then reoptimized at the ωB97X-D/6-311+G(d,p) level in vacuo. Final optimizations were run at the ωB97X-D/6-311+G(d,p) level including the universal solvent model (SMD) for MeCN. The procedure afforded two minima for lentiquinone B (**8**), the most stable of which had a population >98%, and three minima for lentiquinone C (**9**), the two most stable of which had an overall population >99%. For the solid-state ECD/TDDFT approach, the X-ray geometry of lentiquinone C (**9**) was refined by optimizing only the hydrogen atoms at ωB97X-D/6- 31G(d) level in vacuo. TDDFT calculations were run with various functionals (B3LYP, CAM-B3LYP, M06) and def2-TZVP basis set, including SMD for MeCN. Average ECD spectra were computed by weighting component ECD spectra with Boltzmann factors at 300 K estimated from DFT internal energies. ECD spectra were generated using the program SpecDis, (Bruhn *et al.*, 2013; Bruhn *et al.*, 2019) applying the dipole-length rotational strengths formalism; the difference with dipole-velocity values was negligible in all cases.

4.4 Extraction of mycelium and purification of secondary metabolites from *Ascochyta lentis* [2]

The mycelium (30.5 g) obtained after culture filtration was lyophilized and stored at −20°C until use. It was suspended in EtOAc and subsequently macerated for a night and filtered. The obtained organic extract was evaporated under reduced pressure. The organic residue (800 mg) was chromatographed on silica gel column eluted with *n*-hexane-EtOAc (8:2) obtaining 12 groups of homogeneous fractions (Scheme 3). The residue of fourth and the fifth fractions were combined (234.2 mg) and further purified by column chromatography on silica gel eluted with CH_2Cl_2-*i*-PrOH (99:1). From the second fraction of this latter column, a yellow amorphous solid compound was obtained, identified, as

below reported, as pachybasin (**11**, 214.7 mg, 7 mg/g, R_f 0.8, Fig. 22). The residue of second fraction (8.7 mg) of the first column was purified by analytical TLC eluted with *n*-hexane-EtOAc (7:3), yielding a yellow amorphous solid, that proved to be, as below reported the ω-hydroxypachybasin (**12**, 1.2 mg, 0.04 mg/g, R_f 0.3, Fig. 22). The residue obtained from two other bands, were combined and further purified by analytical TLC eluted with *n*-hexane-*i*-PrOH (9:1), to provide two yellow amorphous compounds identified, as below reported, as 1,7-dihydroxy-3-methylanthracene-9,10-dione (**13**, 1.5 mg, 0.04 mg/g, R_f 0.7, Fig. 22) and phomarin (**14**, 2.5 mg, 0.08 mg/g, R_f 0.7, Fig. 22), respectively.

4.4.1 Pachybasin (11)

Pachybasin, obtained as an amorphous solid, had: ^{1}H NMR (500 MHz, in $CDCl_3$), δ 12.55 (s, OH), 8.25 (dd, *J* = 8.2, 3.4 Hz, H-5 and H-8), 7.77 (m, H-6), 7.59 (m, H-4 and H-7), 7.06 (d, *J* = 2.5 Hz, H-2), 2.44 (s, OCH_3). These data agree with those previously reported (Sun *et al.*, 2013; Bick and Rhee, 1966; De Stefano and Nicoletti, 1999; Borges and Pupo, 2006; Xia *et al.*, 2007); ESIMS (+) *m/z* 239 $[M+H]^+$.

4.4.2 *ω*-Hydroxypachybasin (12)

ω-Hydroxypachybasin, obtained as a yellow amorphous solid, had: ^{1}H NMR (500 MHz, in $CDCl_3$), δ 12.64 (s, OH-1), 8.32 (m, H-5 and H-8), 7.62 (m, H-7, H-6 and H-4), 7.36 (m, H-2), 4.84 (brs, CH_2); ^{13}C NMR (500 MHz, in $CDCl_3$), δ 188.4 (s, C-9), 182.6 (s, C10), 163.2 (s, C-1), 151.1 (s, C-3), 133.8 (d, C-6), 134.4 (d, C-7), 133.4 (s, C-4a), 134.8 (s, C-8a), 133.7 (s, C- 10a), 127.1 (d, C-8), 127.1 (d, C-5), 121.4 (d, C-2), 121.4 (d, C-4), 117.5 (s, C-9a), 64.4 (t, CH_2OH). These data agree with those previously reported (Sun *et al.*, 2013; Imre, Sar and Thomson, 1976; Kuo *et al.*, 1995; Khamthong *et al.*, 2012); ESIMS (+) *m/z* 255 $[M+H]^+$.

4.4.3 *1,7-Dihydroxy-3-methylanthracene-9,10-dione* (13)

1,7-Dihydroxy-3-methylanthracene-9,10-dione, isolated as a yellow amorphous solid, had: ^{1}H NMR (500 MHz, in $CDCl_3$), δ 12.49 (brs, OH-1), 8.14 (d, *J*=8.6 Hz, H-5), 7.60 (s, H-8), 7.57 (s, H-4), 7.15 (d, *J*=8.6, H-6), 7.04 (s, H-2), 2.78 (s, CH_3); ^{13}C NMR (500 MHz, in $CDCl_3$), δ 163.2 (s, C-1), 123.7 (d, C-2), 149.7 (s, C-3), 120.7 (d, C-4), 133.9 (s, C-4a), 129.5 (d, C-5), 121.6 (d, C-6), 165.5 (s, C-7), 112.2 (d, C-8), 133.9 (s, C-8a), 188.5 (s, C-9), 115.1 (s, C-9a), 181.5 (s, C-10), 126.6 (s, C-10a), 29.4 (q, CH_3). These data agree with those previously reported (Sun *et al.*, 2013; Borges and Pupo, 2006); ESIMS (+) *m/z* 255 $[M+H]^+$.

4.4.4 Phomarin (14)

Phomarin, obtained as a yellow amorphous : ^{1}H NMR (500 MHz, in $CDCl_3$), δ 12.70 (brs, OH-1), 8.24 (d, *J*=8.6 Hz, H-8), 7.66 (d, *J*=2.6 Hz, H-5), 7.63 (s, H-4), 7.22 (dd, *J*=8.6, 2.6 Hz, H-7), 7.09 (s, H-2), 2.46 (s, CH_3). These data agree with those previously reported (Sun *et al.*, 2013; Bick and Rhee, 1966; Borges and Pupo, 2006); ESIMS (+) *m/z* 255 $[M+H]^+$.

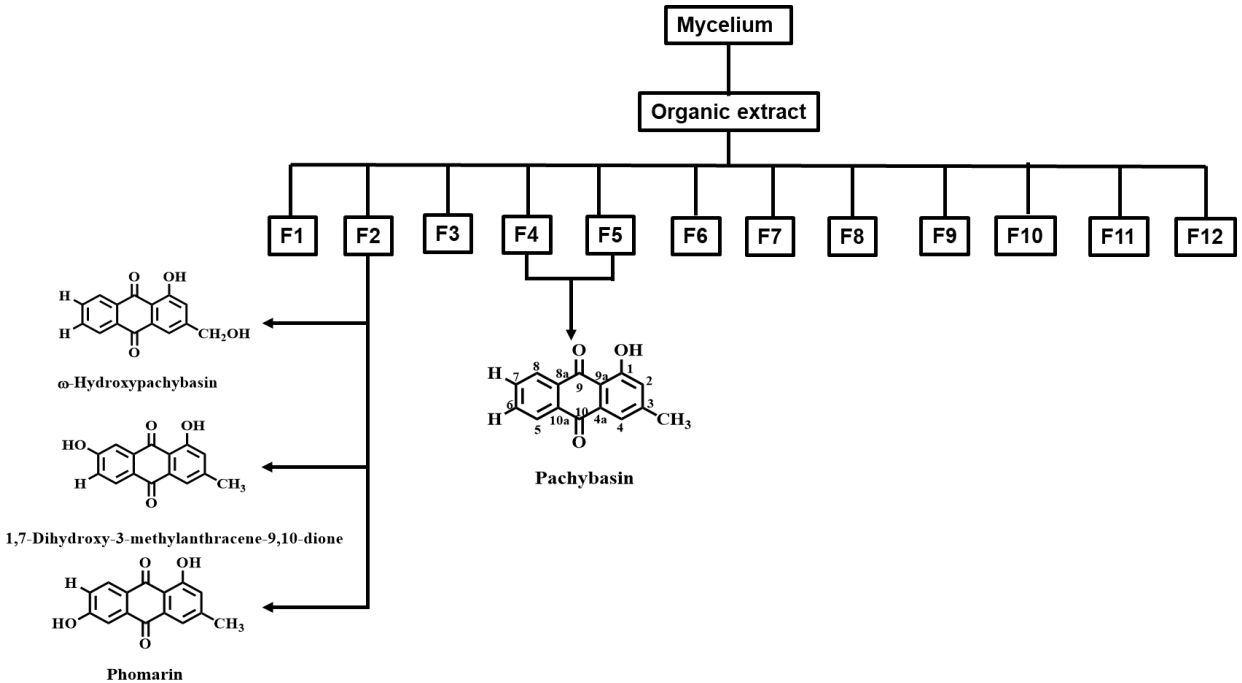

Scheme 3. Extraction and purification of *Ascochyta lentis* mycelium.

4.5 Production, extraction and purification of secondary metabolites from *Colletotrichum lupini* culture filtrates [3]

The fungus was grown for 4 weeks at 25 °C in the dark using a 1L Roux flasks which contained 200 mL of a defined mineral medium (M1D). The fungal cultures were first filtered through gauze and then vacuum filtered through filter paper (Whatman No. 4) to remove the mycelium, and the collected filtrates (10.0 L) were lyophilized and stored at −20 °C until use. Distilled water at 1/10 of its initial volume was used to redissolved the culture filtrate which was then extracted with EtOAc. The obtained organic extract was firstly dried with Na_2SO_4 and then evaporated under reduced pressure. The organic extract (923.0 mg) was purified by silica gel column chromatography with $CHCl_3$-MeOH (85:15), obtaining nine groups of homogeneous fractions (Scheme 4). The first fraction (99.2 mg) was further purified by silica gel column chromatography, eluted with CH_2Cl_2-*i*-PrOH (95:5), yielding seven groups of homogeneous fractions. The third fraction (8.2 mg) was purified by reverse phase TLC, eluted with EtOH-H_2O (6:4), yielding an amorphous solid named lupindolinone (**15**, 1.9 mg, 0.2 mg/L, R_f 0.5, Fig. 55). The second fraction (61.3 mg) of the initial column was further purified by silica gel column chromatography, eluted with CH_2Cl_2-*i*-PrOH (9:1), affording six fractions. The third fraction (33.8 mg) of this latter column was further purified on preparative TLC, eluted with CH_2Cl_2-*i*-PrOH (93:7), yielding an amorphous solid named lupinlactone (**16**, 6.0 mg, 0.6 mg/L R_f 0.6, Fig. 55). Other two known fungal metabolites were obtained from the same fraction, identified, as below reported, as (3*R*)-mevalolactone (**17**, 1.0 mg, 0.1 mg/L R_f 0.7, Fig. 55) and tyrosol (**18**, 1.0 mg, 0.1 mg/L R_f 0.6, Fig. 55).

4.5.1 Lupindolinone (15)

Lupindolinone, obtained as an amorphous solid, had: IRν_{max} 1703, 1620, 1470 cm^{-1} (Fig. 62); UV λ_{max} (log ε) 282 (2.73), 249 (3.46) nm (Fig. 63); ^{1}H and ^{13}C

NMR spectra (Fig. 56 and 57) are reported in Table 6; HRESIMS (+) *m/z*: 162.0919 $[M+H]^+$ (calcd for $C_{10}H_{11}NO$ 162.0914) (Fig. 61).

4.5.2 Lupinlactone (16)

Lupinlactone, obtained as an amorphous solid, had: $[\alpha]^{25}_D$ -11.1 (c 0.6); $IR_{\nu max}$ 3358, 1765 cm^{-1} (Fig. 70); UV λ_{max} (log ε) < 220 nm; ^1H and ^{13}C NMR spectra (Fig. 64 and 65) are reported in Table 7; HRESIMS (+) *m/z*: 283 $[2M+Na]^+$, 261 $[2M+H]^+$, 169 $[M+K]^+$, 153 $[M+Na]^+$, 131.0709, $[M+H]^+$ (calcd for $C_6H_{10}O_3$ 131.0703113) and $[MH-H_2O]^+$ (Fig. 69).

4.5.3 (3*R*)-Mevalolactone (17)

(3*R*)-Mevalolactone had: $[\alpha]^{25}_D$ -17.3 (c 0.5) (Evidente *et al*., 2003); ^1H NMR (500 MHz, in $CDCl_3$) δ 1.41 (3H, s, CH_3), 1.92 (2H, m, H-4), 2.54 (d, *J*=17.5 Hz, H-2A), 2.80 (d, *J*=17.5 Hz, H-2B), 4.35 (m, H-5A), 4.61 (m, H-5B); ESIMS (+), *m/z*: 283 $[2M+Na]^+$, 261 $[2M+H]^+$, 153 $[M+Na]^+$, 131 $[M+H]^+$. These data agree with that previously reported (Varejão *et al*., 2013).

4.5.4 Tyrosol (18)

Tyrosol had: ^1H NMR (500 MHz, in $CDCl_3$), δ: 7.10 (d, *J*=8.2 Hz, H-2 and H-6), 6.79 (d, *J*=8.2 Hz, H-3 and H-5), 3.82 (t, *J*=6.6 Hz, H_2-8), 2.80 (t, *J*=6.6 Hz, H_2-7). ESIMS (+), *m/z*: 295 $[2M+Na]^+$, 159 $[M+Na]^+$. These data agree with those previously reported (Kimura and Tamura, 1973; Capasso *et al.*, 1992; Cimmino *et al.*, 2017).

4.5.5 5-*O*-(*S*)-MTPA ester of lupinlactone (19)

5-*O*-(*S*)-α-methoxy-α-trifluoromethyl-α-phenylacetate (MTPA) ester of lupinlactone (**16**) was obtained as follow: (*R*)-(-)-MPTA-Cl (10 μL) was added to lupinlactone (**16**) (0.5 mg) dissolved in dry pyridine (100 μL). The mixture was kept at room temperature for 1 h and then the reaction was stopped by adding MeOH. The azeotrope formed by addiction of C_6H_6 was removed by an N_2 stream. The residue was purified by analytical TLC, eluted with CH_2Cl_2-*i*-PrOH (9:1), yielding the (*S*)-MPTA ester of lupinlactone (**19**) as a homogeneous

oil (0.9 mg R_f 0.7, Fig. 55). It had: ^{1}H NMR spectrum (Fig. 72) reported in Table 8; ESIMS (+) *m/z* 347 $[M+H]^+$ (Fig. 73).

4.5.6 *5-O-(R)*-MTPA ester of lupinlactone (20)

5-*O*-(*R*)-α-methoxy-α-trifluoromethyl-α-phenylacetate (MTPA) ester of lupinlactone was obtained as follow: (*S*)-(+)-MPTA-Cl (10 μL) was added to lupinlactone (**16**) (0.5 mg) dissolved in dry pyridine (100 μL). The reaction was carried out under the same conditions used to prepare 5-*O*-(*S*)-MTPA ester of lupinlactone (**19**). The purification of the crude residue by analytical TLC, eluted with CH_2Cl_2-*i*-PrOH (9:1), allowed to obtain (*R*)-MTPA ester of lupinlactone (**20**) as a homogeneous oil (0.9 mg R_f 0.7, Fig. 55). It had: ^{1}H NMR spectrum (Fig. 74) reported in Table 8; ESIMS (+) *m/z* 347 $[M+H]^+$ (Fig. 75).

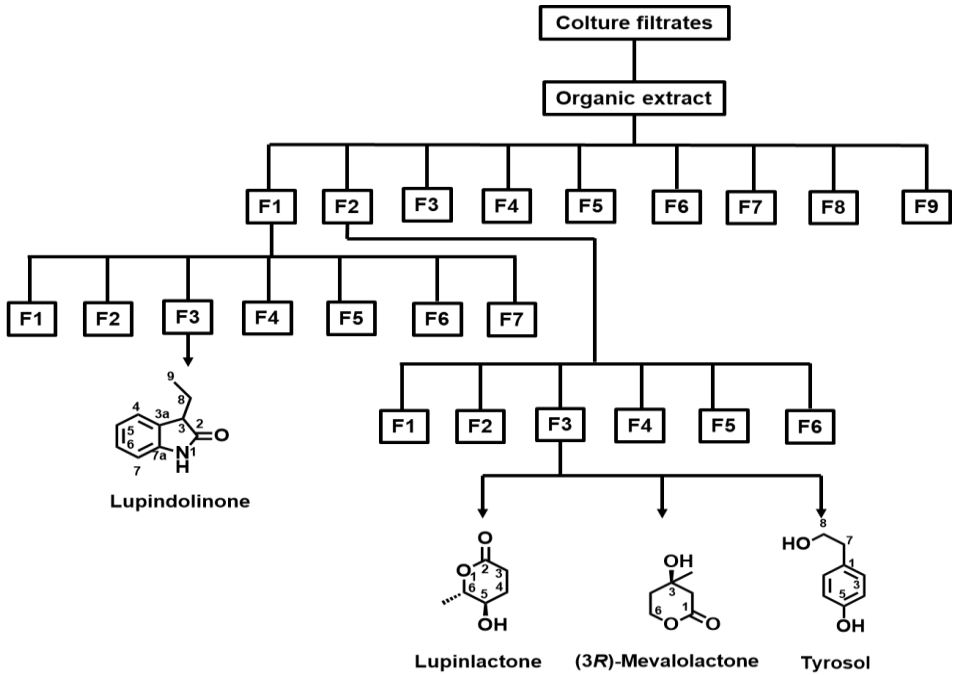

Scheme 4. Extracton and purification of *Colletotrichum lupini* culture filtrates.

4.6 Production, extraction and purification of secondary metabolites from *Neofusicoccum batangarum* culture filtrates [4]

The fungal culture filtrate (12 L), was stored at -20°C until use. It was concentrated, under reduced pressure at 35 °C, to 1 L exhaustively extracted with EtOAc. The obtained organic extract was firstly dried with Na_2SO_4 and then evaporated under reduced pressure. The oily residue (1.84 g) was fractioned by column chromatography on silica gel eluted with $CHCl_3$-*i*-PrOH (9:1), obtaining twelve groups of homogeneous fractions (Scheme 5). The residue of first and second fractions (47.5 mg) were combined and further purified by preparative TLC eluted with *n*-hexane-EtOAc (85:15), obtaining two pure metabolites in the form of amorphous solids, that were identified, as below reported, as (-)-(*R*)-mellein (**21**, 8.6 mg, 0.7 mg/L, R_f 0.4, Fig. 76) and as (±)-botryoisocoumarin A (**22**, 3.4 mg, 0.3 mg/L, R_f 0.3, Fig. 76). The residue of fourth fraction (41.6 mg) of the column chromatography was purified by two preparative TLC eluted with petroleum ether-Me_2CO (8:2), obtaining two pure metabolites identified as below reported as (-)-(3*R*,4*R*)-4-hydroxymellein (**23**, 2.4 mg, 0.2 mg/L, R_f 0.3, Fig. 76) and (-)-(3*R*,4*S*)-4-hydroxymellein (**24**, 3.6 mg, 0.3 mg/L, R_f 0.4, Fig. 76). The residue of fifth fraction (123.4 mg) of the original column was further purified by column chromatography eluted with CH_2Cl_2-*i*-PrOH (95:5) obtaining eleven groups of homogeneous fractions. The seventh and eighth fractions (27.5 mg) were combined and purified by analytical TLC eluted with CH_2Cl_2-*i*-PrOH (95:5), obtaining a pure metabolite as an amorphous solid, that was identified, as below reported, as (-)-terpestacin (**25**, 6.0 mg, 0.5 mg/L, R_f 0.4, Fig. 76). The residue of fifth and sixth fractions (40.8 mg,) were combined and purified by preparative TLC eluted with CH_2Cl_2-*i*-PrOH (97:3), obtaining a pure metabolite identified, as below reported, as (+)-(3R*,4S*)-3,4-dihydro-4,5,8-trihydroxy-3methyl-isocoumarin, named neoisocumarin (**26**, 8.0 mg, 0.7 mg/L, R_f 0.3, Fig. 76).

4.6.1 (-)-(*R*)-Mellein (21)

(-)-(*R*)-Mellein, obtained as an amorphous solid, had: $[\alpha]^{25}_{D}$ -90 (c 0.2); ^{1}H NMR (500 MHz, in $CDCl_3$), δ: 11.03 (s, HO-8), 7.41 (t, *J*=8.4 Hz, H-6), 6.89 (d, *J*=8.4 Hz, H-7), 6.69 (d, *J*=8.4 Hz, H-5), 4.74 (tq, *J*=6.9 and 6.3 Hz, H-3), 2.93 (d, *J*=6.9 Hz, H_2-4), 1.53 (d, *J*=6.3 Hz, Me-3). ESIMS (+), *m/z*: 179 $[M+H]^+$. These data agree with those previously reported (Cole and Cox, 1981; Cabras *et al.*, 2006; Evidente *et al.*, 2010; Abou-Mansour *et al.*, 2015; Cimmino *et al.*, 2017d).

4.6.2 (±)-Botryoisocoumarin A (22)

(±)-Botryoisocoumarin A, obtained as an amorphous solid, had: ^{1}H NMR (500 MHz, in $CDCl_3$), δ 11.03 (s, HO-8), 7.41 (t, *J*=8.3 Hz, H-6), 6.89 (d, *J*=8.3 Hz, H-7), 6.69 (d, *J*=8.3, H-5), 3.40 (OMe), 3.23 (d, *J*=16.0 Hz, H-4A) 3.16 (d, *J*=16.0 Hz, H-4B), 1.69 (s, Me-C3). These data agree with those previously reported (Xu *et al.*, 2012); ESIMS, *m/z*: 439 $[2M+Na]^+$, 209 $[M+H]^+$, 172 $[M+H+MeOH]^+$.

4.6.3 (-)-(3*R*,4*R*)-4-Hydroxymellein (23)

(-)-(3*R*,4*R*)-4-Hydroxymellein had: $[\alpha]^{25}_{D}$ -29.0 (c 1.2); ^{1}H NMR (400 MHz, in $CDCl_3$), δ: 10.99 (s, HO-8), 7.55 (t, *J*=7.0 Hz, H-6), 7.03 (d, *J*=7.0 Hz, H-7), 7.00 (d, *J*=7.0 Hz, H-5), 4.68 (brq, *J*=7.0, H-3), 4.60 (brs, H-4), 1.53 (d, *J*=7.0 Hz, Me-C3). ESIMS (+), *m/z*: 195 $[M+H]^+$. These data agree with those previously reported (Cole and Cox, 1981; Cabras *et al.*, 2006; Djoukeng *et al.*, 2009; Evidente *et al.*, 2010; Abou-Mansour *et al.*, 2015).

4.6.4 (-)-(3*R*,4*S*)-4-Hydroxymellein (24)

(-)-(3*R*,4*S*)-4-Hydroxymellein had: $[\alpha]^{25}_{D}$ -27.0 (c 1.1); ^{1}H NMR (500 MHz, in $CDCl_3$) and ESIMS (+) data are very similar to those of (-)-(3*R*,4*R*)-4-hydroxymellein. These data are also in agreement with those previously reported (Cole and Cox, 1981; Devys *et al.*, 1992; Cabras *et al.*, 2006; Djoukeng *et al.*, 2009; Evidente *et al.*, 2010; Abou-Mansour *et al.*, 2015).

4.6.5 (-)-Terpestacin (25)

(-)-Terpestacin, obtained as an amorphous solid, had: $[\alpha]^{25}_{D}$ -17.7 (c 0.4); ^{1}H NMR (400 MHz, in $CDCl_3$), δ: 5.38 (m, H-12), 5.25 (dd, *J*=10.6 and 5.4 Hz, H-2), 5.13 (m, H-6), 4.07 (dd, *J*=9.7 and 3.6, H-10), 3.85 (dd, *J*=10.4 and 7.0 Hz, H-24A), 3.80 (dd, *J*=10.4 and 5.5 Hz, H-24B), 2.66 (m, H-19), 2.36 (dd, *J*=13.7 and 10.6 Hz, H-1A), 2.44 (d, *J*=17.0 Hz, H-14), 2.26 and 2.11 (2H, both m, H_2-5), 2.24 and 2.10 (2H, both m, H_2-4), 2.18 and 1.78 (2H, both m, H_2-8), 1.92 (m, H-13A), 1.75 (m, H-1B), 1.75 and 1.70 (both m, H_2-9), 1.67 (s, Me-20) 1.64 (s, Me-21), 1.56 (s, Me-22), 1.29 (d, *J*=7.3 Hz, Me-25), 0.99 (s, Me-23); ESIMS (+) *m/z*: 425. $[M+Na]^+$. These data agree with those previously reported (Oka *et al*., 1993; Trost, Dong and Vance, 2007; Cimmino *et al*., 2016).

4.6.6 (+)-Neoisocoumarin (26)

(+)-Neoisocoumarin: $[\alpha]^{25}_{D}$ + 50 (c 0.4); ^{1}H NMR (400 MHz, in Acetone-d_6), δ: 10.68 (s, HO-8), 7.16 (d, *J*=9.0 Hz, H-6), 6.84 (d, *J*=9.0 Hz, H-7), 5.03 (d, *J*=4.1 Hz, H-4), 4.90 (dq, 6.7 and 4.4 Hz, H-3), 1.35 (d, *J*=6.7 Hz, Me-C3) (Fig. 79); ESIMS (+), *m/z*: 443 $[2M+Na]^+$, 233 $[M+Na]^+$, 211 $[M+H]^+$, 193 $[M+H-H_2O]^+$, 175 $[M+H-2H_2O]^+$ (Fig. 81). These data were very similar to that already reported (Yang *et al*., 2011).

4.6.7 5,8-*O*,*O*'-Dimethyl ether of neoisocoumarin (27)

5,8-*O*,*O*'-dimethyl ether of neoisocoumarin was obtained as follow: neosisocoumarin (**26**, 1 mg) was dissolved in MeOH (200 μL) and ethereal solution of diazomethane was added until a persistent yellow color. The reaction was carried out at room temperature overnight and stopped by evaporation of solvent under nitrogen stream. The residue (1.2 mg) was purified by TLC, eluted with $CHCl_3$-*i*-PrOH (95:5) to yield 5,8-*O*,*O*'-dimethyl ether of neoisocoumarin (**27**) as a homogeneous oil (1.1 mg R_f 0.4, Fig. 82). It had ^{1}H NMR, δ: 7.29 (d, *J*=8.8 Hz, H-6), 7.07 (d, *J*=8.8 Hz, H-7), 5.49 (d, *J*=2.4 Hz, H-4), 4.48 (dq, *J*=6.3 and 2.4 Hz, H-3), 3.90 and 3.88 (s, 3H each 2x OMe), 0.85 (d, *J*=6.5 Hz,

Me-11) (Fig. 82); ESIMS (+), *m/z*: 499 $[2M+Na]^+$, 277 $[M+K]^+$, 261 $[M+Na]^+$, 239 $[M+H]^+$, 221 $[M+H-H_2O]^+$ (Fig. 83).

4.6.8 5-*O*-(*S*)-MTPA ester of 5,8-*O*,*O*'-dimethyl ether of neoisocoumarin (28)

5-*O*-(*S*)-α-methoxy-α-trifluoromethyl-α-phenylacetate (MTPA) ester of 5,8-*O*,*O*'-dimethyl ether of neoisocoumarin was obtained as follow: (*R*)-(-)-MPTA-Cl (10 μL) was added to 5,8-*O*,*O*'-dimethyl ether of neoisocoumarin (**27**, 1.1 mg) dissolved in dry pyridine (100 μL). The mixture was kept at room temperature for 1 h and then the reaction stopped by adding MeOH and the azeotrope, formed by addition of C_6H_6, was removed by an N_2 stream. The residue (1.3 mg) was purified by analytical TLC, eluted with CH_2Cl_2-*i*-PrOH (97:3), yielding 5-*O*-(*S*)-(MTPA) ester of 5,8-*O*,*O*'-dimethyl ether of neoisocoumarin as a homogeneous oil (0.6 mg R_f 0.7). ^{1}H NMR spectrum (Fig. 84) is reported in Table 10; ESIMS (+) *m/z* 477 $[M+Na]^+$, 455 $[M+H]^+$ (Fig. 85).

4.6.9 5-*O*-(*R*)-MTPA ester of 5,8-*O*,*O*'-dimethyl ether of neoisocoumarin (29)

5-*O*-(*R*)-α-methoxy-α-trifluoromethyl-α-phenylacetate (MTPA) ester of 5,8-*O*,*O*'-dimethyl ether of neoisocoumarin was obtained as follow: (*S*)-(+)-MPTA-Cl (10 μL) was added to 5,8-*O*,*O*'-dimethyl ether of neoisocoumarin (1.1 mg) dissolved in dry pyridine (100 μL). The reaction was carried out under the same conditions used for preparing **28** from **27**. The crude residue was purified by analytical TLC eluted with CH_2Cl_2-*i*-PrOH (97:3), affording 5-*O*-(*R*)-(MTPA) ester of 5,8-*O*,*O*'-dimethyl ether of neoisocoumarin as a homogeneous oil (0.4 mg R_f 0.7). ^{1}H NMR spectrum (Fig. 86) is reported in Table 10; ESIMS (+) *m/z* 477 $[M+Na]^+$, 455 $[M+H]^+$ (Fig. 87).

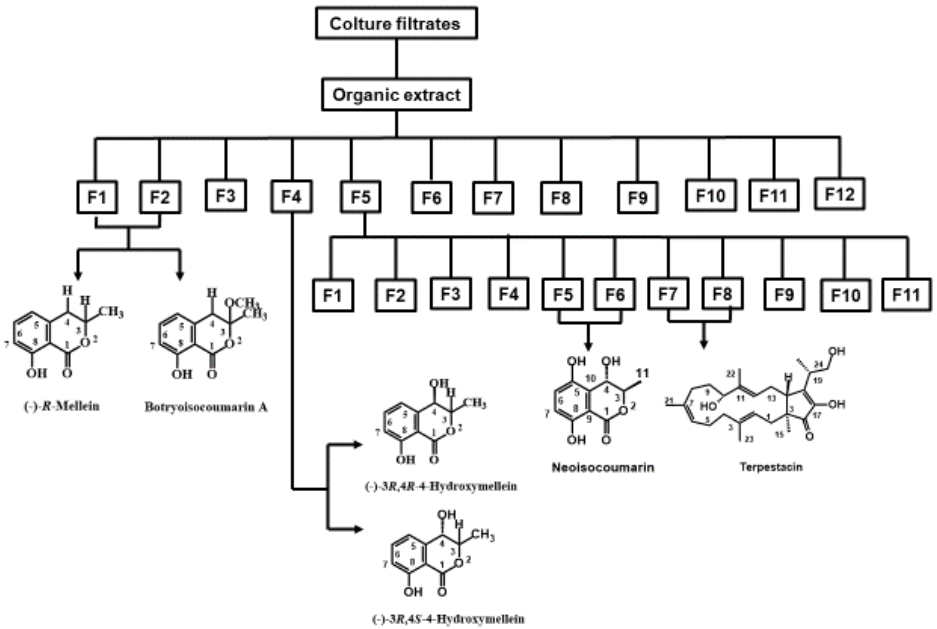

Scheme 5. Extracton and purification of *Neofusicoccum batangarum* culture filtrates.

4.7 Biological assays

4.7.1 Leaf puncture assay

The metabolites **1**-**5** and **7**-**18** were tested at 2 µg/µL concentration on seven different plant species, belonging to different botanical families, i.e., *Lupinus albus*, *Lens culinaris*, *Phaseolus vulgaris* (Fabaceae family), *Sonchus oleraceus* (Asteraceae), *Convolvulus arvensis* (Convolvulaceae), *Lycopersicon esculentum* (Solanaceae), *Mercurialis annua* (Euphorbiaceae). Droplets (20 µL) of the solution containing the compound **1**-**5** and **7**-**18** were applied to detached leaves previously punctured with a needle. Five replications were used for each plant species tested. Leaves were kept in a moistened chamber under continuous fluorescent lights at 25°C. The eventual appearance of symptoms, consisting in circular necrosis, was observed three days after droplet application. Control treatments were carried out by applying droplets of a methanol solution (MeOH 1%).

The metabolites **21**-**26** were tested on young cladodes of host plant cactus pear [*Opuntia ficus-indica* (L.) Mill.] and on non-host plant, using tomato (*Solanum lycopersicum* L.) leaves. Pure metabolites were first dissolved in MeOH, and then diluted to the desired final concentrations with distilled water (final concentration of MeOH, 4%). For each metabolite, 50 µL of the solution was pipetted into cladodes at concentrations of 0.05, 0.1, 0.25, 0.5 or 1 mg/mL. Phytotoxicity of pure metabolites of *N. batangarum* was also tested by a puncture assay on tomato leaves. A droplet (10 µL) of each metabolite, at concentrations of 0.05, 0.1, 0.25, 0.5 or 1 mg/mL, was placed on the leaf lamina previously punctured by a needle. One cladode of a single plant of cactus pear and four leaves of tomato were employed as replicates, and each treatment was repeated twice. MeOH (4%) and sterile distilled water were used as controls. Symptoms of phytotoxicity of inoculated cladodes and leaves, kept in a climatic

chamber under controlled conditions, were observed each day for 7 days. The size (mm^2) of necrotic area surrounding the punctures was measured.

4.7.2 Assay on seed germination of the parasitic weed *Phelipanche ramosa*.

Phelipanche ramosa seeds, collected from infested tomato and tobacco fields in Southern Italy, were surface sterilized with 1% sodium hypochlorite for 10 min, rinsed with sterile tap water and then placed on wet glass microfiber filters (GF/A Whatman) cut to fit in large glass petri dishes (16 cm diameter). Seeds were kept at 25–26 °C in the dark room for 3 weeks. Filters were then cut in small pieces, each containing approximately 100 seeds. Two pieces of the cut filters were placed in small petri dishes (6 cm diameter) containing another filter disk that had been moistened with a solution at 10^{-3} and 10^{-4} M concentrations. This filter disk also contained the synthetic strigolactone analog stimulant GR24 (Wigchert *et al*., 1999). Plates were again kept at 25°C in dark room. Two replications were used for each assayed compound (**1**,**2**, **7**-**18**). After 3 days, the number of germinated seeds was determined by direct observation under a stereomicroscope, and the results were expressed as germination percentage in comparison to the control. Visual estimation of the germination tubes was also performed (Boari and Vurro, 2004).

4.7.3 Assay on *Lepidium sativum* rootlet elongation.

Seeds of *L. sativum* were rinsed for some minutes under a continuous flux of tap water. Thus, they were germinated by placing them on Petri dishes, on a wet paper disk, at 25°C in the dark room for 48 h. Ten uniformly germinated and healthy seedlings were selected and transferred to each small Petri dish, containing the paper disk wetted with 2 mL of the test solutions. Each compound (**1-5, 7-18**) was tested at 2×10^{-4} M concentration, in triplicate. Disks were kept under continuous fluorescent lights for 3 days. Thus, the rootlet length

was measured, and the results were expressed as percentage reduction of rootlet length in comparison to the respective control.

4.7.4 *Lemna minor* assay.

A bioassay for detecting the effects of metabolites on chlorophyll degradation was performed on *Lemna minor*. The wells of sterile, polystyrene 96-well microtiter plates were filled with a 100 µL aliquot of solutions containing the metabolites (**7**-**18**) to be tested at 2 µg/µL concentration, and one frond of actively growing axenic *L. minor*. For each compound were prepared four replications. The plates were incubated in a growth chamber with 12/24 h fluorescent lights and observed daily up to 4 days. One day after the application of the test solution, 100 µL of distilled H_2O was added to each well. The appearance of necrosis or chlorosis was assessed visually by comparison to the respective control (Cimmino *et al*., 2012b). Moreover, plantlet fresh weight was measured, and chlorophyll contents were determined by using a protocol previously described (Marr *et al*., 1995).

4.7.5 Antifungal assay.

For the antifungal bioassay, PDA (150 µL), under sterile conditions, was added to each well of a 96-well-plate. In each well were also placed 5 µL of solvent containing 10 µg of each metabolite (**7**-**14**). In an Eppendorf tube containing 1 mL of water, a fungal conidial suspension was added. The suspension was obtained by placing a PDA plug (around 1 cm diameter) with the actively growing mycelia of each fungus and mixing the material by using a Vortex. To each plate was added 5 µL of the obtained fungal suspension. *Verticillium dahliae*, *Fusarium solani*, *Aspergillus carbonarius*, *Penicillium allii*, *Colletotrichum fioriniae*, *Rhizoctonia* sp., *Phoma exigua*, *Alternaria alternata*, and *Cladosporium halotolerans* (all available from the ISPA fungal collection) were tested with the eight compounds, with four replications for each. After 2

days was visually evaluated the appearance of the fungal colony overgrowing PDA.

4.7.6 Antibiotic assay.

This assay was performed on *Bacillus subtilis* and *Escherichia coli* by using a published protocol (Bottalico *et al*., 1990). 4 μL of the solvent (MeOH or DMSO) containing each compound (**7**-**14**) at 10^{-1} M were applied on a diskette. The eventual appearance of a growth inhibition halo around the diskette, revealing an antibiotic effect, was visually estimated 24 h after the application of the compounds.

5 RESULTS AND DISCUSSION

5.1 Structural identification of secondary metabolites from *Ascochyta lentis* var. *lathyri* culture filtrates [1]

The organic extract obtained from the culture filtrates of *A. lentis* var. *lathyri* was purified, as detailed in the Experimental section (Scheme 1), obtaining five pure metabolites (**1**-**5**) that were isolated and identified (Fig. 6). Two of them appeared to be, from a preliminary ^{1}H NMR investigation, new phenol derivatives and were named lathyroxins A and B (**1** and **2**, respectively). The other three compounds proved to be well-known metabolites, *p*-hydroxybenzaldehyde (**3**), *p*-methoxyphenol (**4**), and tyrosol (**5**) respectively. They were identified by comparing their spectroscopic data with those reported in the literature: (Ren-Yi *et al*., 2015) for *p*-hydroxybenzaldehyde (**3**), (Liu and Ackermann, 2013) for *p*-mehoxyphenol (**4**), and (Kimura and Tamura, 1973; Capasso *et al*., 1992; Cimmino *et al*., 2017d) for tyrosol (**5**).

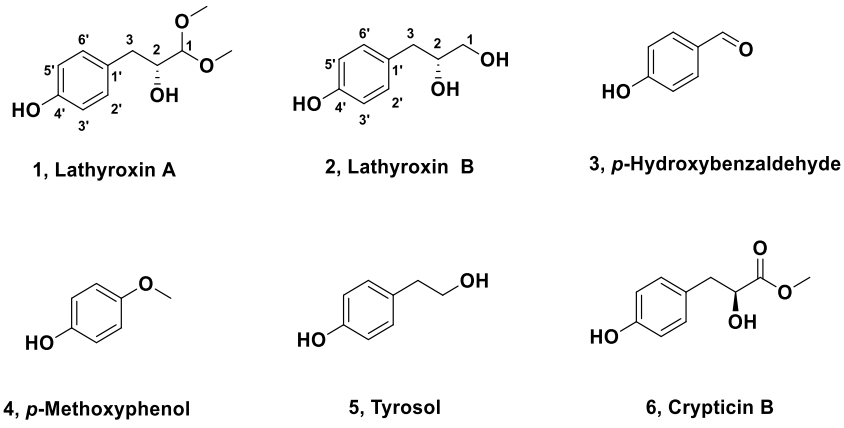

Figure 6. *Ascochyta lentis* var. *lathyri* secondary metabolites (**1**-**5**) and crypticin (**6**)

5.1.1 Structural identification of lathyroxin A.

Lathyroxin A (**1**) has the molecular formula $C_{11}H_{16}O_4$ as deduced from its HRESIMS (Fig. 11) and consistent with 4 hydrogen deficiencies. Its ^1H and ^{13}C data (Fig. 7 and 8) showed signal systems like those of a substituted derivative of phenol. These data are also consistent with the bands of hydroxy and aromatic groups observed in the IR spectrum at ν_{max} 3358, 1613, 1516, 1549 cm^{-1} (Fig. 13) (Nakanishi, 1977), as well as with the absorption maxima observed at 278 and 223 nm in the UV spectrum (Fig. 12) (Badertscher *et al*., 2009). The ^1H spectrum (Fig. 7) showed the typical pattern system of a *para*-disubstituted benzene ring with two doublets (J = 8.3 Hz) at δ 7.15 (H-2′,6′) and 6.79 (H-3′,5′) respectively and with the latter *ortho*-located to the hydroxy phenol group (Berger and Braun, 2004). The same spectrum showed signals of an ABXY system appearing as a doublet (J=5.7Hz), a multiplet, and two double doublets (J =14.1 and 3.7 Hz; 14.1 and 8.5 Hz) at δ 4.17, 3.83, 2.92, and 2.67, respectively, and assigned to H-1, H-2, and H-3A and H-3B. The chemical shift of H-1 is typical of a dioxolanemethine, attached to two methoxy groups resonating as singlets at δ 3.48 and 3.46, respectively. As expected, the ^1H NMR spectrum (Fig. 7) also showed two broad singlets due to two hydroxy groups at δ 4.78 and δ 2.10 (Badertscher *et al*., 2009). The couplings observed in the HSQC spectrum (Fig. 9) permitted the assignment of the signals observed in the ^{13}C NMR spectrum (Fig. 8 and Table 1) at δ 106.0, 72.1, 37.2, 130.6, 115.2, and 54.8 (overlapped signal) to the protonated carbons C-1, C-2, C-3, C-2′,6′, and C-3′,5′ and to the two methoxy groups, respectively (Berger and Braun, 2004; Breitmaier and Voelter, 1987). The couplings observed in the HMBC spectrum (Fig. 10 and Table 1) between the tertiary oxygenated sp^2 carbon C-4′ and H-2′,6′ and H-3′,5′ allowed to assign this carbon at δ 154.1 (Berger and Braun, 2004). Similarly, the coupling observed between the quaternary sp^2 carbon C-1′ and the same protons (H-2′,6′ and H-3′,5′) and with H-2 and H_2-3 allowed to

assign this carbon at δ 130.2. Thus, the chemical shifts were assigned to all the protons and to all the unsaturated carbons as reported in Table 1, and lathyroxin A (**1**) was formulated as 4-(2-hydroxy-3,3-dimethoxypropyl)-phenol. The structure assigned to lathyroxin A (**1**) was confirmed by all the other couplings observed in the HMBC spectrum (Fig. 10 and Table 1) and the data from the HRESIMS spectrum (Fig. 11). The latter, showed the sodiated dimer $[2M+Na]^+$ and the sodium cluster $[M+Na]^+$ at *m/z* 447 and 235.0931, respectively.

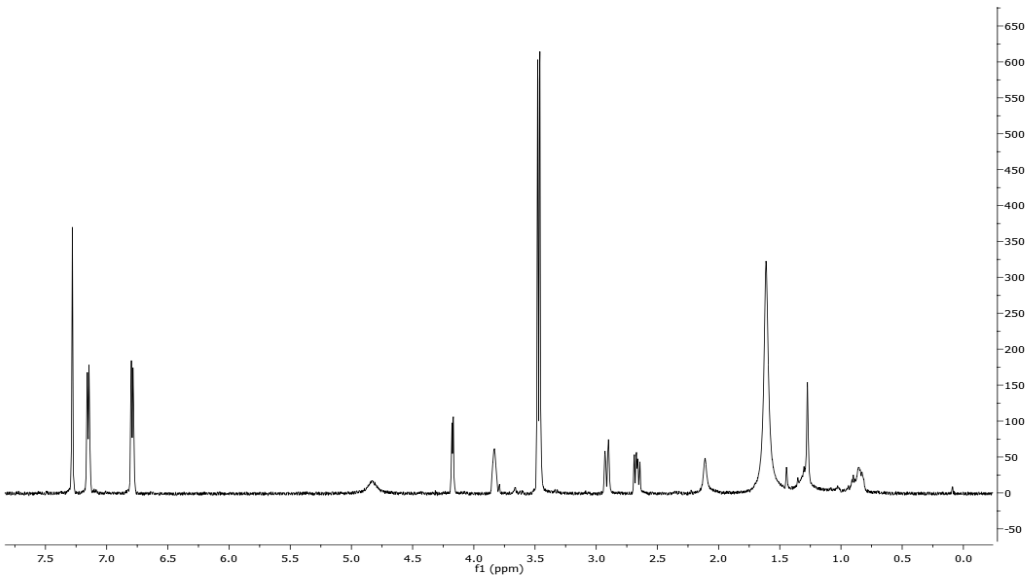

Figure 7. ^{1}H NMR spectrum of lathyroxin A ($CDCl_3$, 500 MHz).

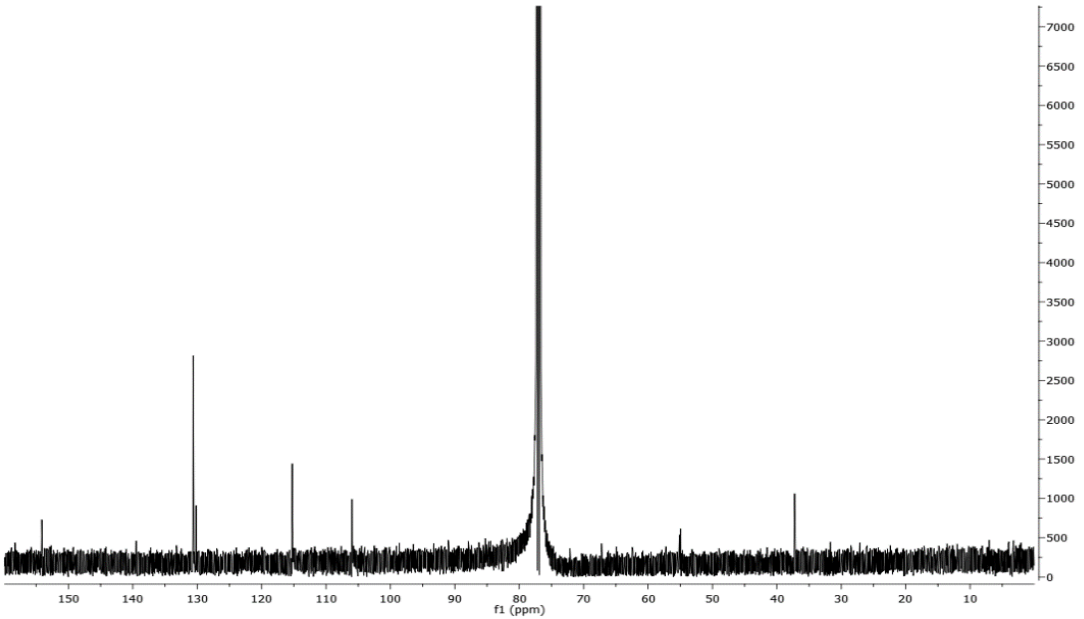

Figure 8. ^{13}C NMR spectrum of lathyroxin A ($CDCl_3$, 500 MHz).

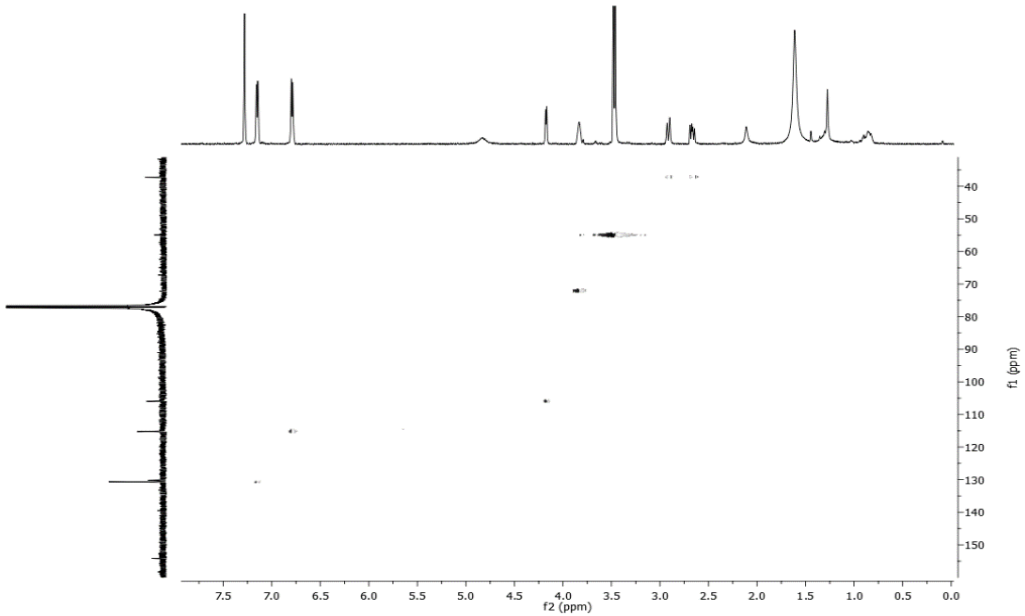

Figure 9. HSQC spectrum of lathyroxin A ($CDCl_3$, 500 MHz).

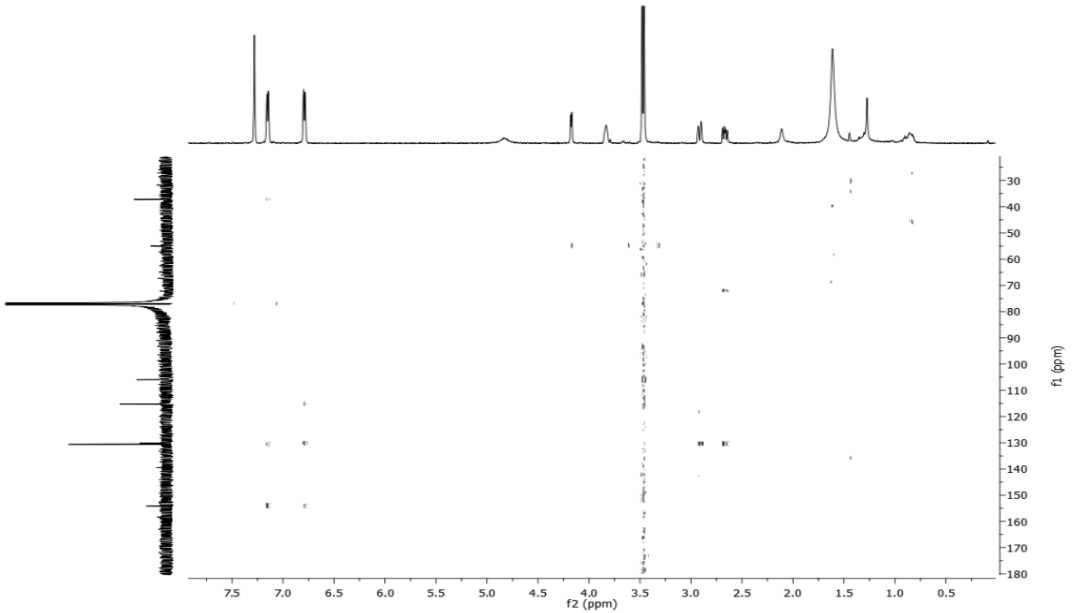

Figure 10. HMBC spectrum of lathyroxin A ($CDCl_3$, 500 MHz).

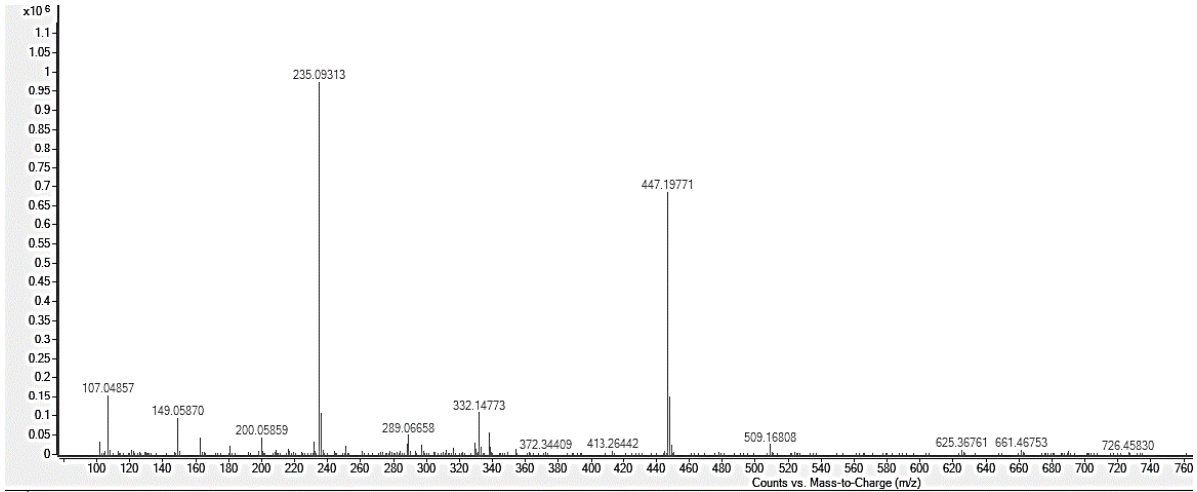

Figure 11. HRESIMS spectrum of lathyroxin A.

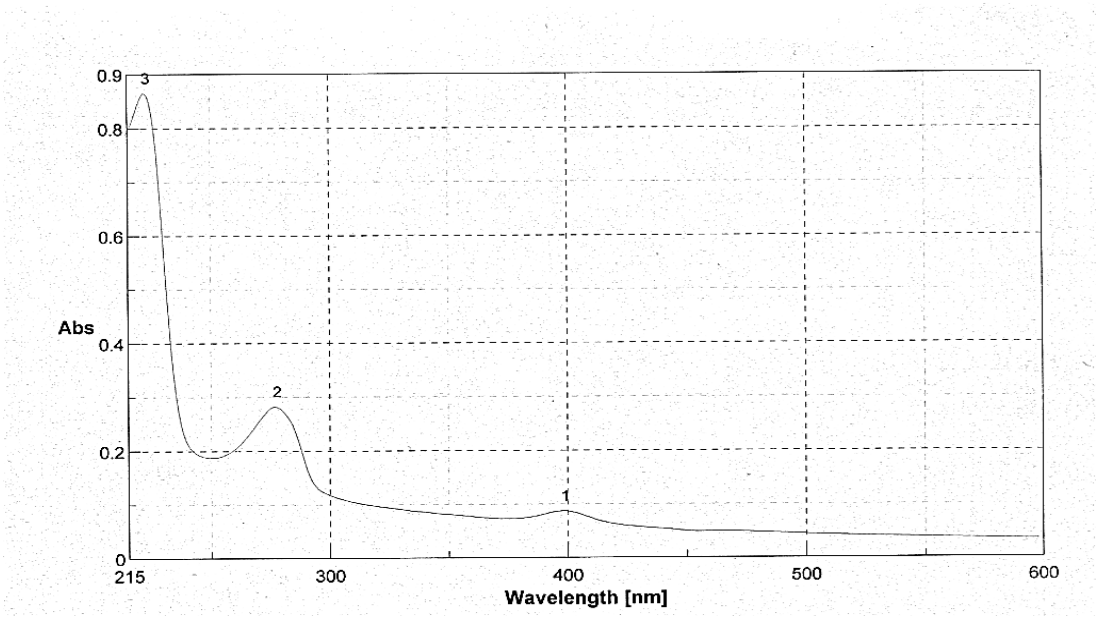

Figure 12. UV spectrum of lathyroxin A.

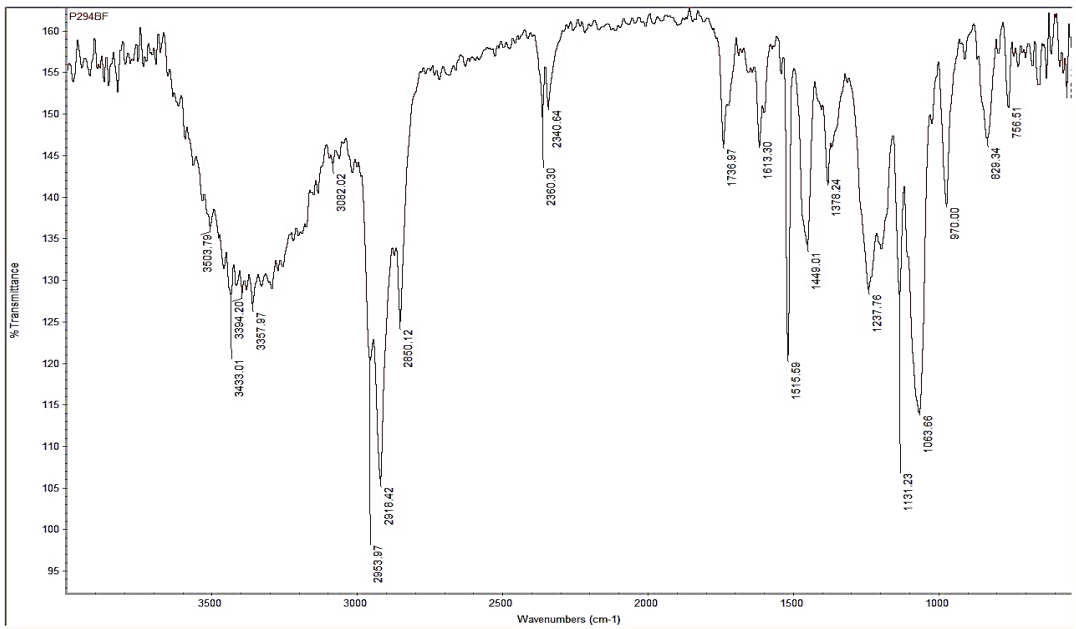

Figure 13. IR spectrum of lathyroxin A.

5.1.2 Structural identification of lathyroxin B.

Lathyroxin B (**2**) (Fig. 6) has a molecular formula of $C_9H_{12}O_3$ as deduced from its HRESIMS (Fig. 18) and consistent with 4 hydrogen deficiencies. It appeared to be related to lathyroxin A from which differs only by the side chain attached to C-1′, which is a 2,3-diolpropyl instead of 2-hydroxy-3,3-dimethoxypropyl. Indeed, the comparison of their ^{1}H and ^{13}C NMR data (Fig. 14 and 15 and, Table 1) showed that the shift and the multiplicity of the signal of C-1 were changed. These were the only substantial differences between the two compounds. Being a hydroxymethyl in **2** and a dimethoxymethine in **1**. The ^{1}H NMR spectrum of lathyroxin B (Fig. 14) showed two double doublets (*J*=11.2 and 4.4 Hz; 11.2, and 6.3 Hz, respectively) typical of a hydroxymethyl group at δ 3.50 and 3.43, (Badertscher *et al*., 2009) which in the HSQC spectrum (Fig. 16) also coupled with the carbon (C-1) at δ 65.1 (Breitmaier and Voelter, 1987). As expected, the ^{1}H NMR spectrum also showed broad singlets due to three hydroxy groups at δ 3.46, 1.31, and 0.91, respectively. Conversely, the signals present in the ^{1}H and ^{13}C NMR spectra of lathyroxin A (**1**) for the dioxolanemethine and the two methoxy groups were absent in the spectra of lathyroxin B (**2**). The couplings observed in the HSQC and HMBC spectra of this latter (Fig. 16 and 17 and, Table 1) supported the assignment of chemical shifts of all the protons and the corresponding carbons of **2** as reported in Table 1 and to formulate lathyroxin B as 3-(4-hydroxyphenyl)-propane-1,2- diol. The structure assigned to **2** was also supported by the data of its HRESIMS spectrum (Fig. 18), which showed the sodiated dimer $[2M+Na]^+$ and the sodium cluster $[M+Na]^+$ at *m/z* 359 and 191.0663, respectively. Furthermore, the significant corresponding tropylium ion $[HO\text{-}Ph\text{-}CH_2]^+$ was recorded at *m/z* 107, probably generated from the pseudomolecular ion by loss of the 1,2-diolpropyl residue.

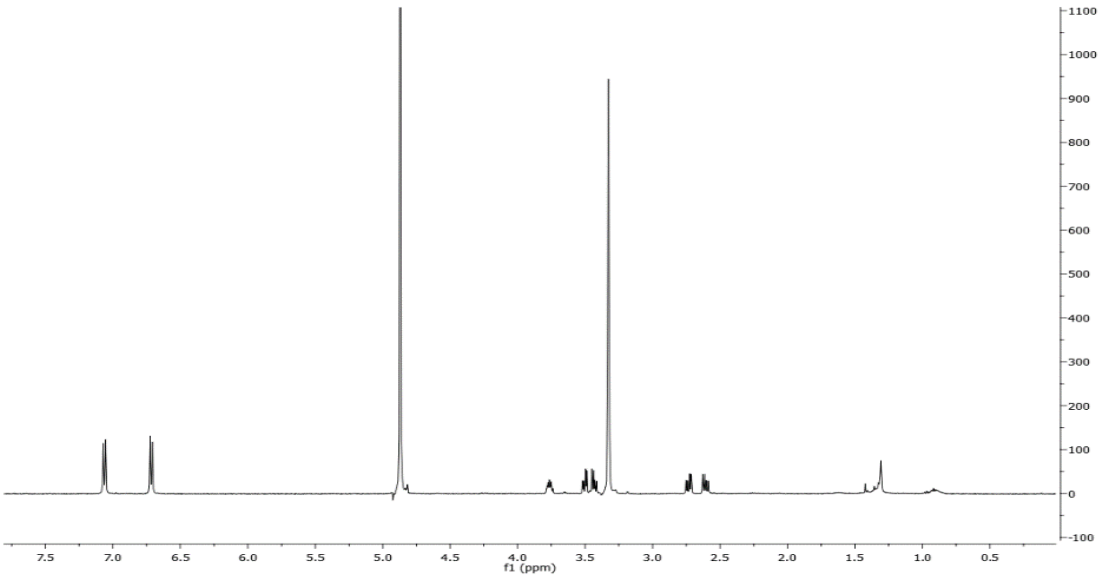

Figure 14. ^{1}H NMR spectrum of lathyroxin B (MeOD, 500 MHz).

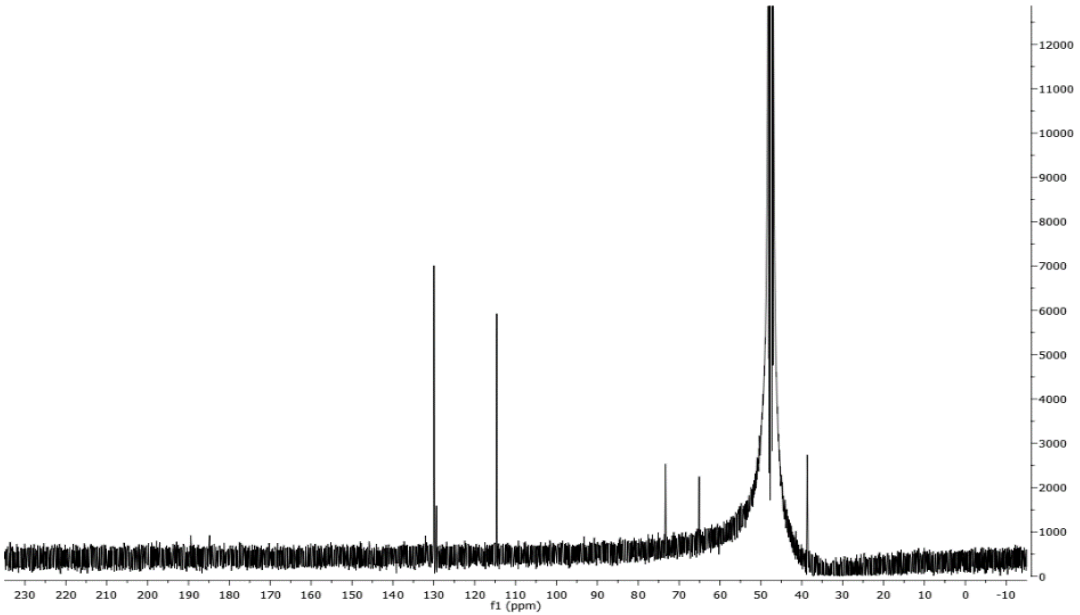

Figure 15. ^{13}C NMR spectrum of lathyroxin B (MeOD, 500 MHz).

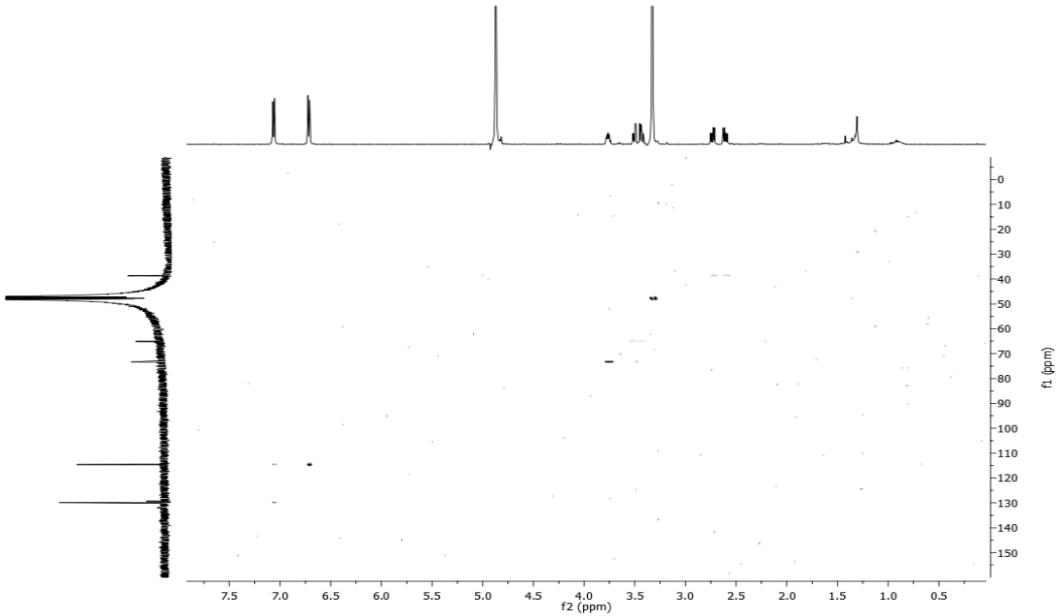

Figure 16. HSQC spectrum of lathyroxin B (MeOD, 500 MHz).

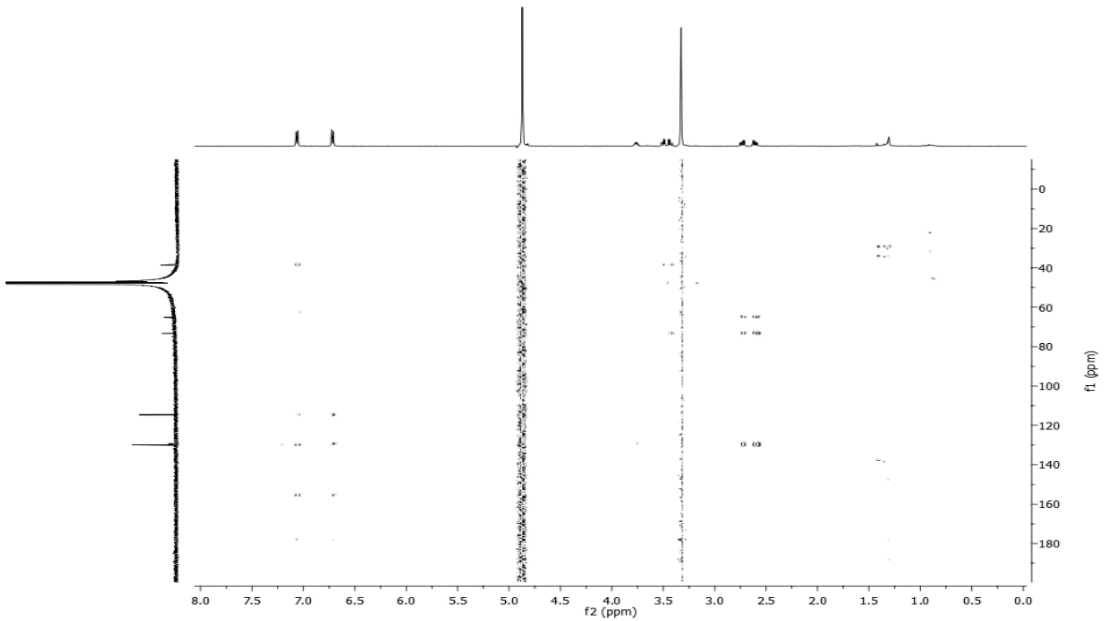

Figure 17. HMBC spectrum of lathyroxin B (MeOD, 500 MHz).

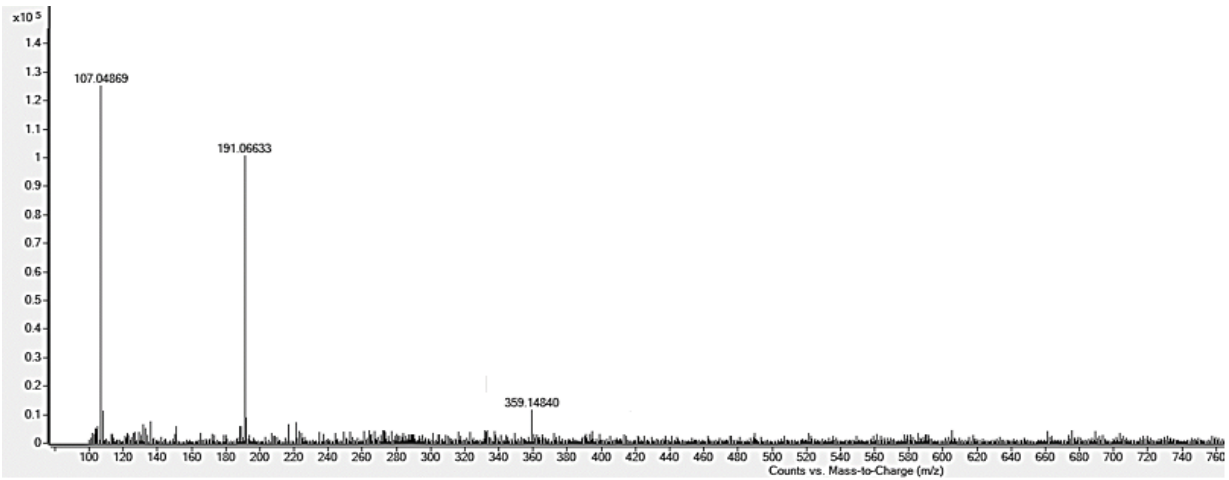

Figure 18. HRESIMS spectrum of lathyroxin B

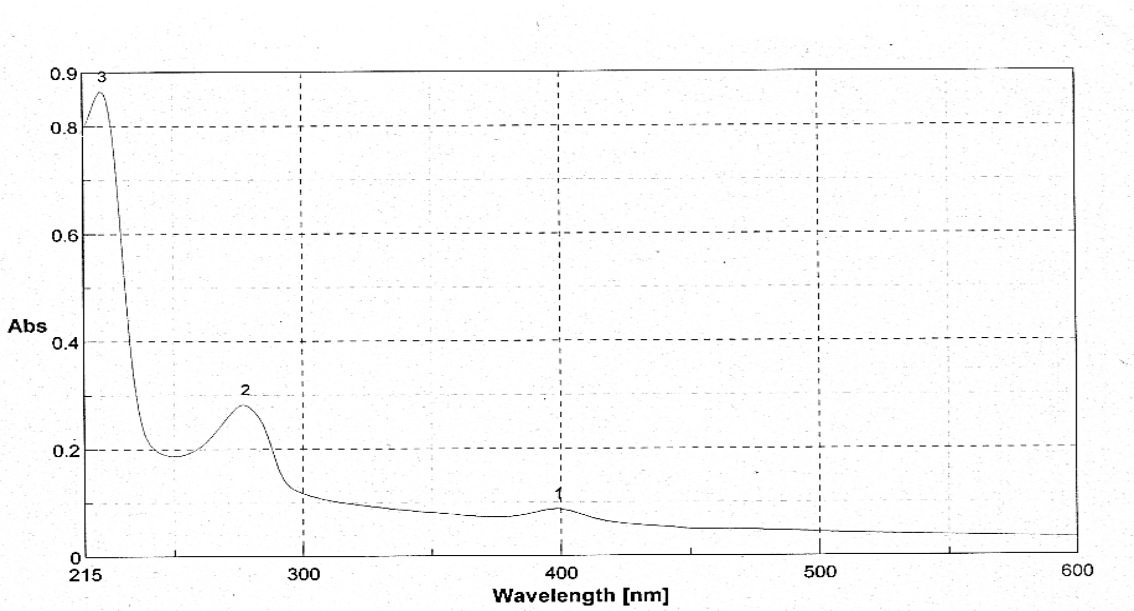

Figure 19. UV spectrum of lathyroxin B.

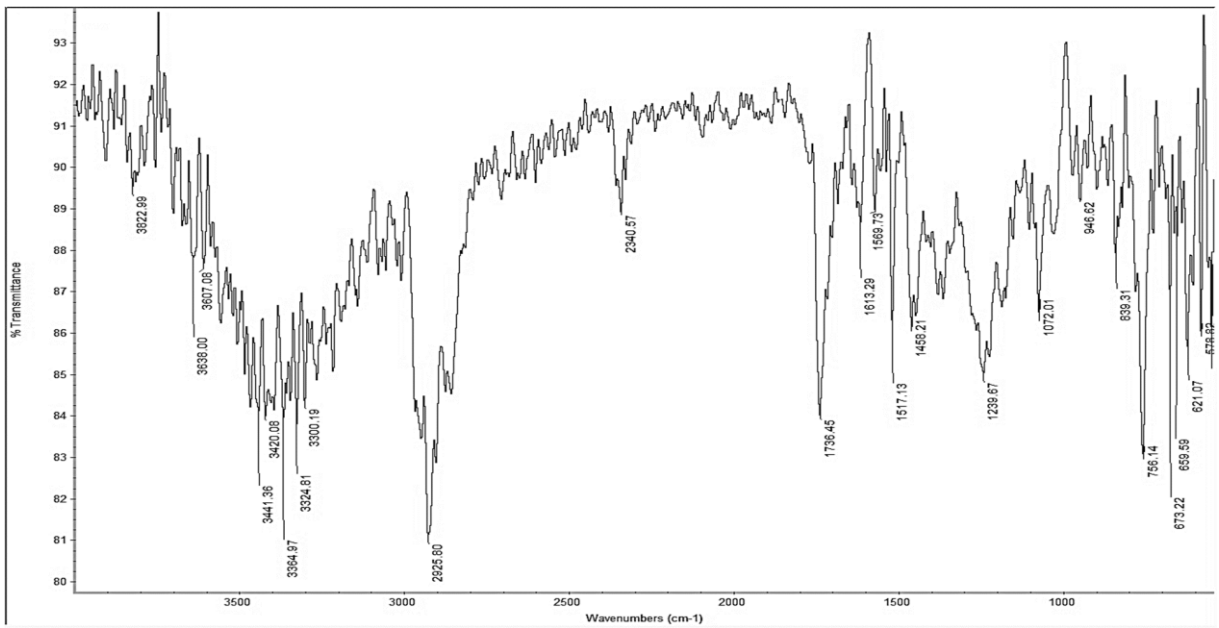

Figure 20. IR spectrum of lathyroxin B.

Table 1. ^{1}H and ^{13}C NMR Data of lathyroxins A and B (**1** and **2**)

	Lathyroxin A (1)			**Lathyroxin B (2)**		
Position	δC[c]	δH (*J* in Hz)	HMBC	δC[c]	δH (*J* in Hz)	HMBC
1	106.0 d	4.17 (1H) d (5.7)	H_2-3, H-2, OMe	65.1 t	3.50 (1H) dd (11.2, 4.4) 3.43 (1H) dd (11.2, 6.3)	H_2-3, H-2
2	72.1 d	3.83 (1H) m	H_2-3, OMe	73.3 d	3.76 (1H) m	H-2',6', H_2-1, H_2-3
3	37.2 t	2.92 (1H) dd (14.1, 3.7) 2.67 (1H) dd (14.1, 8.5)	H-2',6', H-1	38.7 t	2.73 (1H) dd (13.8, 5.9) 2.61 (1H) dd (13.8, 7.4)	H-2',6', H-2,
1'	130.2 s		H-3',5', H-2',6', H_2-3, H-2	129.4 s		H-3',5', H-2, H_2-3
2', 6'	130.6 d	7.15 (2H) d (8.3)	H-3',5', H_2-3, H-2	129.9 d	7.06 (2H) d (8.4)	H_2-3
3', 5'	115.2 d	6.79 (2H) d (8.3)	H-2',6'	114.6 d	6.72 (2H) d (8.4)	H-2',6'
4'	154.1 s		H-2',6', H-3',5',	155.4 s		H-2',6', H-3',5'
MeO	54.8 q	3.48 (3H) s				
MeO	54.8 q	3.46 (3H) s				
OH					0.91 (1H) br s	
OH		2.10 (1H) br s			1.31 (1H) br s	
OH		4.78 (1H) br s			3.46 (1H) br s	

[a]The chemical shifts are in δ values (ppm) from TMS. [b]2D ^{1}H, ^{1}H (COSY) ^{13}C, ^{1}H (HSQC) NMR experiments delineated the correlations of all the protons and the corresponding carbons. [c]Multiplicities were assigned by DEPT spectrum.

5.1.3 Absolute configuration of lathyroxins A and B.

The absolute configuration at C-2 of the side chain of both lathyroxins A and B (**1** and **2**) was assigned by recording their electronic circular dichroism (ECD) spectra (Fig. 21), which were compared to that of the structurally related crypticin B (**6**, Fig. 6), having the same chromophore. This latter was recently isolated from the culture filtrates of *Diaporthella cryptica*, the causal agent of halzenut trunk and branch dieback in Sardinia, Italy, and its C-2 (*S*) configuration was assigned by experimental and computed ECD spectra (Cimmino *et al*., 2018). The comparison of its spectrum (**6**) with those of lathyroxins A and B (**1** and **2**) supported the assignment of an *R* absolute configuration for C-2 of their side chains.

3-(4-hydroxyphenyl)-propane-1,2-diol was previously reported as a fungal (Ayres, 1981) (Forseth *et al*., 2013) and a plant (Yang *et al*., 2014) metabolite, but the absolute stereochemistry and biological activities were not reported. The racemic 3-(4-hydroxyphenyl)propan-1,2-diol has also been synthesized starting from 4-chlorophenol and 2-propenol (Escudero-Adán *et al*., 2014). The enantiomer of lathyroxin B (**2**) was prepared from acid hydrolysis of the (*S*)-3-[4-(benzyloxy)phenyl]propane-1,2- diol (Manet *et al*., 2005). This diol was, in turn, obtained from the reduction of the optically pure (*S*)-3-*p*-benzyloxyphenyllactic acid, synthesized starting from *O*-benzyl-L-tyrosine (Zeng *et al*., 2007). Thus, this is the first report of lathyroxin B (**2**) as a natural product.

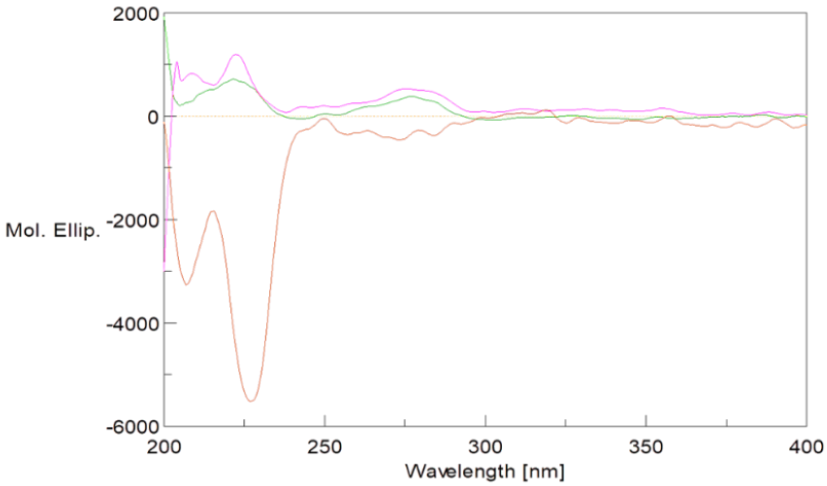

Figure 21. ECD spectra of lathyroxin A (pink line), lathyroxin B (green line), and cripticin B (brown line)

5.1.4 Biological activities of secondary metabolites from *Ascochyta lentis* var. *lathyri* culture filtrates

5.1.4.1 Leaf puncture assay

Assayed by puncture on different leaves (*Lupinus albus* L., *Lens culinaris* Medik., *Phaseolus vulgaris*, *Sonchus oleraceus*, *Convolvulus arvensis* L., *Lycopersicon esculentum* (L.) Karsten ex Farw., and *Mercurialis annua* L.) at 2 µg/µL, Lathyroxin B (**2**) caused clear necrosis on all the tested plants. The clearest effects were visible on *Sonchus oleraceus* L., *Lycopersicon esculentum* (L.) Karsten ex Farw., *Phaseolus vulgaris* L., and *Lens culinaris* Medik. Lathyroxin A (**1**) was active only on *Lupinis albus* L. and *Sonchus oleraceus*, whereas *p*-hydroxybenzaldehyde (**3**) was active only on *L. albus* and *L. culinaris*. *p*-methoxyphenol and tyrosol (**4** and **5**) were inactive at the tested concentration.

5.1.4.2 Assay on seed germination of parasitic weed *Phelipanche ramosa*

On seeds of the parasitic weed *Phelipanche ramosa*, lathyroxin B (**2**) reduced germination by 63% (Table 2). Lathyroxin A (**1**) caused approximatively 36% inhibition. Both compounds clearly shortened the germination tubes of the seeds.

5.1.4.3 Assay on *Lepidium sativum* rootlet elongation

On *Lepidium sativum*, lathyroxin B (**2**) reduced the rootlet length of the germinated seeds by over 50% (Table 2). Lathyroxin A and tyrosol (**1** and **5**) showed a modest but still significant reduction of rootlet elongation by around 15% (Table 2), whereas the other three compounds (**2**, **3** and **4**) were inactive.

Table 2. Biological activities of secondary metabolites from *Ascochyta lentis* var. *lathyri* on *P. ramosa* and *L. sativus*

Compound	***Phelipanche ramosa****		***Lepidium sativus****	
	10^{-3} M	10^{-4} M	10^{-3} M	10^{-4} M
Lathyroxin A (**1**)	36	13	11	4
Lathyroxin B (**2**)	63	11	48	5
p-Hydroxybenzaldeyde (**3**)	nt	nt	4	nt
p-Methoxyphenol (**4**)	nt	nt	3	nt
Tyrosol (**5**)	nt	nt	15	nt
*Inhibition of seed germination (% of control)				
**Reduction of rootlet growth (% of control)				
nt – not tested				

5.2 Structural identification of secondary metabolites from *Ascochyta lentis* culture filtrates and mycelium [2]

The fungal liquid cultures were separated by filtration into the two components: the cultures filtrates and the mycelium. Both were subjected to extraction by organic solvents (Scheme 2 and 3). The bio-guided purification of the organic extracts, as detailed in Experimental section, allowed to obtain eight main metabolites (Fig. 22). Four metabolites were isolated from the culture filtrates: lentiquinones A-C (**7**-**9**) and lentisone (**10**). Four metabolites were isolated from the mycelium: pachybasin (**11**), ω-hydroxypachybasin (**12**), 1,7-dihydroxy-3-methylanthracene-9,10-dione (**13**), and phomarin (**14**) (Fig. 22).

From preliminary ^{1}H NMR investigations, all metabolites appeared to be structurally related, being anthraquinone derivatives and appearing as yellow-colored compounds. Three compounds isolated from the culture filtrates proved to be new and were named lentiquinones A, B, and C (**7**-**9**, Fig. 22). The other five metabolites proved to be well-known fungal and/or plant metabolites, namely lentisone (**10**), pachybasin (**11**), ω-hydroxypachybasin (**12**), 1,7-dihydroxy-3-methylanthracene-9,10-dione (**13**), and phomarin (**14**).

Pachybasin (**11**) proved to be the metabolite produced in larger amount by the fungus into the mycelium (7 mg/g of dried mycelium), whereas lentiquinone B (**8**) was the main metabolite in the culture filtrates (0.6 mg/L). The known metabolites were identified by comparing their data with those reported in the literature. For lentisone (**10**) (Andolfi *et al*., 2013); for all the other metabolites (**10**-**14**): (Sun *et al*., 2013). Specifically, for pachybasin (**11**) (Bick and Rhee, 1966; De Stefano and Nicoletti, 1999; Borges and Pupo, 2006; Xia *et al.*, 2007); for ω-hydroxypachybasin (**12**) (Imre, Sar and Thomson, 1976; Kuo *et al.*, 1995; Khamthong *et al.*, 2012); for 1,7-dihydroxy-3-methylanthracene-9,10-dione (**13**) (Borges and Pupo, 2006); for phomarin (**14**) (Bick and Rhee, 1966; Borges and Pupo, 2006).

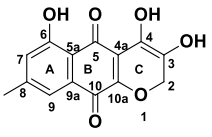

7, lentiquinone A

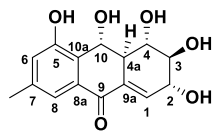

8, lentiquinone B

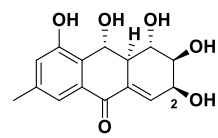

9, lentiquinone C

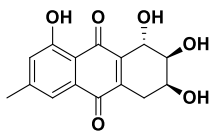

10, lentisone

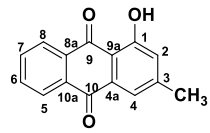

11, pachybasin

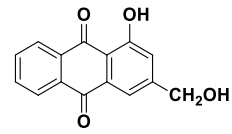

12, ω-hydroxypachybasin

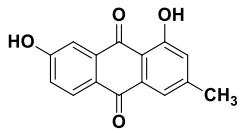

13, 1,7-dihydroxy-3-methylanthracene-9,10-dione

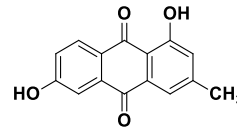

14, phomarin

Figure 22. *Ascochyta lentis* secondary metabolites.

5.2.1 Structural identification of lentiquinone A.

Lentiquinone A (**7**) has the molecular formula $C_{14}H_{10}O_6$ as deduced by its HRESIMS (Fig. 28) consistent with 10 hydrogen deficiencies. Its ^{1}H and ^{13}C spectra (Fig. 23 and 24) showed spin systems in accord with those of a substituted anthraquinone. The data were also consistent with the bands of hydroxy, α,β-conjugated carbonyl, and aromatic groups as observed in the IR spectrum at ν_{max} 3362, 1660, 1640 cm^{-1} (Fig. 30) (Nakanishi, 1977) as well as with the absorption maxima observed in the UV spectrum at 419, 278, 250 and, 220 nm (Fig. 29) (Badertscher *et al*., 2009). The ^{1}H and COSY data (Fig. 23 and 25) showed the typical spin system of a 1,2,3,5-tetrasubstituted benzene ring (A ring) with two singlets of the meta-located protons at δ 7.37 (H-9) and 6.98 (H-7), being shielded by the *ortho*-located to the phenolic group (Berger and Braun, 2004). The phenolic group, being linked by a hydrogen bond to the carbonyl (O=C-5) of the adjacent quinone ring (B ring), appeared, as expected, as a sharp singlet at δ 11.99 (Affolter *et al*., 2000). Furthermore, the same spectra showed the presence of two singlets and a broad signal typical of an oxymethylene (H_2C-2), a benzylic methyl (Me-8) and another hydroxy group (HO-3) at the typical chemical shift values of 4.01, 2.37, and 2.80, respectively (Badertscher *et al*., 2009) suggesting also the presence of a 1,2,3,4-tetrasubstituted dihydro-2*H*-pyran ring (C ring) fused to the B ring. The couplings observed in the HSQC spectrum (Fig. 26) permitted the assignment of the signals observed in the ^{13}C NMR spectrum (Fig. 24) at δ 123.6, 120.3, 67.2, and 22.4, to the protonated carbons C-7, C-9, C-2, and Me-8, respectively (Berger and Braun, 2004; Breitmaier and Voelter, 1987). The same spectrum showed 10 sp^2 carbons, two of which were the quinone carbonyls assigned by the long-range coupling observed in the HMBC spectrum (Fig. 27 and Table 3) for C-10 at δ 183.9 with H-9 and consequently C-5 was at δ 182.5 (Berger and Braun, 2004). The remaining eight sp^2 carbons belong to both the

tetrasubstituted aromatic, quinone, and pyran rings (A, B, and C rings) four of which (5a and 9a, and 4a and 10a) were the bridgehead carbons of the junction between the A and B, and B and C rings. Six of them were assigned based on the other couplings observed in the HMBC spectrum (Fig. 27). In fact, the couplings between C-3 and H_2C-2 and HO-3, C-5a and HO-6, H-7 and Me-8, C-4 with HO-3, C-6 and HO-6, and H-7, C-8 with H-9 and H-7, C-9 with H-7 and Me-8, C-9a with Me-8, allowed the assignment of the signals at δ 141.5, 131.8, 161.3, 161.5, 123.8, 120.3, and 147.8 to C-3, C-5a, C-6, C-4, C-8, C-9, and C-9a, respectively, and of the remaining two sp^2 carbons at δ 142.5 and 142.4 to C-10a and C-4a (which could be interchangeable). Thus, the signals were assigned to all the protons and the corresponding carbons as reported in Table 3, and lentiquinone A (**7**) was formulated as 3,4,6-trihydroxy-8-methyl-2*H*-benzo[γ]chromene-5,10-dione. The structure assigned was confirmed by all the other couplings observed in the HMBC data (Table 3) and the data from the HRESIMS spectrum (Fig. 28). The latter showed the sodiated dimer $[2M+Na]^+$, the sodium adduct ion $[M+Na]^+$, and the protonated ion $[M+H]^+$ at *m/z* 571, 297, and 275.0559 respectively.

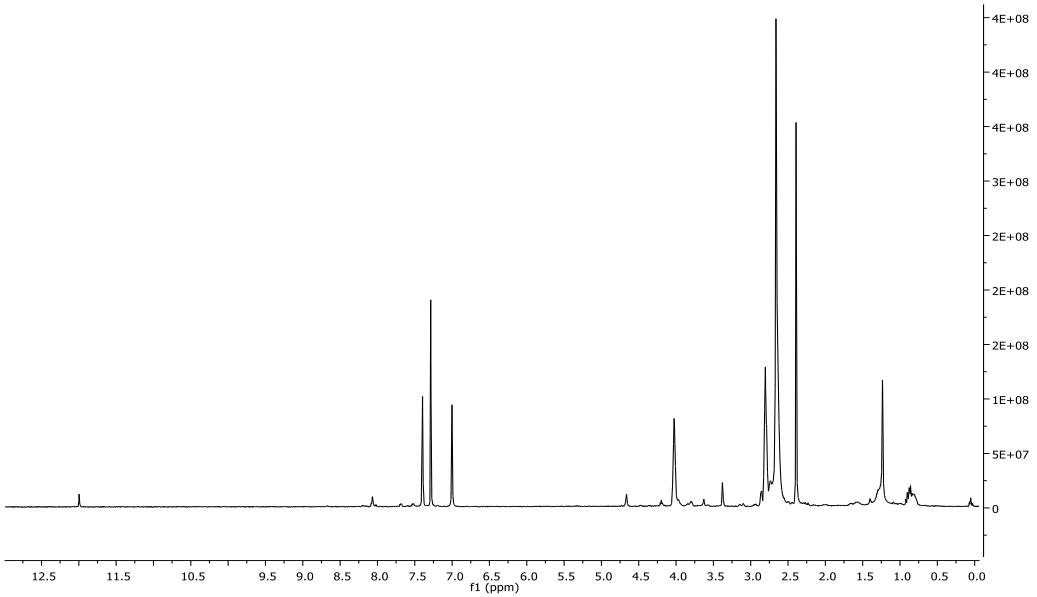

Figure 23. ^{1}H NMR spectrum of lentiquinone A ($CDCl_3$, 400 MHz).

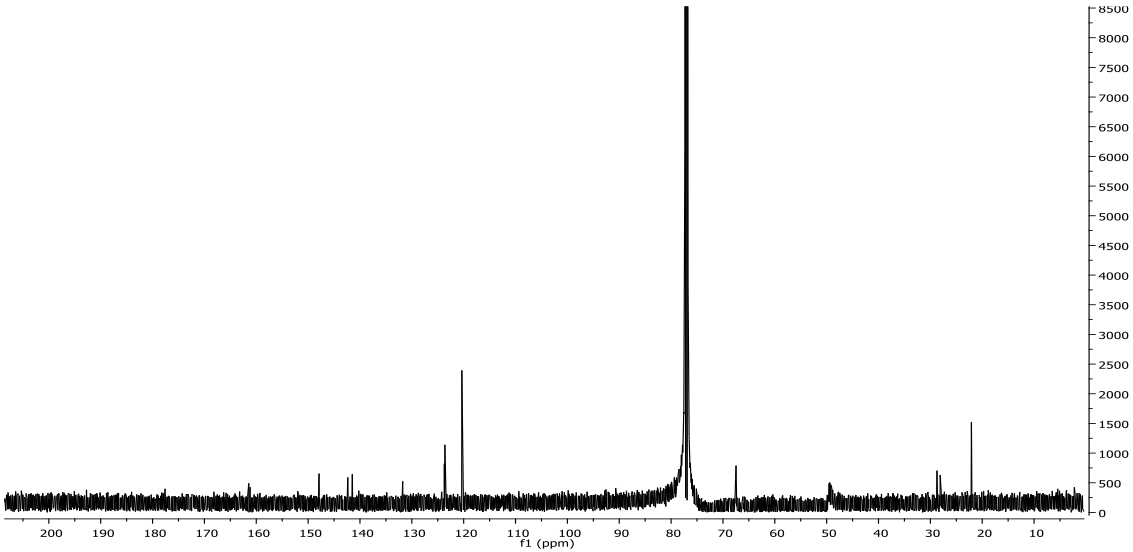

Figure 24. ^{13}C NMR spectrum of lentiquinone A ($CDCl_3$, 400 MHz).

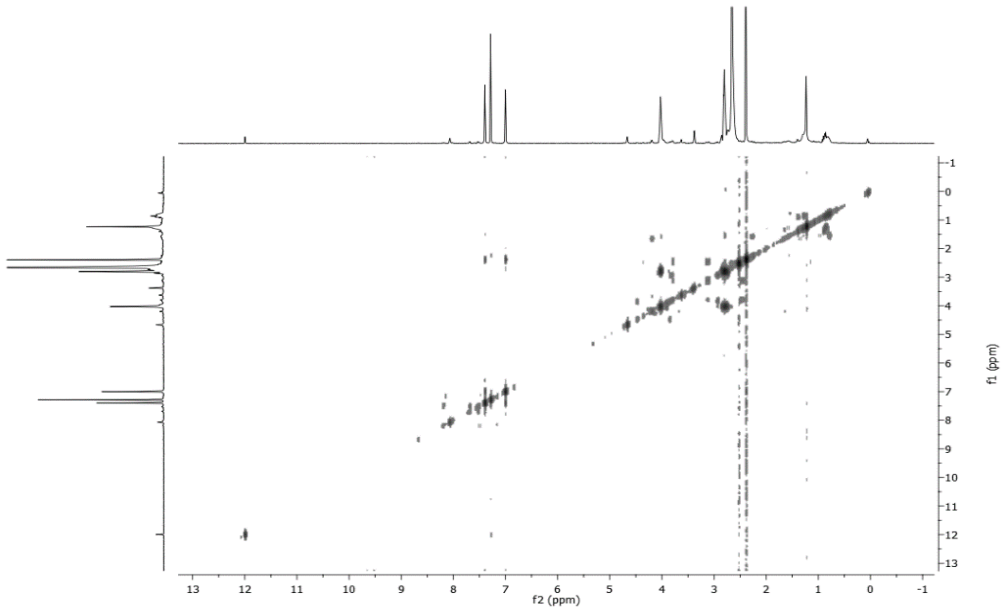

Figure 25. COSY spectrum of lentiquinone A ($CDCl_3$, 400 MHz).

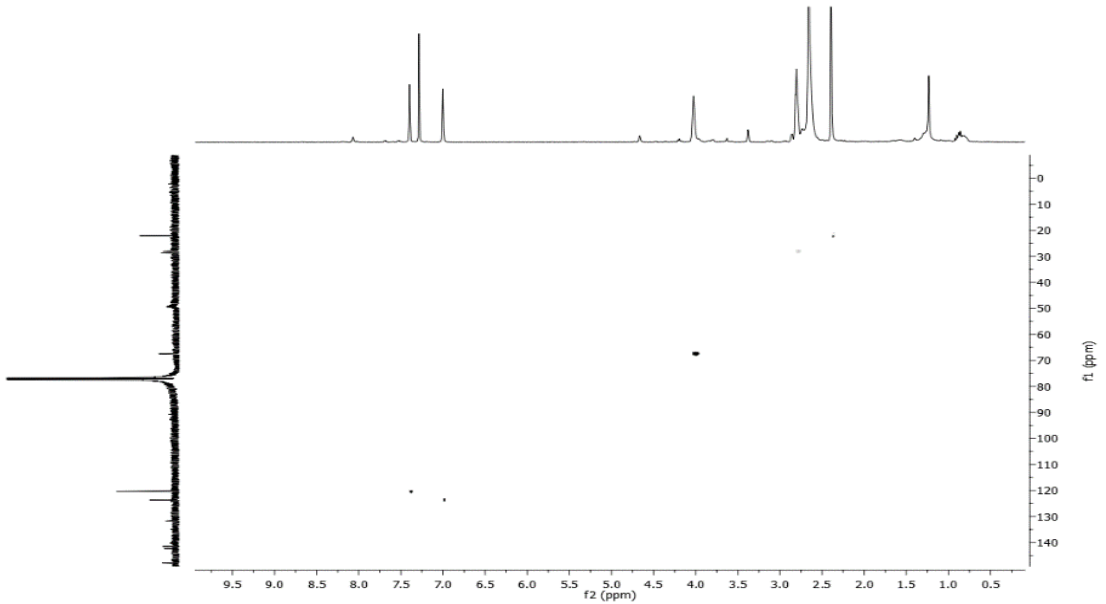

Figure 26. HSQC spectrum of lentiquinone A ($CDCl_3$, 400 MHz).

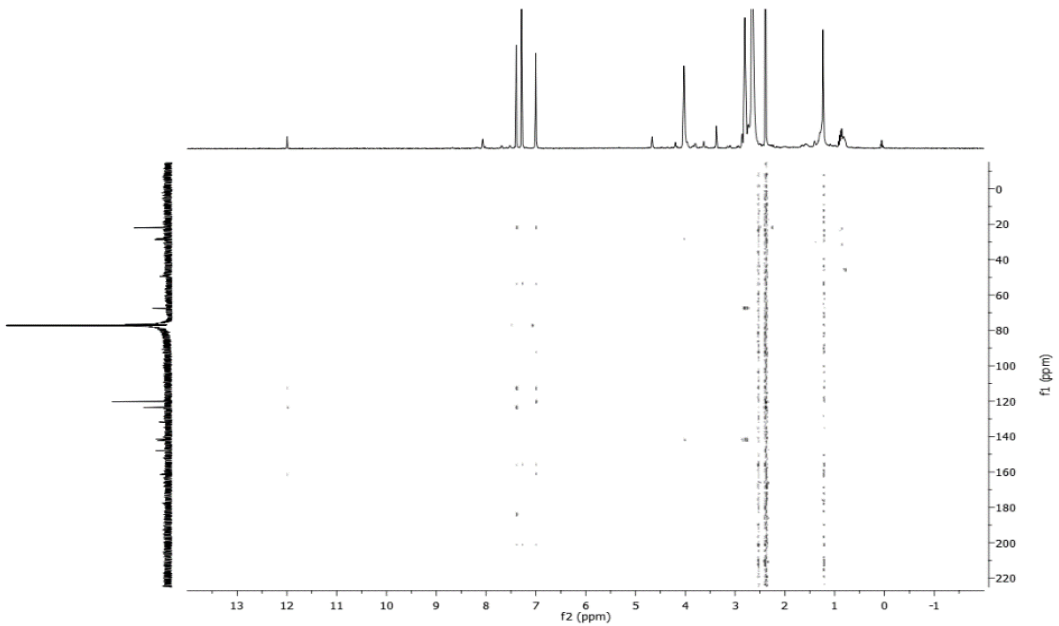

Figure 27. HMBC spectrum of lentiquinone A ($CDCl_3$, 400 MHz).

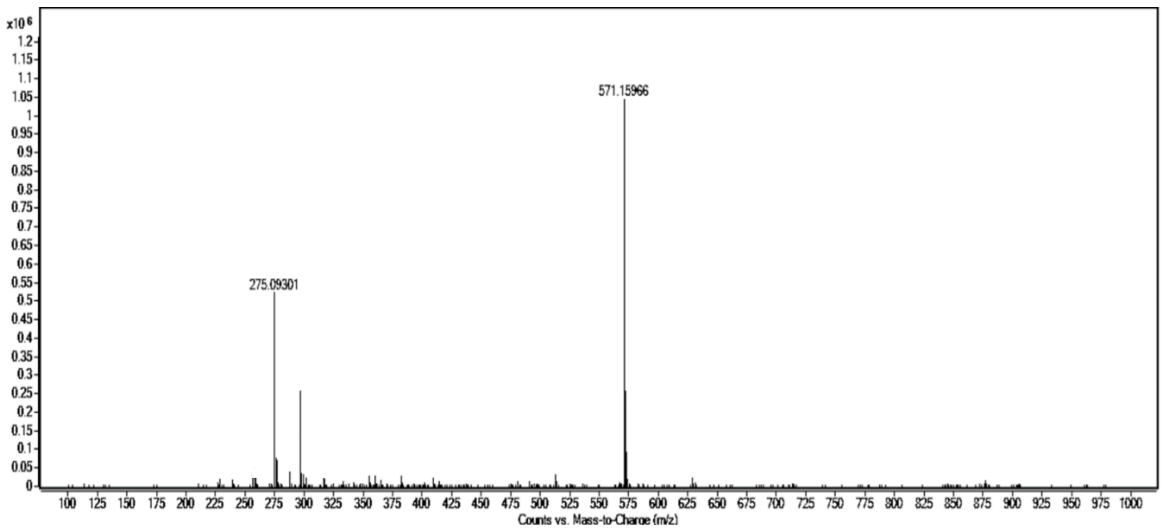

Figure 28. HRESIMS spectrum of lentiquinone A.

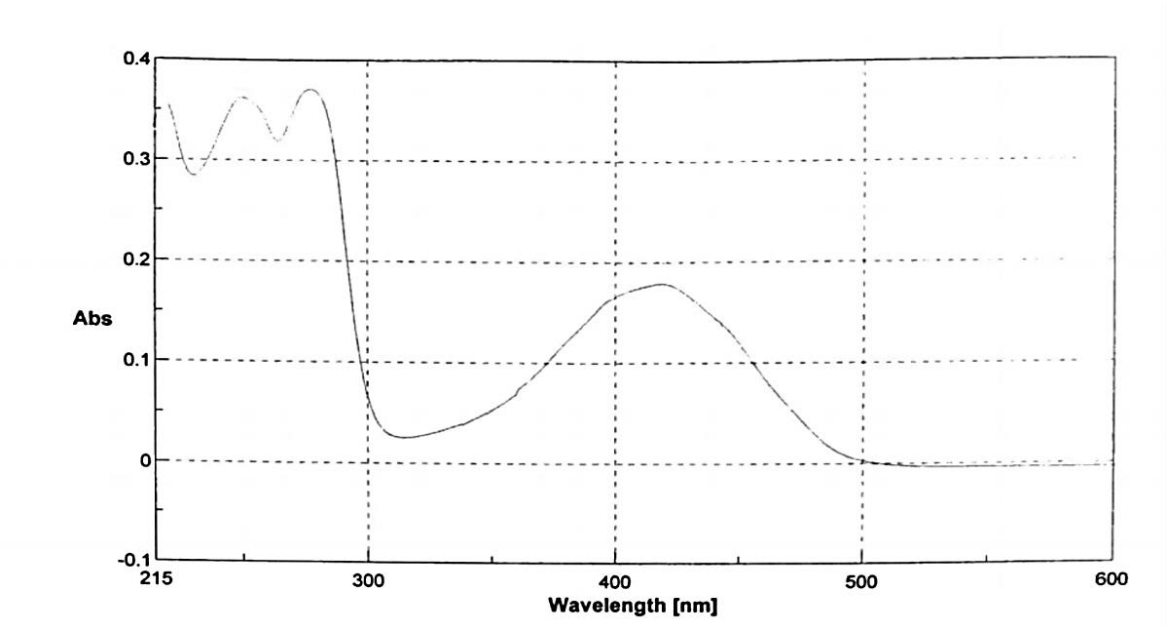

Figure 29. UV spectrum of lentiquinone A.

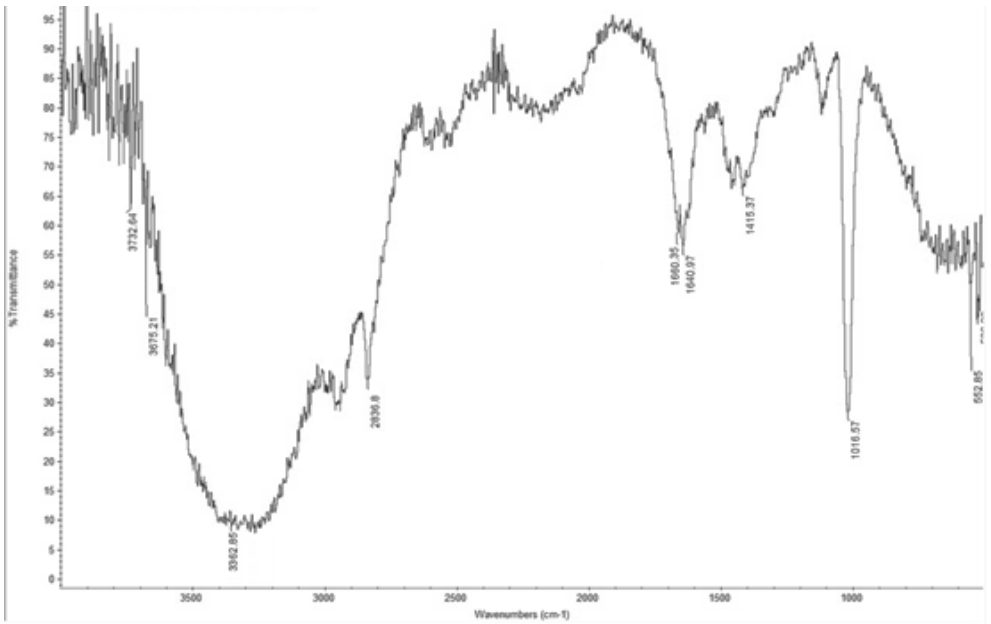

Figure 30. IR spectrum of lentiquinone A.

5.2.2 Structural identification of lentiquinone B.

Lentiquinone B (**8**) has a molecular formula of $C_{15}H_{16}O_6$ as deduced by its HRESIMS (Fig. 36) consistent with eight indices of hydrogen deficiencies. Lentiquinones A and B (**7** and **8**) differ for one carbon and six hydrogens due to the different functionalization of the B and C rings, while the A ring is the same. This was confirmed by comparing the ^{1}H and ^{13}C NMR data (Table 3), which highlighted the nature of a hemiquinone and a trihydroxycyclohexene for the B and C rings, respectively. Indeed, the ^{13}C NMR spectrum (Fig. 32) of lentiquinone B shows a single α,β-unsaturated carbonyl (C-9) at δ 185.7 and lacks any oxygenated methylene carbon for a pyran ring. The ^{1}H NMR spectrum (Fig. 31) lacks the signal of a hydrogen-bounded phenolic group, while an olefinic proton was present, and the complexity of the region, corresponding to the protons attached to the oxygenated carbons, was significantly increased. In particular, the ^{13}C and ^{1}H NMR spectra (Fig. 31 and 32) showed a secondary hydroxylated carbon at δ 73.4 (d, C-10)/5.27 (d, J = 10.1 Hz). H-10 showed a COSY correlation with H-4a of the adjacent tertiary carbon (Fig. 33), which appeared at δ 2.94 as a complex signal due to its coupling also with H-4 (C ring) and its allylic and homoallylic coupling with H-1 and H-2, respectively (Badertscher, Bühlmann and Pretsch, 2009; Sternhell, 1969). Thus, C-4a at δ 48.0 constituted one of bridgehead carbons between the B and C rings. H-4 resonates as a doublet of doublets (J=10.1 and 8.4 Hz) at δ 3.96, being also coupled with H-3, the proton of the secondary hydroxylated carbon (C-3) of the same C ring, which appeared as a doublet of doublets (J=10.1 and 8.2 Hz) at δ 3.53. In turn, H-3 was coupled with H-2 of the adjacent hydroxylated carbon (C-2), which resonated as a doublet of doublets of doublets (J=8.2, 4.2, and 2.6 Hz), at δ 4.24. H-2 also coupled with the adjacent olefinic protons (H-1) resonating as a triplet (J=2.6 Hz) at δ 6.84, being also allylically coupled with H-4a. The ^{13}C NMR spectrum (Fig. 32), besides the cited carbonyl group, showed the olefinic

protonated carbon, the signals of the other three protonated secondary carbons, the benzylic methyl, and those of the four aromatic and the olefinic sp^2 carbons, which were attributed by the couplings observed in the HSQC and HMBC spectra (Fig. 34 and 35). Thus, the chemical shifts were assigned to all the protons and the corresponding carbons of lentiquinone B (**8**) as reported in Table 3, and it was formulated as 2,3,4,5,10-pentahydroxy-7-methyl-3,4,4a,10-tetrahydroanthracen-9(2*H*)-one. The structure assigned was confirmed by the other couplings observed in the HMBC data (Fig. 35 and Table 3) and the data from the HRESIMS spectrum (Fig. 36). The latter showed the sodiated dimer $[2M+Na]^+$ and the protonated molecular ion $[M+H]^+$ at *m/z* 607 and 293.1013, respectively.

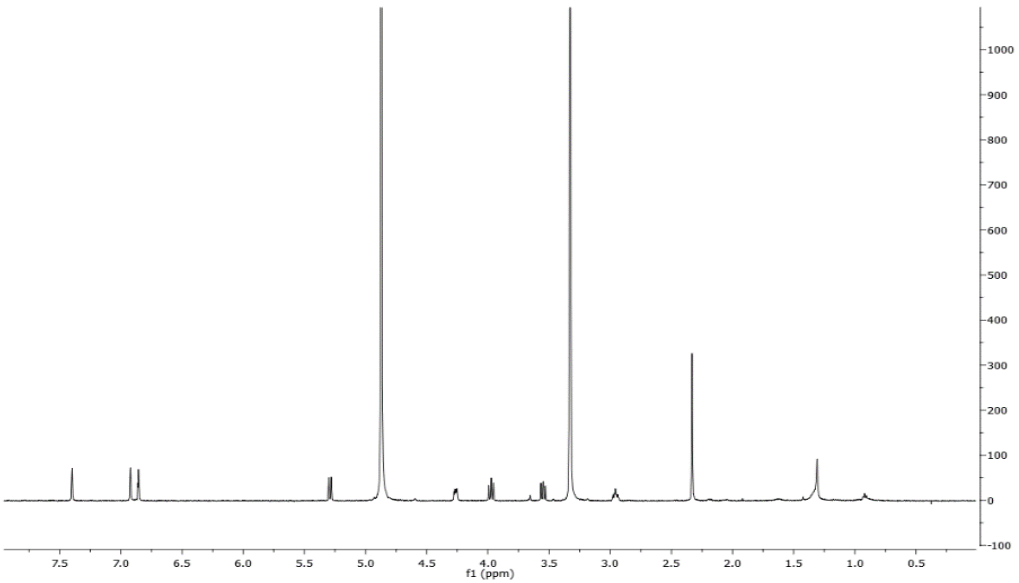

Figure 31. ^{1}H NMR spectrum of lentiquinone B (MeOD, 400 MHz).

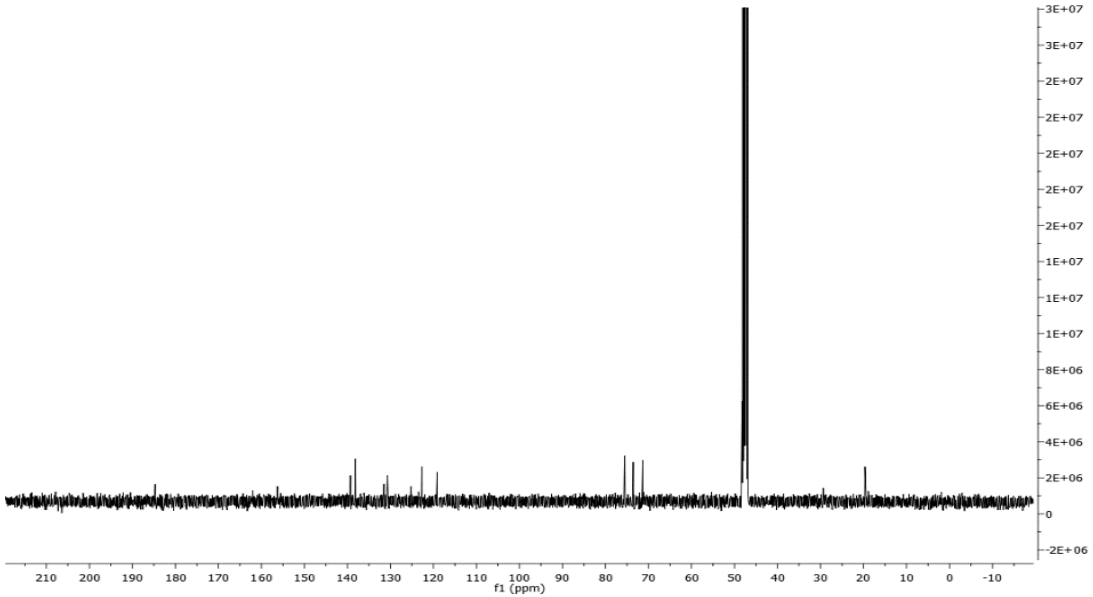

Figure 32. ^{13}C NMR spectrum of lentiquinone B (MeOD, 400 MHz).

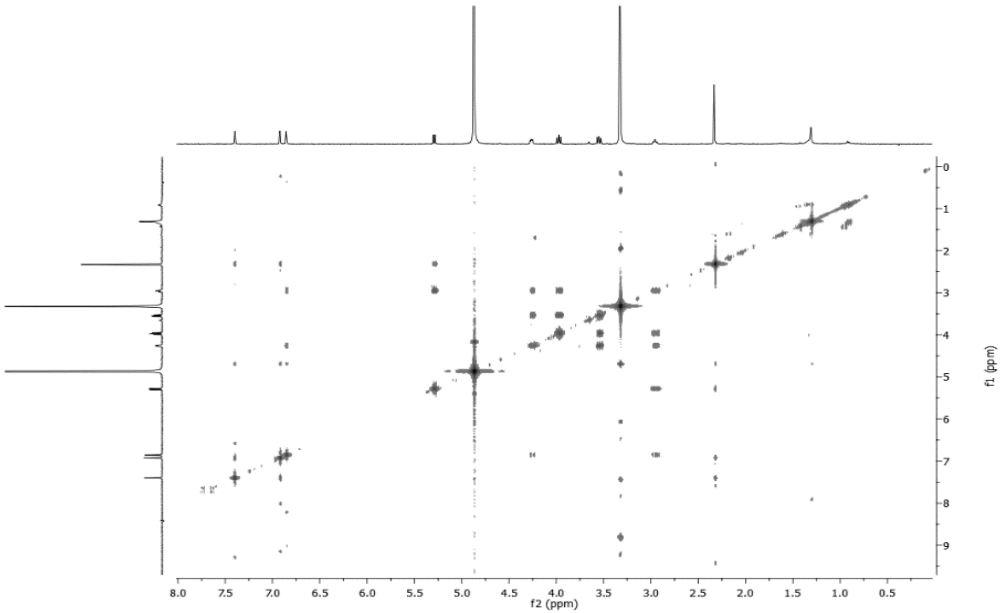

Figure 33. COSY spectrum of lentiquinone B (MeOD, 400 MHz).

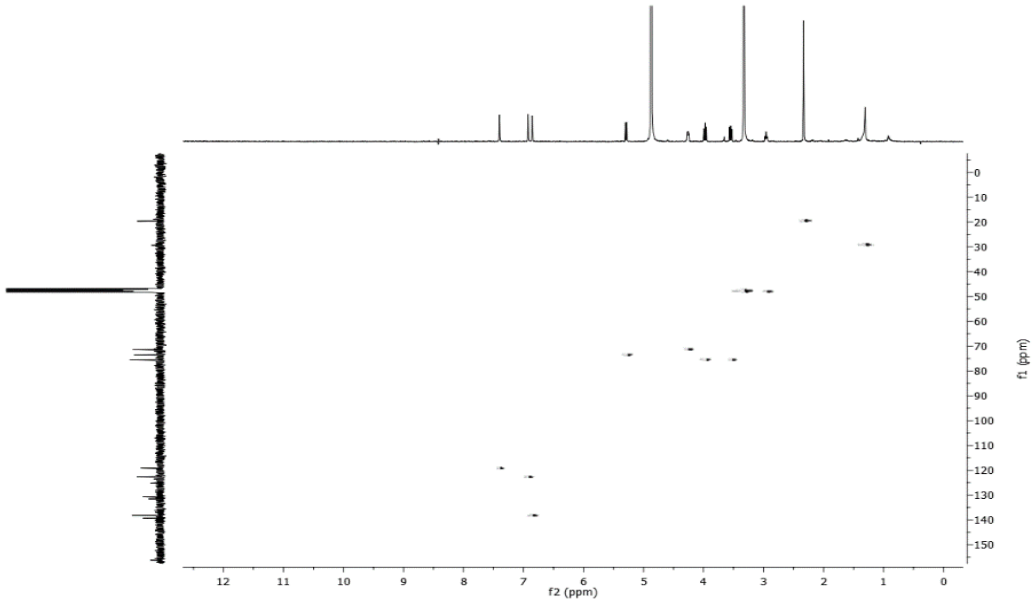

Figure 34. HSQC spectrum of lentiquinone B (MeOD, 400 MHz).

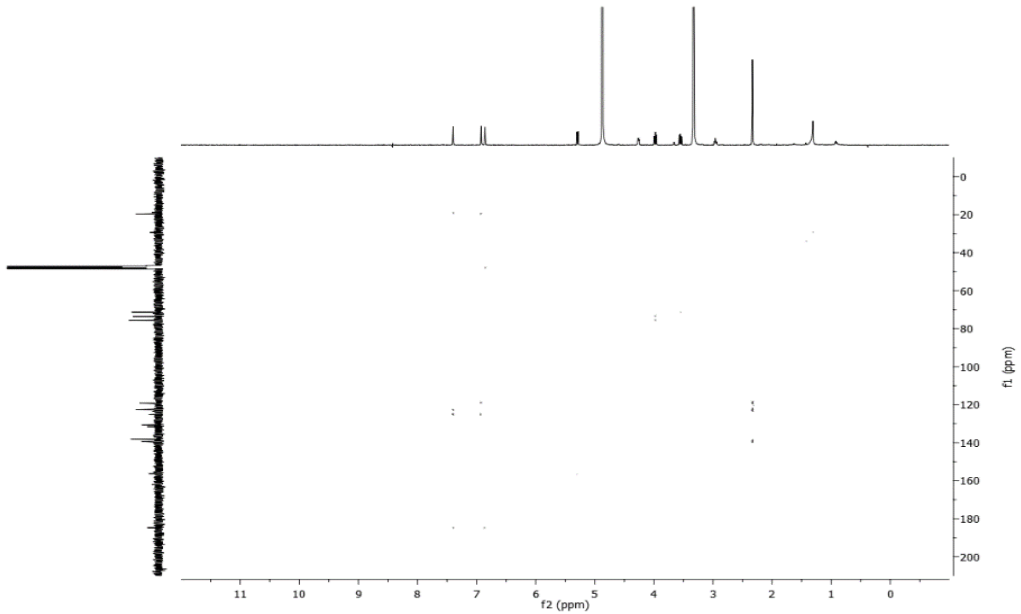

Figure 35. HMBC spectrum of lentiquinone B (MeOD, 400 MHz).

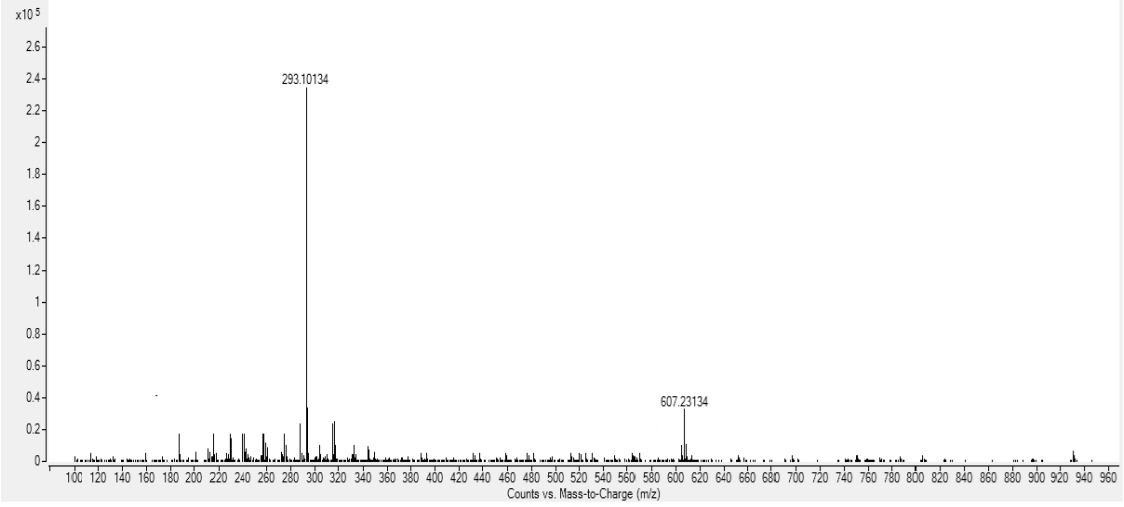

Figure 36. HRESIMS spectrum of lentiquinone B.

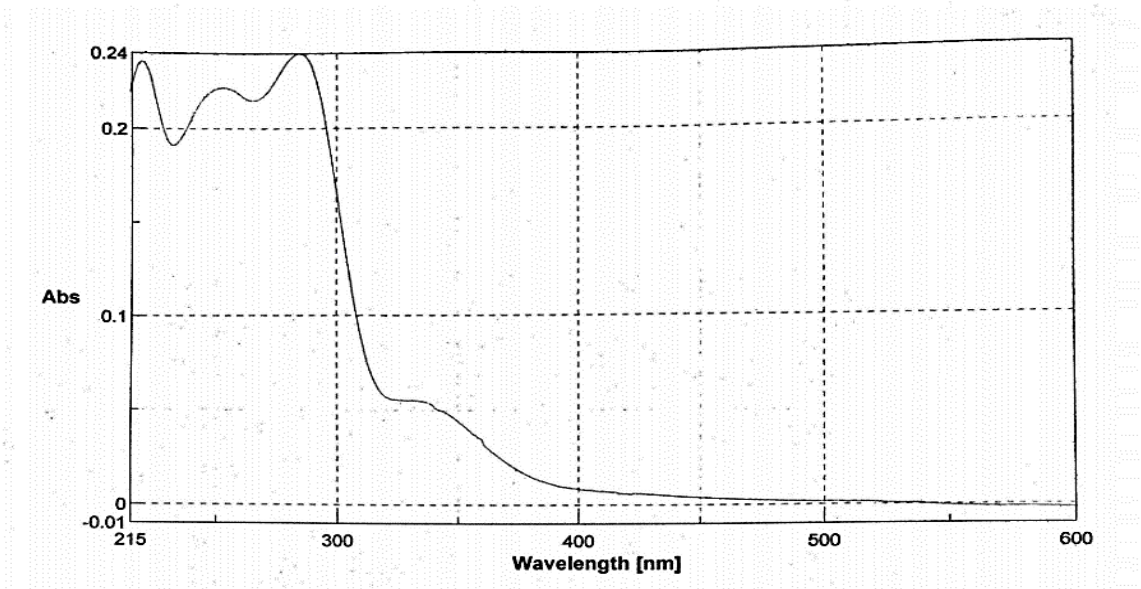

Figure 37. UV spectrum of lentiquinone B.

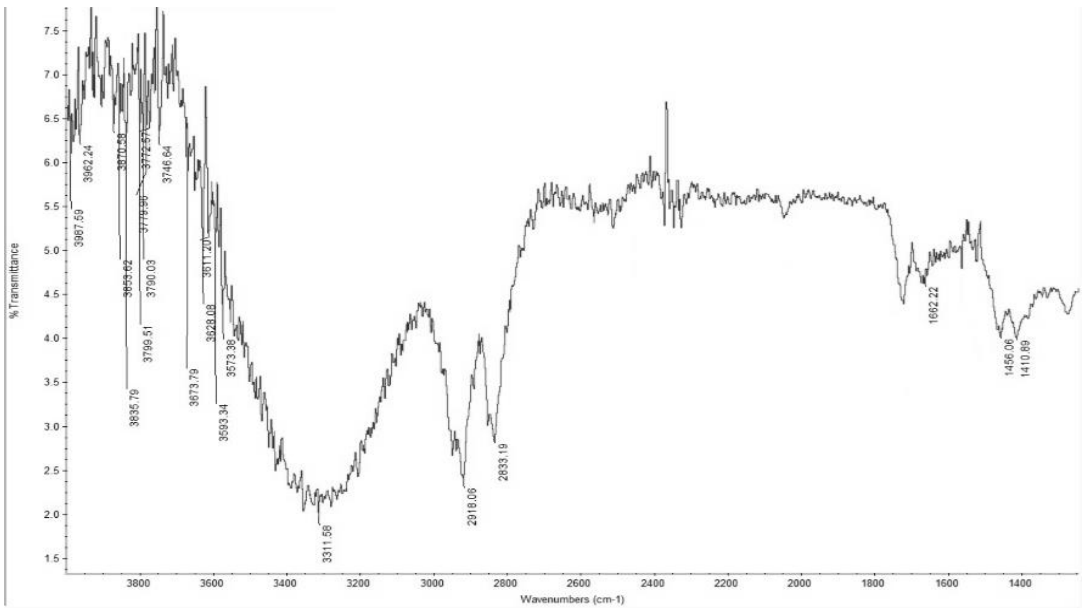

Figure 38. IR spectrum of lentiquinone B.

5.2.3 Structural identification of lentiquinone C.

Lentiquinone C (**9**) showed the same molecular formula $C_{15}H_{16}O_6$ as lentiquinone B (**8**), as deduced by its HRESIMS and ^{13}C NMR data (Fig. 44 and 40), and the same eight hydrogen deficiencies. Comparison of ^{1}H and ^{13}C NMR data (Fig. 31, 32 and 39, 40) of lentiquinone B and C (**8** and **9**) showed similar spin systems (Table 3). The most significant differences were the upfield shifts ($\Delta\delta$ 4.1) observed for C-2 in the ^{13}C NMR spectrum of lentiquinone C (**9**, Fig. 40), and the significantly different value recorded for the coupling between H-2 with both H-3 (*J*=4.2Hz) and H-1 (*J*=4.2 Hz), while the other *J*-couplings remained practically unchanged. The value measured for the coupling between H-2 and H-3 is typical for an axial-equatorial coupling in a half-chair conformation for a cyclohexene derivative (Badertscher, Bühlmann and Pretsch, 2009; Sternhell, 1969). Thus, lentiquinone C (**9**) appears to be the 2-epimer of lentiquinone B (**8**). The couplings observed in the COSY, HSQC, and HMBC data (Fig. 41-43) permitted the assignment of the chemical shifts for all the protons and the corresponding carbons of lentiquinone C (**9**) as reported in Table 3, and the structure of lentiquinone C (**9**) was characterized as (2*S**,3*S**,4*S**,4a*S**,10*R**)-2,3,4,5,10-pentahydroxy-7-methyl-3,4,4a,10 tetrahydroanthracen-9(2*H*)-one. The structure assigned to lentiquinone C (**9**) was also supported by the data of its HRESIMS spectrum (Fig. 44) which showed the sodiated dimer $[2M+Na]^+$ and the protonated molecular ion $[M+H]^+$ at *m/z* 607 and 293.1028, respectively.

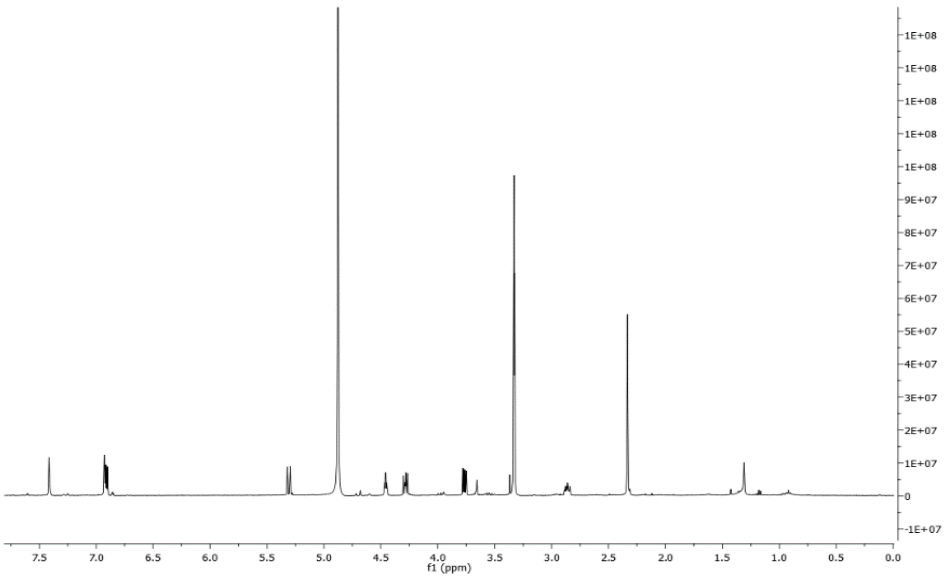

Figure 39. ^{1}H NMR spectrum of lentiquinone C (MeOD, 400 MHz).

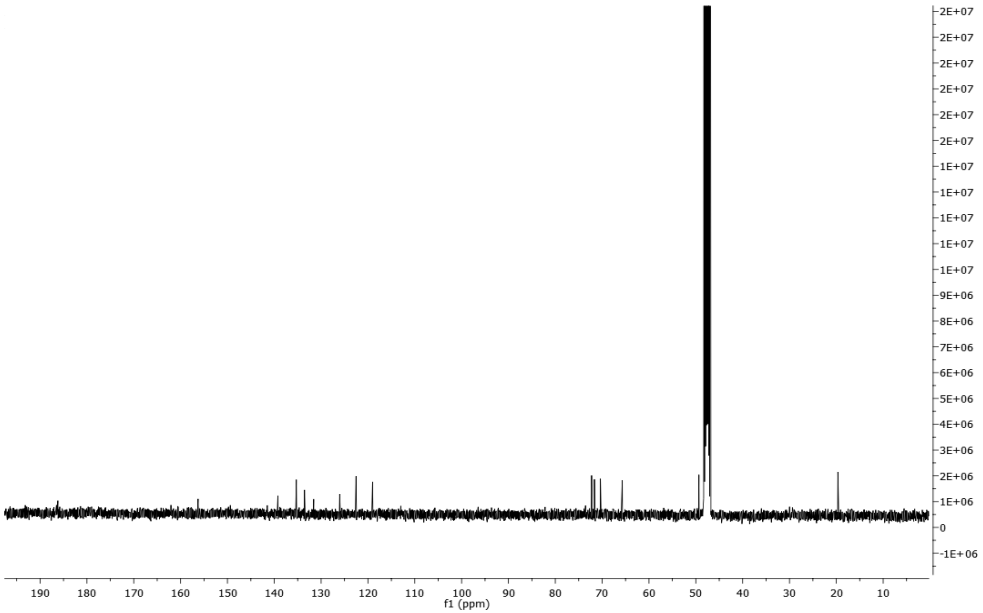

Figure 40. ^{13}C NMR spectrum of lentiquinone C (MeOD, 400 MHz).

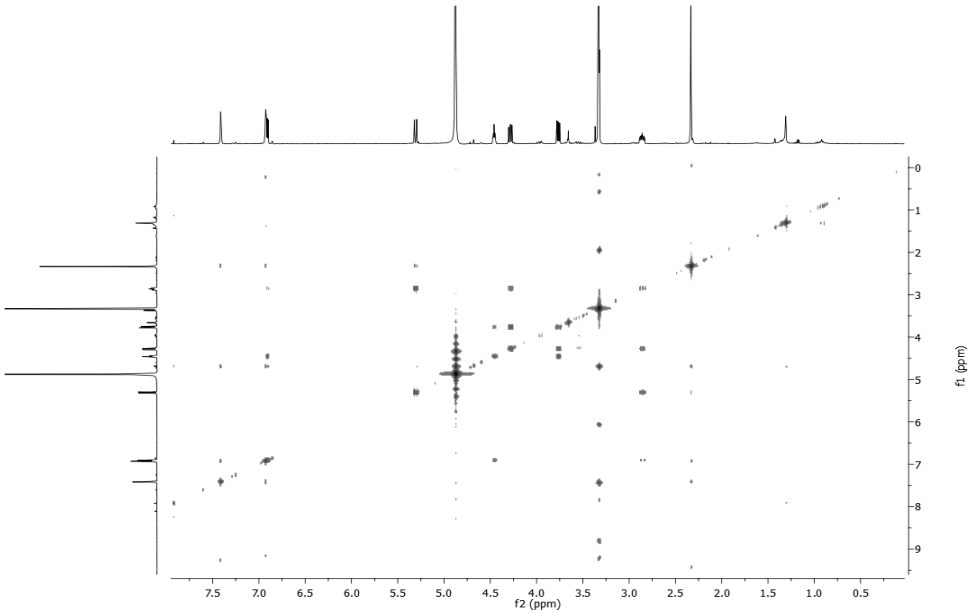

Figure 41. COSY spectrum of lentiquinone C (MeOD, 400 MHz).

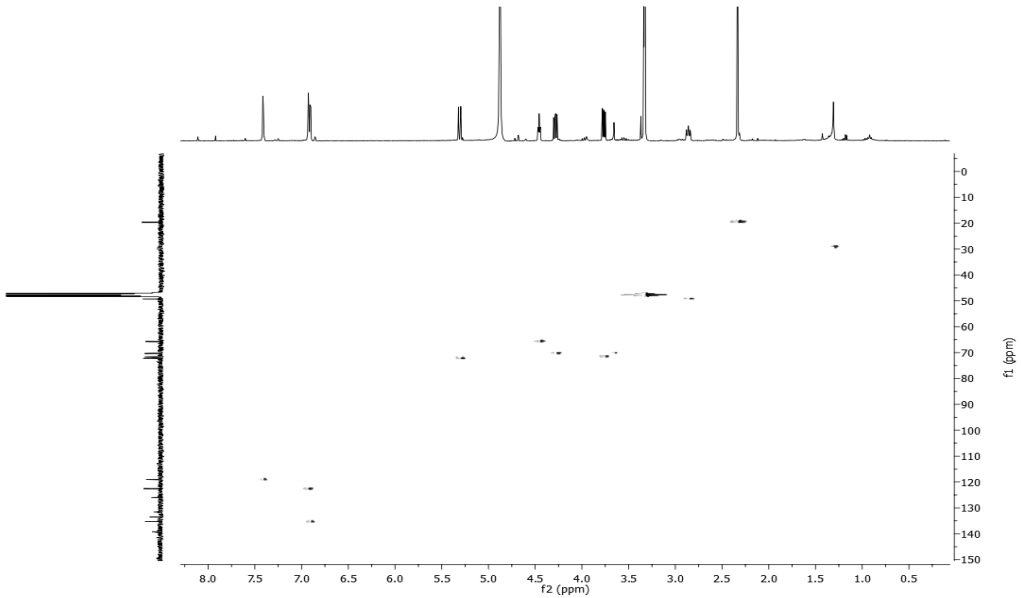

Figure 42. HSQC spectrum of lentiquinone C (MeOD, 400 MHz).

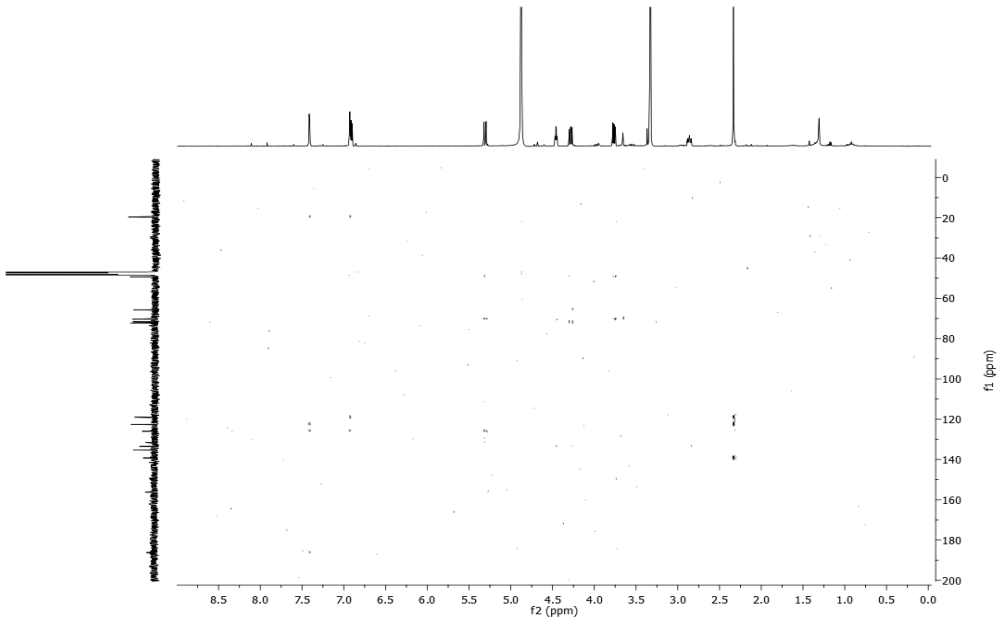

Figure 43. HMBC spectrum of lentiquinone C (MeOD, 400 MHz).

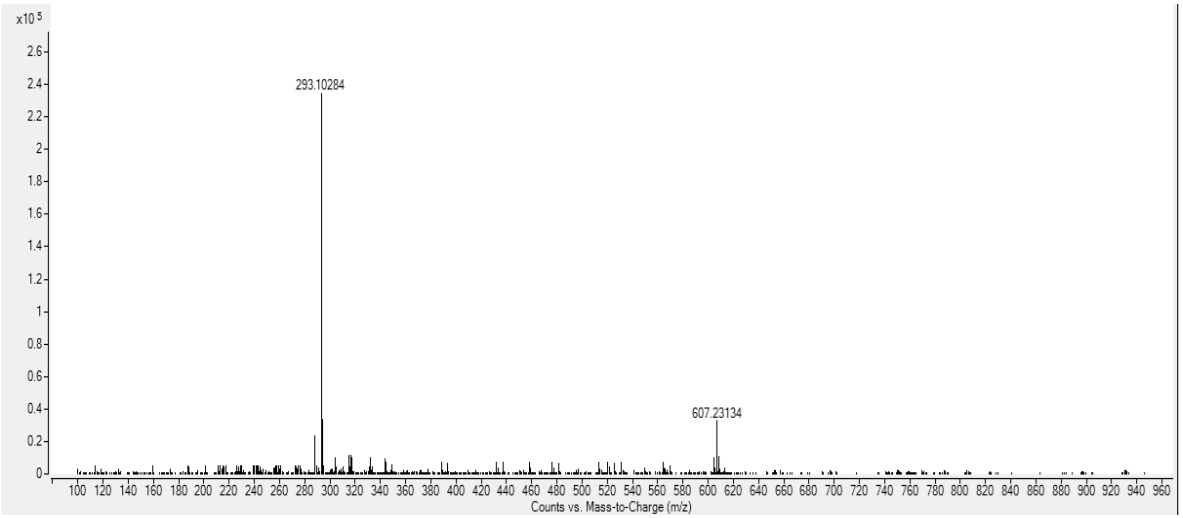

Figure 44. HRESIMS spectrum of lentiquinone C.

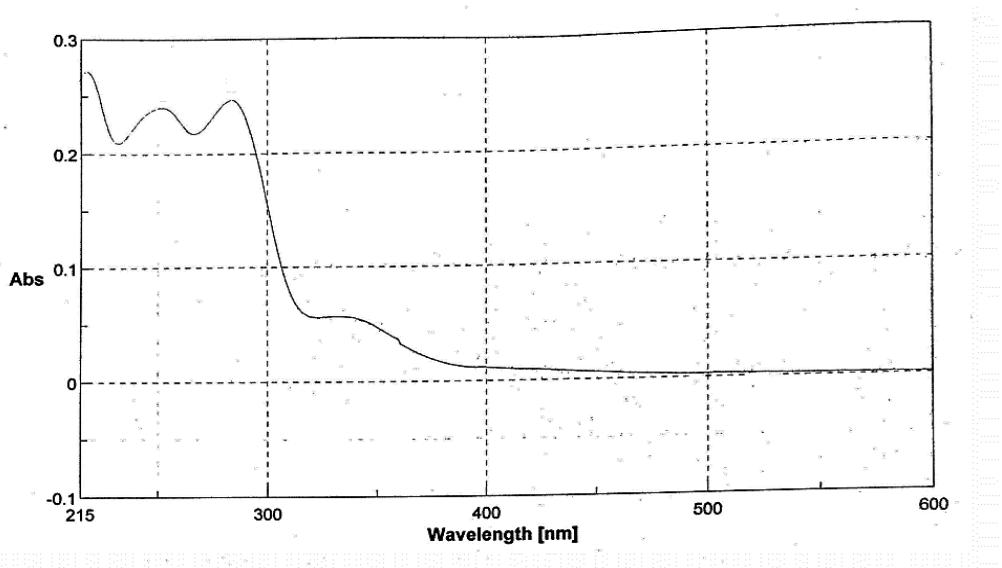

Figure 45. UV spectrum of lentiquinone C.

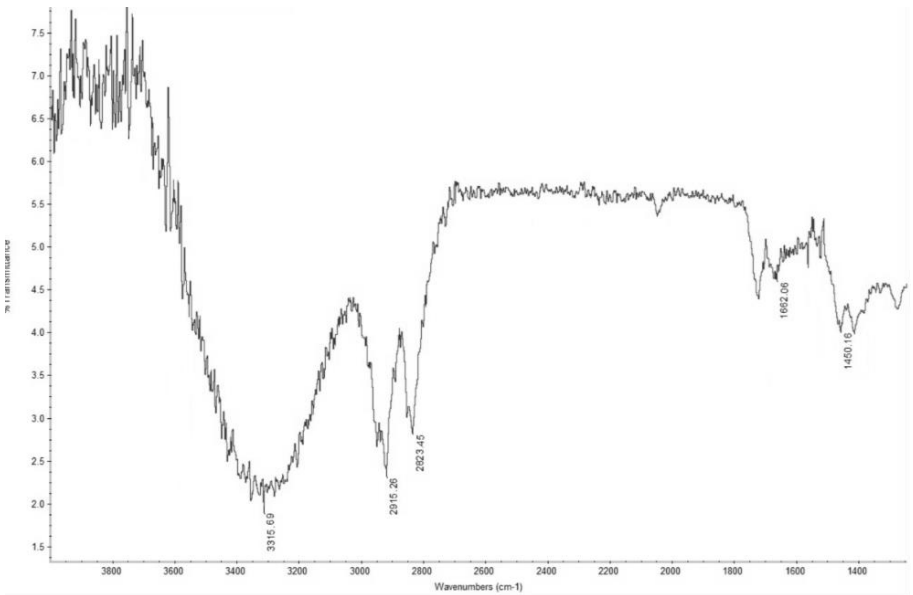

Figure 46. IR spectrum of lentiquinone C.

Table 3. ^{1}H and ^{13}C NMR Data of Lentiquinones A (**7**)[a,b] continue…

Lentiquinone A (7)							
Position	δC[c]	δH (*J* in Hz)	HMBC	Position	δC[c]	δH (*J* in Hz)	HMBC
1				8	123.8 s		H-9, H-7
2	67.2 t	4.01 (2H) s	HO-3	9	120.3 d	7.37 (1H) s	H-7, Me-C(8)
3	141.5 s		H_2-2, HO-3	9a	147.8 s		Me-C(8)
4	161.5 s		HO-3	10	183.9 s		H-9
4a	142.4 s[d]			10a	142.5 s[d]		
5	182.5 s			Me-C(8)	22.4 q	2.37 (3H) s	H-9, H-7
5a	131.8 s		HO-6, H-7, Me-C(8)	HO-3		2.80 (1H) br s	
6	161.3 s		HO-6, H-7	HO-6		11.99 (1H) br s	
7	123.6 d	6.98 (1H) s	HO-6, H-9, Me-C(8)				

[a]The chemical shifts are in δ values (ppm) from TMS. [b]2D ^{1}H, ^{1}H (COSY) ^{13}C, ^{1}H (HSQC) NMR experiments delineated the correlations of all the protons and the corresponding carbons. [c]Multiplicities were assigned by DEPT spectrum. [d]These attributions could be exchanged. [e]This is a complex signal due to the coupling of H-4a with the proton (H-4 and H-10) of the adjacent secondary carbons C-4 and C-10 of C and B rings and also of its allylic and homoallylic coupling with H-1 and H-2 (Badertscher, Bühlmann and Pretsch, 2009; Sternhell, 1969).

Table 3. ^{1}H and ^{13}C NMR Data of Lentiquinones B (**8**)[a,b] continue…

Lentiquinone B (8)							
Position	δC[c]	δH (*J* in Hz)	HMBC	Position	δC[c]	δH (*J* in Hz)	HMBC
1	138.2 d	6.84 (1H) t (2.6)	H-4a	8	119.0 d	7.38 (1H) d (1.2)	H-6, Me-C(7)
2	71.2 d	4.24 (1H) ddd (8.2, 4.2, 2.6)	H-4, H-3	8a	139.2 s		Me-C(7)
3	75.6 d	3.53 (1H) dd (10.1, 8.2)	H-4	9	185.7 s		H-1, H-8
4	75.5 d	3.96 (1H) dd (10.1, 8.4)	H-10	9a	130.7 s		H-1
4a	48.0 d	2.94 (1H) m[e] (10.1, 8.4, 4.2, 2.6)	H-1, H-3, H-4	10	73.4 d	5.27 (1H) d (10.1)	H-4
5	156.3 s		H-6, H-10	10a	131.5 s		H-10
6	122.6 d	6.91 (1H) d (1.2)	H-8, Me	Me-C(7)	19.6 q	2.31 (3H) s	H-6, H-8
7	125.2 s		H-6, H-8, Me-C(7)				

[a]The chemical shifts are in δ values (ppm) from TMS. [b]2D ^{1}H, ^{1}H (COSY) ^{13}C, ^{1}H (HSQC) NMR experiments delineated the correlations of all the protons and the corresponding carbons. [c]Multiplicities were assigned by DEPT spectrum. [d]These attributions could be exchanged. [e]This is a complex signal due to the coupling of H-4a with the proton (H-4 and H-10) of the adjacent secondary carbons C-4 and C-10 of C and B rings and also of its allylic and homoallylic coupling with H-1 and H-2 (Badertscher, Bühlmann and Pretsch, 2009; Sternhell, 1969).

Table 3. ^{1}H and ^{13}C NMR Data of Lentiquinones C (**9**)[a,b]

Lentiquinone C (9)							
Position	δC[c]	δH (*J* in Hz)	HMBC	Position	δC[c]	δH (*J* in Hz)	HMBC
1	136.8 d	6.88 (1H) dd (4.2, 2.8)		8	120.3 d	7.39 (1H) d (1.2)	H-6, Me-C(7)
2	67.1 d	4.43 (1H) td (4.2, 1.8)	H-4	8a	140.6 s		Me-C(7)
3	73.0 d	3.74 (1H) dd (8.2, 4.2)	H-4	9	187.7 s		H-8
4	71.4 d	4.26 (1H) dd (8.2, 6.1)	H-10, H-3	9a	133.0 s		H-10
4a	50.8 d	2.83 (1H) m[e] (10.0, 6.1, 2.8, 1.8)	H-10, H-3	10	73.6 d	5.28 (1H) d (10.0)	H-4
5	157.9 s		H-6	10a	134.9 s		H-4
6	124.0 d	6.90 (1H) d (1.2)	H-8, Me-C(7)	Me-C(7)	21.1 q	2.31 (3H) s	H-6, H-8
7	127.4 s		H-6, H-8				

[a]The chemical shifts are in δ values (ppm) from TMS. [b]2D ^{1}H, ^{1}H (COSY) ^{13}C, ^{1}H (HSQC) NMR experiments delineated the correlations of all the protons and the corresponding carbons. [c]Multiplicities were assigned by DEPT spectrum. [d]These attributions could be exchanged. [e]This is a complex signal due to the coupling of H-4a with the proton (H-4 and H-10) of the adjacent secondary carbons C-4 and C-10 of C and B rings and also of its allylic and homoallylic coupling with H-1 and H-2 (Badertscher, Bühlmann and Pretsch, 2009; Sternhell, 1969).

5.2.4 Relative and absolute configuration of lentiquinones B and C

The relative configuration of lentiquinone B (**8**) was deduced by the ^{1}H NMR coupling constants (Table 3). In fact, as the ring C assumes the most stable half-chair conformation, the typical $^{3}J_{H,H}$ values recorded for the coupling between H-4a and H-4 (J=8.4 Hz), H-4 with H-3 (J=10.1 Hz), and H-3 with H-2 (J=8.2 Hz), demonstrated that all four protons have pseudoaxial positions (Badertscher, Bühlmann and Pretsch, 2009; Sternhell, 1969) and permitted assignment of the relative configuration of lentiquinone B as (2*R**,3*S**,4*S**,4a*S**,10*R**).

The structure and the relative configuration of lentiquinone B (**8**) were confirmed by X-ray diffraction data analysis carried out on the colorless block-shaped crystals obtained by the slow addition of water to a solution of lentiquinone B (**8**) in MeOH, followed by slow evaporation of the aqueous alcoholic mixture. An ORTEP view of lentiquinone B is shown in Figure 47. All bond lengths and angles are in the normal range. Lentiquinone B (**8**) crystallizes in the orthorhombic $P2_12_12_1$ space group with one molecule of lentiquinone B (**8**) and one H_2O solvent molecule contained in the asymmetric unit. The structure of lentiquinone B (**8**) comprises three six membered rings, whose bond lengths, pattern, and geometry disclose the aromatic nature of ring A, the hemiquinone nature of ring B, and the cyclohexene nature of ring C. In the ring systems the sp^2 hybridization of C-9, C-9a, and C-1 and the planarity of ring A allow a near all-planar shape of the molecule. A degree of flexibility is found in the B and C rings, which adopts an envelope conformation of ring B (atom C-4a at the flap), and the half-chair conformation of ring C (C-3 and C-4 atoms up and down the mean plane C-1/C-2/C-4a/C-9a). Five stereogenic centers are present in the molecule with the relative configuration 2R*,3S*,4S*,4aS*,10*R confirmed by the X-ray structure analysis. The methine H atoms at C-2, C-3, C-4, C-4a, and C-10 are in the axial positions with a mutually *trans* configuration. All the hydroxy groups are in the equatorial positions and are involved in intra-

and intermolecular H-bonding that also includes the solvent H_2O molecule (Fig. 48).

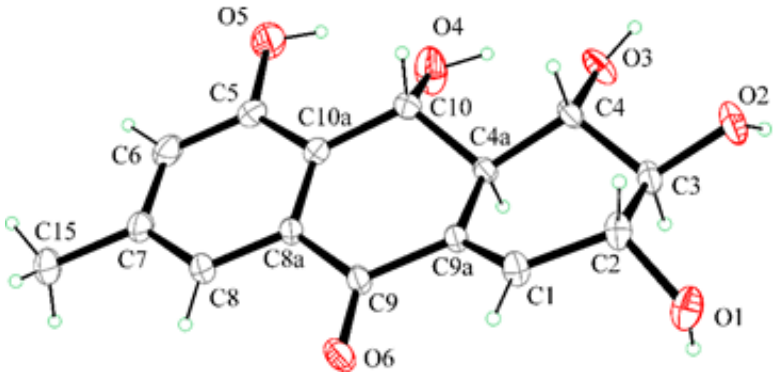

Figure 47. Ortep view of lentiquinone B.

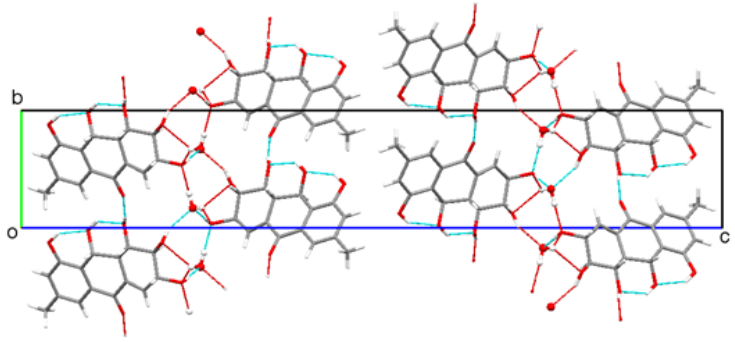

Figure 48. Crystal packing of lentiquinone B.

The structure and the relative configuration of lentiquinone C (**9**) were confirmed by the X-ray diffraction data analysis carried out on its orange block-shaped crystals obtained by the same procedure described for lentiquinone B (**8**). An ORTEP view of lentiquinone C is shown in Figure 49. All bond lengths and angles are in the normal range. Lentiquinone C (**9**) crystallizes in the monoclinic $P2_1$ space group with one molecule contained in the asymmetric unit. Crystal structure analysis shows that the molecular geometry of lentiquinone C (**9**) is similar to lentiquinone B (**8**). The two molecules perfectly overlay each other, except the hydroxy atom at C-2 that in lentiquinone B (**8**) is axial and in lentiquinone C (**9**) is equatorial (Fig. 50). The X-ray diffraction data analysis clearly shows that lentiquinone C (**9**) is the 2-epimer of lentiquinone B (**8**), with 2S*,3S*,4S*,4aS*,10R* relative configuration.

In the crystal packing of lentiquinone C (**9**) all the hydroxy groups are involved in strong OH···O intra- and intermolecular hydrogen bonds and layers of parallel molecules are arranged in a tridimensional H-bonding pattern (Fig. 51).

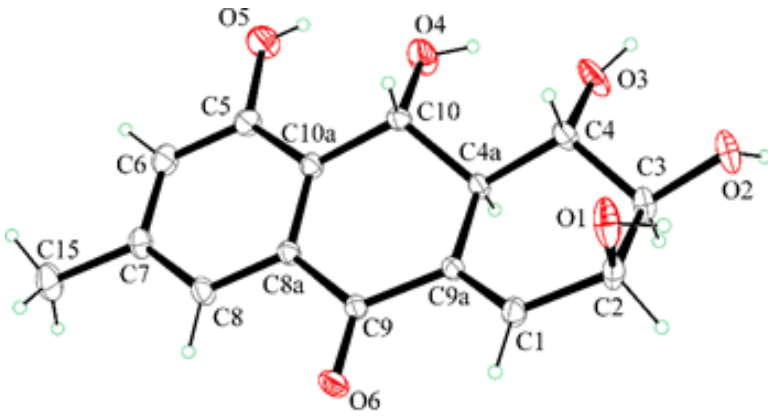

Figure 49. Ortep view of lentiquinone C.

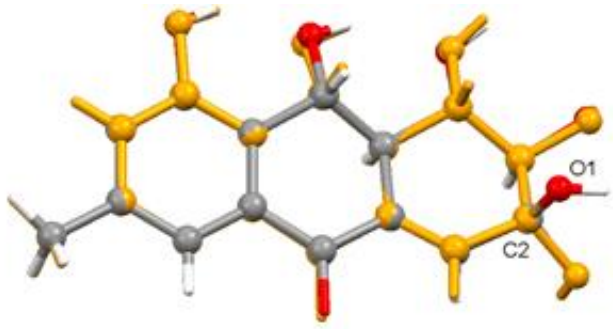

Figure 50. Superimposition of lentiquinone C (element colors) with lentiquinone B (orange)
X-ray geometries.

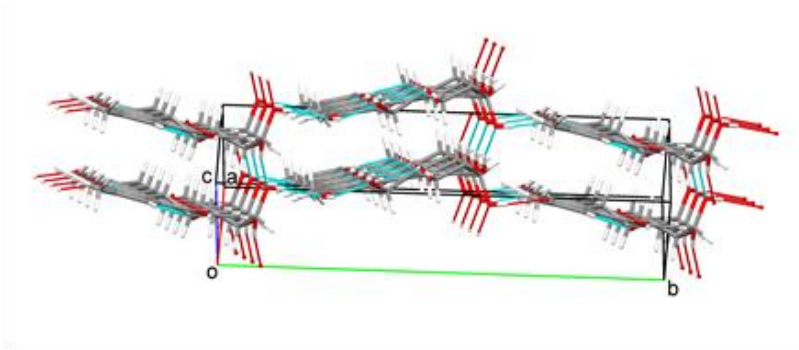

Figure 51. Perspective view of crystal packing of lentiquinone C with H-bonding pattern drawn as light blue dashed lines.

Attempts to assign the absolute configurations of lentiquinones B and C (**8** and **9**) by X-ray diffraction data analysis were made according to literature methods applied to light-atoms structures using Mo Kα radiation (Parsons, Flack and Wagner, 2013; Escudero-Adán, Benet-Buchholz and Ballester, 2014; Parsons, 2017). However, no certainty about the absolute configuration was reached because of a too large standard deviation for the calculated absolute structure parameters [Flack parameters: 0.0(2) for lentiquinone B (**8**) and 0.14(12) for lentiquinone C (**9**)] (Parsons *et al*., 2013).

The absolute configurations of both lentiquinones B (**8**) and C (**9**) were defined *via* electronic circular dichroism (ECD) spectroscopy (Superchi *et al*., 2018). The ECD spectra of lentiquinones B and C (**8** and **9**, Fig. 52 and 53) were measured in MeCN and, for lentiquinone C (**9**), also in the solid state as a KCl pellet (Fig. 54). The spectra show a rich pattern of bands expected for the extended conjugated chromophore. Using a consolidated computational procedure (Pescitelli and Bruhn, 2016), the conformations of lentiquinones B and C (**8** and **9**) were investigated by a conformational search with molecular mechanics (Merck molecular force field, MMFF), followed by geometry optimizations with density functional theory (DFT) run at the ωB97X-D/6-311+G(d,p) level and including a solvent model (SMD) for MeCN. Lentiquinone B (**8**) has a dominant conformation in keeping with NMR (measured *J*-couplings) and X-ray diffraction data results, and a minor conformation with rotated OH groups. For lentiquinone C (**9**) various conformers were found corresponding to the rotamerism of OH groups and ring flipping of ring C. However, the two most stable conformers featured the same ring conformation found in the X-ray geometry and similar to lentiquinone B (**8**). ECD calculations were run with time-dependent DFT (TDDFT) using various functionals (B3LYP, CAM-B3LYP, M06) and the def2-TZVP basis set, with the SMD solvent model. The good agreement between experimental and

calculated ECD spectra, especially using CAM-B3LYP (Fig. 52 and 53), permitted assignment of the absolute configurations as 2*R*,3*S*,4*S*,4a*S*,10*R*-lentiquinone B (**8**) and 2*S*,3*S*,4*S*,4a*S*,10*R*-lentiquinone C (**9**). For the latter, the quantity of crystals used for the X-ray diffraction experiment was large enough (about 50 μg) to apply a variant of the ECD analysis known as the solid-state ECD/TDDFT approach (Pescitelli *et al*., 2009). Here, the ECD spectrum is measured in the solid state as KCl pellet, and the calculation is run with TDDFT on the X-ray geometry, avoiding any uncertainty related to the conformation. The solid-state experimental and calculated ECD spectra are shown in Figure 54. Their good agreement in the long-wavelength region confirms the absolute configuration of lentiquinone C (**9**). The discrepancy at shorter wavelength is most likely a consequence of intercrystalline exciton couplings, which are expected for conjugated chromophores with strong dipole allowed transitions like the present one (Padula *et al*., 2014). Inspection of the crystal packing of lentiquinone C (**9**) confirms that such couplings are viable because of the skewed orientation of distinct molecules along the b axis.

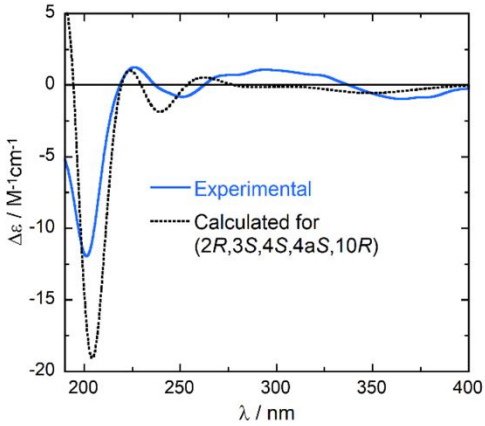

Figure 52. Experimental (solid blue line) and calculated (dotted black line) ECD spectrum of (2*R*,3*S*,4*S*,4a*S*,10*R*)-lentiquinone B.

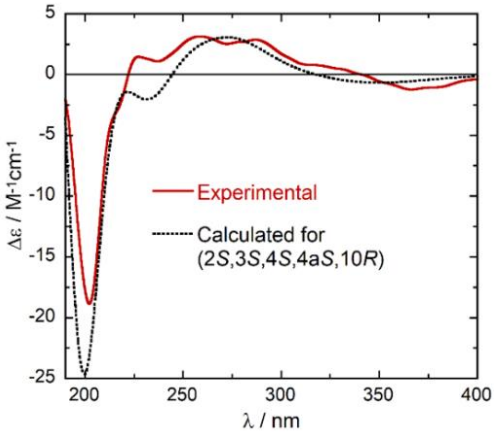

Figure 53. Experimental (solid red line) and calculated (dotted black line) ECD spectrum of (2*R*,3*S*,4*S*,4a*S*,10*R*)-lentiquinone C.

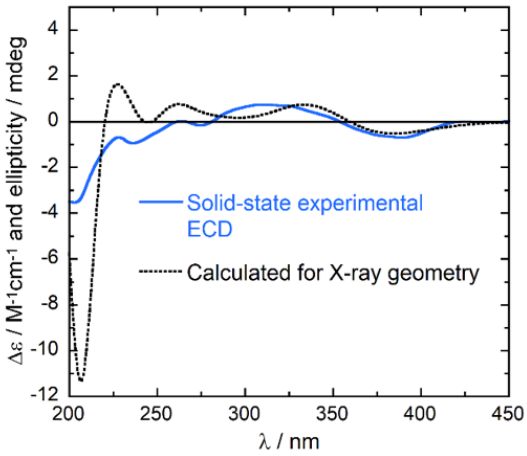

Figure 54. Experimental (solid blue line) ECD spectrum of (2*S*,3*S*,4*S*,4a*S*,10*R*)-lentiquinone C in the solid state (KCl pellet) compared with the spectrum calculated on the X-ray geometry (dotted black line) at CAM-B3LYP/def2-TZVP level.

5.2.5 Biological activities of secondary metabolites from *Ascochyta lentis*

5.2.5.1 Leaf puncture assay

Assayed on punctured leaves of 10 plant species, *Amaranthus retroflexus* L., *Dittrichia viscosa* (L.) Greuter, *Sonchus*, *Chenopodium album* L., *Convolvulus arvensis* L., *Ocimum basilicum* L., *Lens culinaris* L., *Lupinus albus* L., *Setaria*, *Solanum nigrum* L., the compounds (**7**-**14**) showed different activities (Table 4). Lentisone (**10**) was the most active compound, causing the widest necrosis to all the tested leaves. Lentiquinone A (**7**) was active too, but on average less active than lentisone (**10**), whereas lentiquinone B and C (**8** and **9**) were even less, but clearly active. The other tested compounds (**11**-**14**) were modestly active or not active at all. In general, the different sensitivity of the leaves to the tested compounds (**7**-**14**) seemed to be related to the characteristics of leaf surface. For instance, basil leaves have a tiny epidermis, and thus the clear necrosis probably are caused by the active compounds because they can readily diffuse into the parenchyma. The results confirmed those reported by (Andolfi *et al*., 2013) as lentisone (**10**) proved to be toxic in their assay, whereas pachybasin (**11**) was not.

5.2.5.2 Assay on *Lepidium sativum* rootlet elongation

On cress, lentiquinone A (**7**) had the highest activity, reducing almost 70% of rootlet growth compared to the control (Table 5). The other compounds (**8**-**14**) had modest or negligible effects.

5.2.5.3 *Lemna minor* assay

In the bioassay on *Lemna minor*, 1,7 dihydroxy-3-methylantracene-9,10-dione (**13**) was particularly active, together with ω-hydroxypachybasin (**12**), reducing the chlorophyll content in the fronds by over 80% compared to the control. All the other compounds (**7**-**10**, **14**) had a lower effect on chlorophyll, except pachybasin (**11**) that was inactive.

5.2.5.4 Assay on seed germination of parasitic weed *Phelipanche ramosa*

In the assay on seeds of the parasitic weed *Phelipanche ramosa*, lentisone (**10**) caused the total inhibition of seed germination (Table 5). Lentiquinone A (**7**) reduced the germination percentage by 60%, compared to the control, whereas the other tested metabolites (**8**-**14**) had modest or negligible effects.

Considering its effectiveness at 10^{-3} M, lentisone (**10**) was also tested at lower concentrations. At 2×10^{-4} M and 4×10^{-5} M it still caused some phytotoxic effects in terms of reduction of seed germination and germ tube elongation, whereas at 8×10^{-6} M it was inactive.

Thus, regarding the phytotoxicity, it seems that the presence of a B-ring quinone moiety, as in lentiquinone A (**7**) and lentisone (**10**), is an important structural feature to impart activity, while it is missing in lentiquinones B and C (**8** and **9**), which are less active. Also, the nature of the C-ring seems important for the phytotoxicity as the presence of a pyran C-ring, as in lentiquinone A (**7**), compared to lentisone (**10**) decreased the activity. Pachybasin, ω-hydroxypachybasin, 1,7-dihydroxy-3-methylanthracene-9,10-dione and phomarin (**11**-**14**), all quinones, probably did not show phytotoxicity due to the aromatization of the C-ring.

5.2.5.5 Antifungal assay

In the antifungal bioassay, only lentiquinone A (**7**) proved to be modestly effective, by partially inhibiting the mycelial growth of four out of the nine tested strains, namely *Verticillium dahlia*, *Penicillium allii*, *Rhizoctonia* sp., and *Phoma exigua*. All the other compounds (**8**-**14**) proved to be ineffective to all the tested fungi.

5.2.5.6 Antibiotic assay

In the antibiotic assay against Gram (+) and Gram (-) bacteria, lentisone (**10**) and lentiquinone C (**9**) were active against *Bacillus subtilis*, causing clear growth inhibition areas (Table 5). Lentiquinone B (**8**) was active too, but to a

lesser extent; lentiquinone A (**7**) was even less active, although clearly active. The other four bioassayed compounds (**11**-**14**) proved to be completely inactive at the tested concentration. Conversely, all the compounds (**7**-**14**) were inactive against *Escherichia coli*.

Table 4. Effect of *Ascochyta lentis* metabolites in the leaf puncture assay

		Compound							
		Lentiquinone A (7)	Lentiquinone B (8)	Lentiquinone C (9)	Lentisone (10)	Pachybasin (11)	ω-hydroxypachybasin (12)	1,7-dihydroxy-3-methylanthracene-9,10-dione (13)	Phomarin (14)
Plant species	**Family**								
Amaranthus retroflexus L.	Amaranthaceae	2[a]	1	1	3	0	0	0	0
Dittrichia viscosa (L.) Greuter	Asteraceae	3	1	1	3	0	0	0	0
Sonchus	Asteraceae	2	0	0	3	0	0	0	0
Chenopodium album L.	Chenopodiaceae	4	2	3	4	0	0	0	0
Convolvulus arvensis L.	Convolvulaceae	3	2	2	4	0	0	0	0
Ocimum basilicum L.	Lamiaceae	4	2	2	4[b]	0	0	0	0
Lens culinaris L.	Leguminosae	3	2	1	4	0	1	[c]	[c]
Lupinus albus L.	Leguminosae	4	2	4	4	0	2	0	2
Setaria	Poaceae	3	1	2	2[d]	0	0	0	1
Solanum nigrum L.	Solanaceae	4	1	1	4	0	0	0	0

[a]Dimension of leaf necrosis by a visual scale from 0 to 4 (0=no effects; 4=necrosis around 1 cm diameter). [b]Necrosis very wide, out of the scale. [c]Only chlorosis. [d]Necrosis surrounded by an area of chlorophyll retention (green island).

Table 5. Effects of the *Ascochyta lentis* Metabolites in Different Bioassays

		Compound							
		Lentiquinone A (7)	**Lentiquinone B (8)**	**Lentiquinone C (9)**	**Lentisone (10)**	**Pachybasin (11)**	**8-hydroxypachybasin (12)**	**1,7-dihydroxy-3-methylanthracene-9,10-dione (13)**	**Phomarin (14)**
Bioassay	**Plant species**								
Rootlet elongation[a]	*Lepidium sativus*	32.7	89.0	83.9	75.6	100.0	90.4	90.8	102.3
Chlorophyll[b]	*Lemna minor*	77.7	60.2	58.5	60.5	100.0	24.1	17.6	53.6
Seed germination[c]	*Phelipanche ramosa*	40[fe]	79	78	1	93	104[e]	106	106
Antibiosis[d]	*Bacillus subtilis*	11	12	14	14	0	0	0	0

[a]Rootlet elongation (percentage in comparison to the control length). [b]Chlorophyll content (percentage compared to the control content). [c]Seed germination (percentage compared to the control germination). [d]Growth inhibition halo (diameter mm). [e]Germinated tubes shorter than the control ones.

5.3 Structural identification of secondary metabolites from *Colletotrichum lupini* culture filtrates.

The EtOAc organic extract obtained from the culture filtrates of *C. lupini*, showing a strong phytotoxicity on host plant leaves, was purified as detailed in Experimental section (Scheme 4). A 3-substituted indolinone and a 5,6-disubstituted tetrahydro-α-pyrone, named lupindolinone (**15**) and lupinlactone (**16**), (3*R*)-mevalolactone (**17**) and tyrosol (**18**) were obtained (Fig. 55).

(3*R*)-Mevalolactone (**17**) was identified by comparison of its physic (specific optical rotation) and spectroscopic (^{1}H NMR and MS) data with that previously reported in literature (Varejão *et al*., 2013). **17** is the lactone form of (-)-(*R*)-mevalonic acid and an important intermediate in biosynthetic pathways leading to sterols, terpenes, carotenoids, and other isoprenoids (Dewick, 2002). This compound was recently isolated from the fungal cultures of *Diaporthaceae* sp. PSU-SP2/4 (Khamthong *et al*., 2014), *Alternaria euphorbiicola* (Varejão *et al*., 2013), *Pseudallescheria boydii* (Chang *et al*., 2013) and *Phomopsis archeri* (Hemtasin *et al*., 2011).

Tyrosol (**18**) was identified by comparison of its physical and spectroscopic (^{1}H NMR and MS) data with those previously reported in literature (Kimura and Tamura, 1973; Capasso *et al*., 1992; Cimmino *et al*., 2017d). **18** is a well-known fungal phytotoxic metabolite produced by several plant pathogens e.i. *Diplodia seriata* (Venkatasubbaiah and Chilton, 1990), *Alternaria tagetica* (Gamboa-Angulo *et al*., 2001), *Neofusicoccum parvum* (Evidente *et al*., 2010), some *Lasiodiplodia* spp. (Cimmino *et al*., 2017c) and *Diaporthella cryptica* (Cimmino *et al*., 2018).

The preliminary investigation of ^{1}H and ^{13}C NMR spectra of lupinindolinone (**15**) and lupinlactone (**16**) showed that they are derivatives of indolinones and tetrahydro-α-pyrone, respectively.

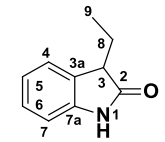

15, Lupindolinone

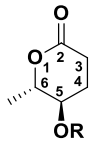

16, Lupinlactone, R=H
19, 5-O-(*S*)-MTPA esters of lupinlactone , R=*R*-MTPA
20, 5-O-(*R*)-MTPA esters of lupinlactone , R=*S*-MTPA

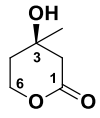

17, (3*R*)-Mevalolactone

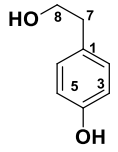

18, Tyrosol

Figure 55. *Colletotrichum lupini* secondary metabolites**.**

5.3.1 Structural identification of lupindolinone

Lupindolinone (**15**) had a molecular formula $C_{10}H_{11}NO$, as deduced from its HRESIMS spectrum (Fig. 60) and consistent with six hydrogen deficiencies. In particular, its ^{1}H NMR and COSY spectra (Fig. 56 and 60) showed the signal systems of 3-substituted indolinone ring with two doublets (*J*=7.5 Hz) and two triplets (*J*=7.5 Hz) at δ 7.23 and 6.86 (H-4 and H-7) and δ 7.21 and 7.03 (H-6 and H-5) (Berger and Braun, 2004). H-3 resonated as a triplet (*J*=6.8 Hz) at δ 3.45 while the NH was observed as a broad singlet at the very typical chemical shift value of 4.68 (Badertscher *et al*., 2009). Furthermore, H-3 was coupled with the protons of the adjacent methylene (CH_2-8) of the side chain observed as a quintet (*J*=6.8 Hz) at δ 2.03, being also coupled with the terminal methyl group (CH_3-9), which appeared as a triplet (*J*=6.8 Hz) at δ 0.92. These findings were in full agreement with the absorption bands typical for carbonyl and aromatic groups observed in the IR spectrum at 1703, 1620, 1470 cm^{-1} (Fig. 62) (Nakanishi, 1977) and the absorption maximum observed in the UV spectrum at 282 and 249 nm (Fig. 63) (Badertscher *et al*., 2009). The couplings observed in the HSQC spectrum (Fig. 58) (Berger and Braun, 2004) allowed to assign the signals resonating in the ^{13}C NMR spectrum (Fig. 57) at δ 127.8, 124.2, 122.3, 109.1, 47.0, 23.6 and 10.0 to protonated carbons C-6, C-4, C-5, C-7, C-3, C-8 and C-9 (Breitmaier and Voelter, 1987). The couplings observed in the HMBC spectrum (Fig. 59) (Berger and Braun, 2004) allowed to assign the signals of the carbonyl and the two quaternary aromatic carbons. In fact, the carbonyl group (C-1), at δ 179.4, coupled with H-3 and H_2-8, C-7a at δ 141.4 with H-3, H-5 and H-6, and C-3a at δ 129.5 with NH, H-3, H-4, H-5, H-7 and H_2-8, respectively (Breitmaier and Voelter, 1987). Consequently, the chemical shifts of all protons and the corresponding carbons of lupindolinone (**15**) were assigned and reported

in Table 6. These findings allowed to formulate lupinindolinone (**15**) as 3-ethylindolin-2-one.

The structure assigned to lupindolinone (**15**) was confirmed by all the other correlations observed in HMBC spectrum (Fig. 59 and Table 6) and by the data of its HRESIMS spectrum (Fig. 61). This latter spectrum showed the protonated molecular ion $[M+H]^+$ at *m/z* 162.0919.

Lupindolinone (**15**) was apparently isolated in a racemic form. Indeed, the optical rotation value was close to zero, and the electronic circular dichroism (ECD) spectrum was negligible in the range 200-400 nm. Indeed, despite a long measurement time, the ECD band around 250 nm was hardly detectable with a γ-factor < $2x10^{-5}$ and a signal-to-noise ratio < 2.

Lupindolinone (**15**) was isolated in racemic mixture but this is not a surprise because some natural products are bio-synthesized in racemic form although this is rarely reported (Zask and Ellestad, 2018). Sometimes, some others are also isolated as racemic mixtures, as in the recent case of colletopyrandione, a tetrasubstituted indolylidenepyrandione isolated from *C. higginsianum* (Masi *et al*., 2017). However, lupindolinone (**15**) has the only stereocenter in simultaneously benzylic and in α position to a carbonyl group, therefore we envisage the possibility of easy racemization via keto-enol tautomerism or enolate formation (Wolf, 2007).

Considering that lupindolinone (**15**) was reported only as a synthetic compound (Li *et al*., 2014), this is its first isolation as a natural occurring compound and as a fungal phytotoxic metabolite produced by *C. lupini*. Its spectroscopic properties are reported by Grigg *et al.,* (2009) and our data are full consistent.

Table 6. ^{1}H and ^{13}C NMR data and HMBC correlations of lupindolinone (**15**) [a,b]

Position	δ_C[c]	δ_H (*J* in Hz)	HMBC
1		4.68 (1H) br s	
2	179.4 C		H-3, H_2-8
3	47.0 CH	3.45 (1H) t (6.8)	H_2-8, H_3-9
3a	129.5 C		H-3, H-4, H-5, H-7, H_2-8, NH
4	124.2 CH	7.23 (1H) d (7.5)	H-5
5	122.3 CH	7.03 (1H) t (7.5)	H-7
6	127.8 CH	7.21 (1H) t (7.5)	H-4
7	109.1 CH	6.86 (1H) d (7.5)	H-5
7a	141.4 C		H-3, H-5, H-6
8	23.6 CH_2	2.03 (2H) quin (6.8)	H-3, H_3-9
9	10.0 CH_3	0.92 (3H) t (6.8)	H-3 H_2-8

[a]The chemical shifts are in δ values (ppm) from TMS. [b]2D ^{1}H, ^{1}H (COSY) ^{13}C, ^{1}H (HSQC) NMR experiments delineated the correlations of all the protons and the corresponding carbons. [c]Multiplicities were assigned by DEPT spectrum.

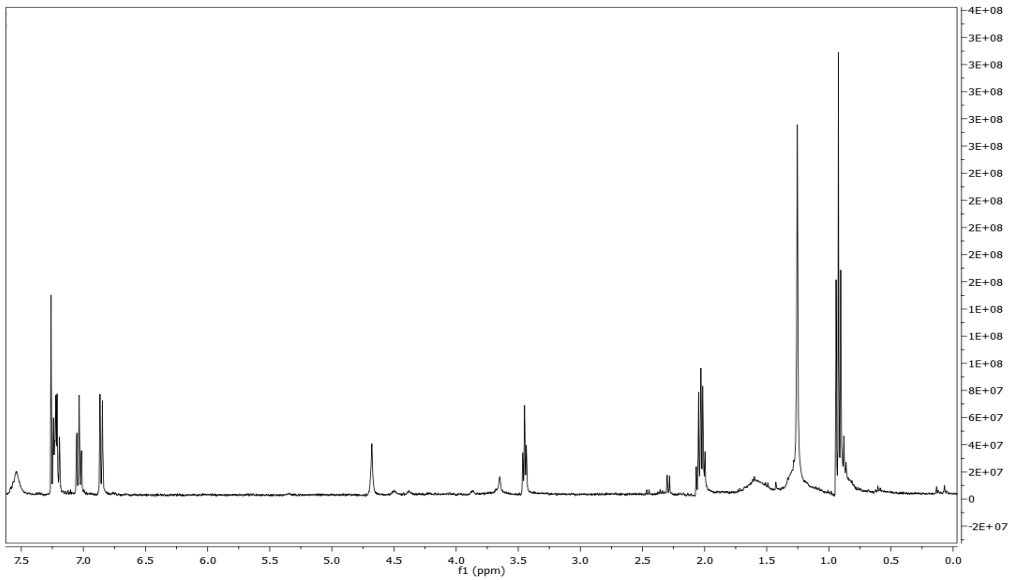

Figure 56. ^{1}H NMR spectrum of lupindolinone ($CDCl_3$, 500 MHz).

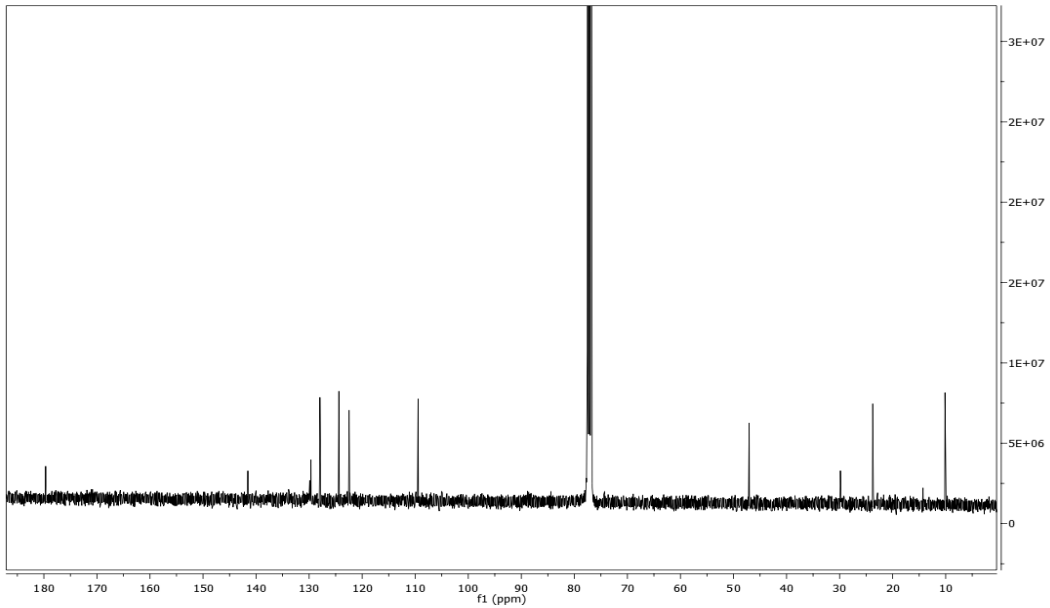

Figure 57. ^{13}C NMR spectrum of lupindolinone ($CDCl_3$, 500 MHz).

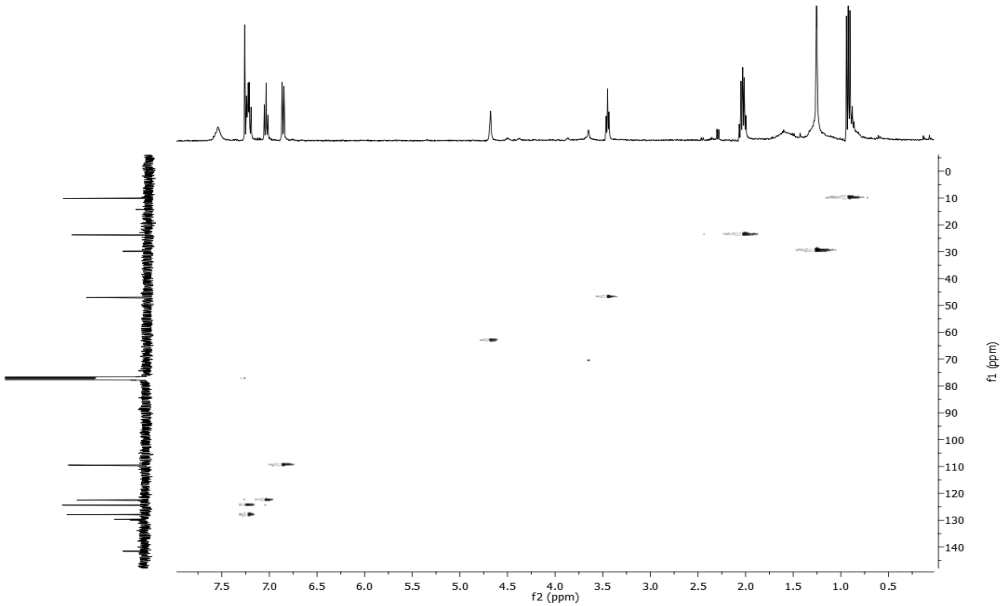

Figure 58. HSQC spectrum of lupindolinone ($CDCl_3$, 500 MHz).

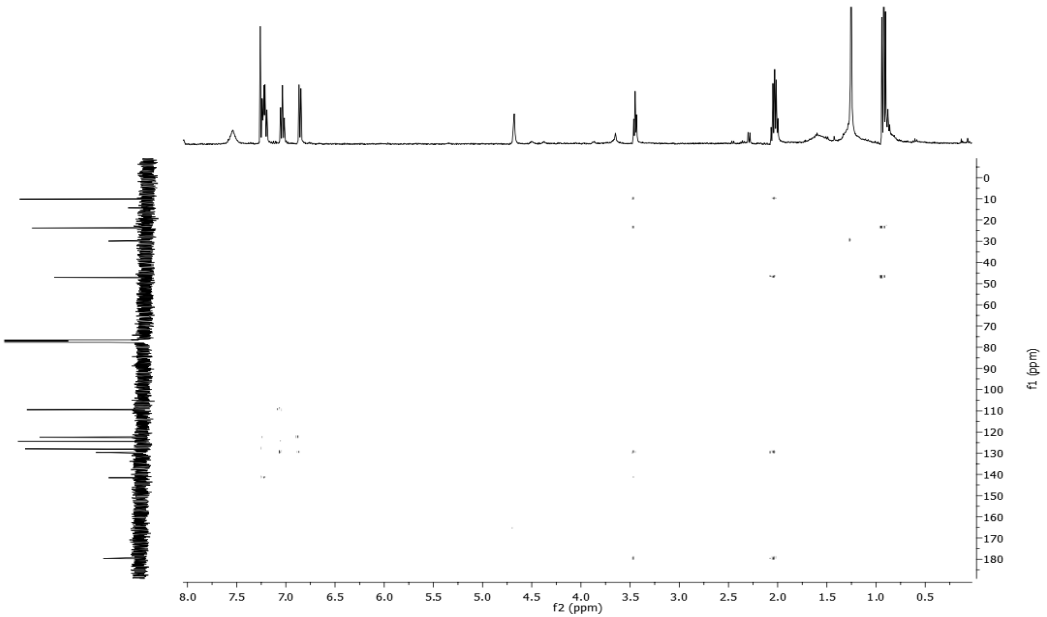

Figure 59. HMBC spectrum of lupindolinone ($CDCl_3$, 500 MHz).

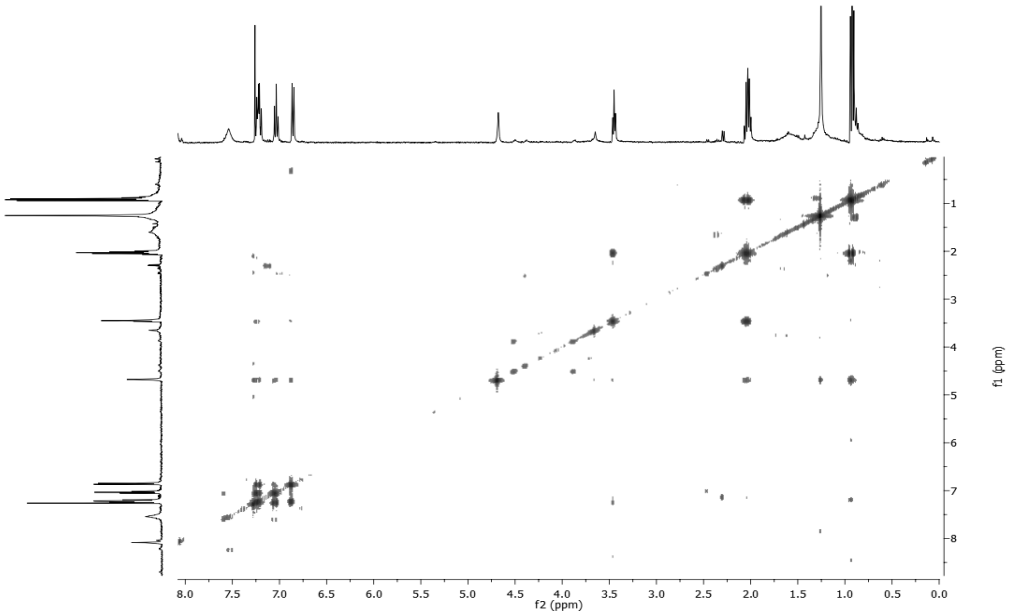

Figure 60. COSY spectrum of lupindolinone ($CDCl_3$, 500 MHz).

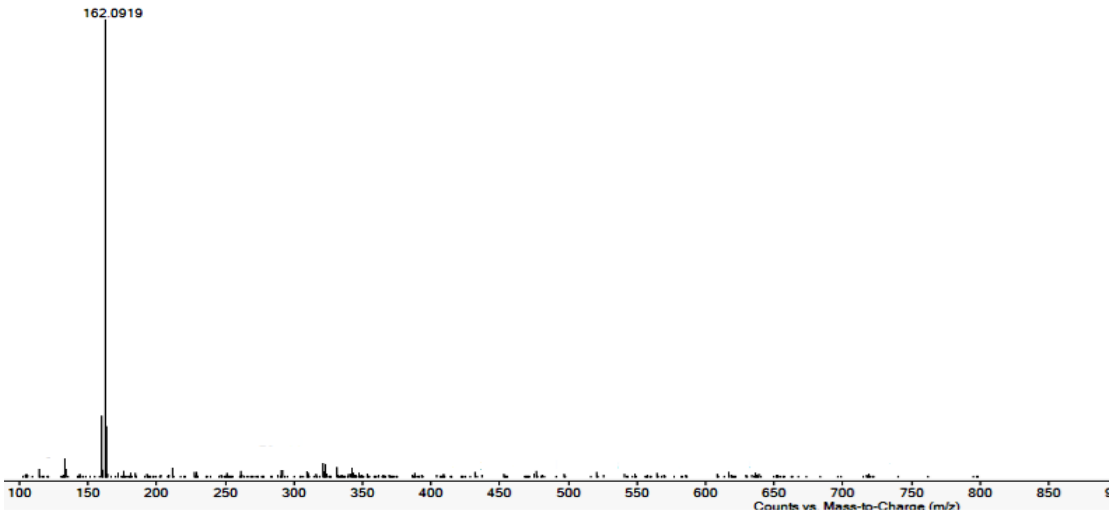

Figure 61. HRESIMS spectrum of lupindolinone.

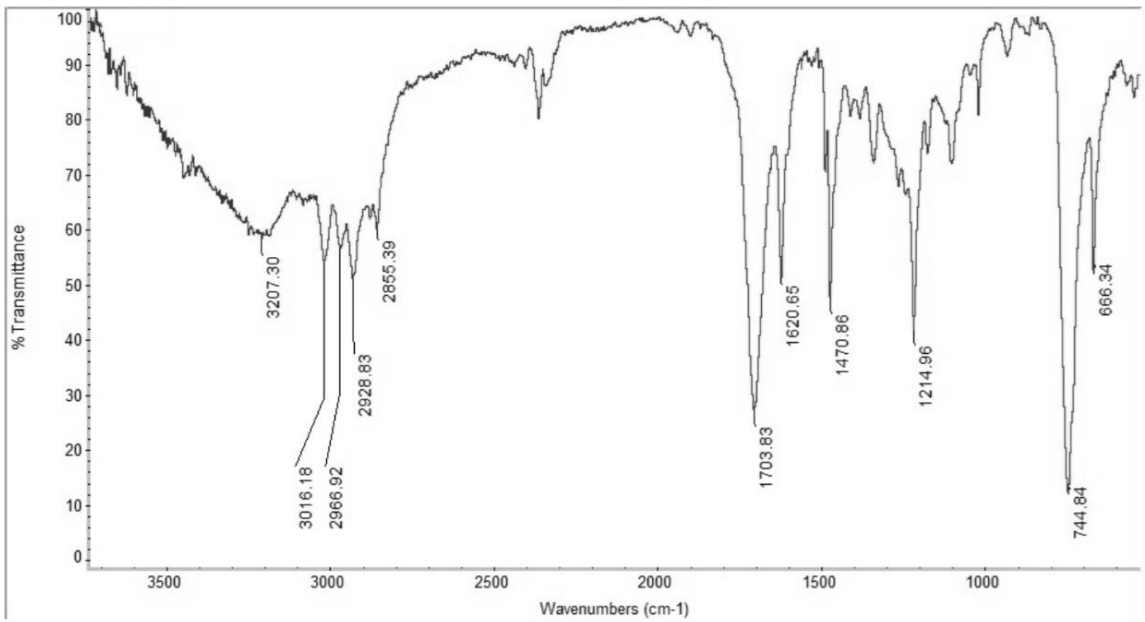

Figure 62. IR spectrum of lupindolinone.

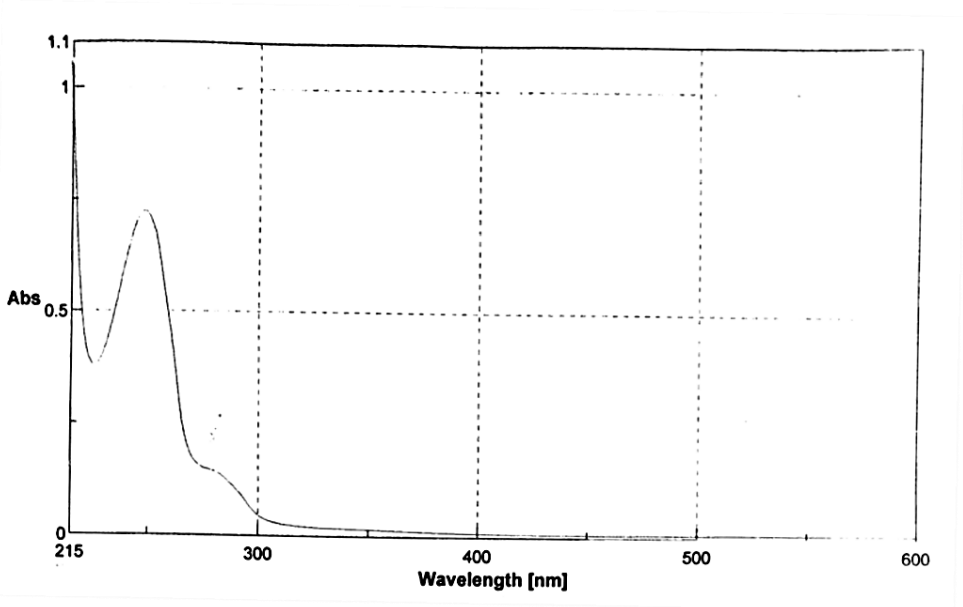

Figure 63. UV spectrum of lupindolinone.

5.3.2 Structural identification of lupinlactone

Lupinlactone (**16**) had a molecular formula $C_6H_{10}O_3$ as deduced from its HRESIMS spectrum (Fig. 69) and consistent with five hydrogen deficiencies. The ^{1}H NMR and COSY spectra (Fig. 64 and 68) showed the signal systems typical of a 5,6-disubstituted tetrahydropran-2-one. Indeed, a broad double doublet (*J*=10.7 and 6.8 Hz) for the proton (H-5) of a secondary hydroxylated carbon was observed at δ 4.34. This latter, in turn, coupled with the adjacent proton (H-6) appearing as a double quartet (*J*=10.7 and 6.8 Hz) at δ 3.78, being also coupled with the geminal methyl group resonating as a doublet (*J*=6.8 Hz) at δ 1.26. H-5 also coupled with the protons of the other adjacent methylene group (H_2C-4) resonating as two multiplets at δ 2.26 and 2.04, being also coupled with the protons of the adjacent methylene (H_2C-3) appearing as two complex multiplets at δ 2.59 and 2.54, respectively (Badertscher *et al*., 2009).

These findings were full consistent with the band typical of hydroxyl and carbonyl groups (Nakanishi, 1977) observed in the IR spectrum at 3358 and 1765 cm^{-1} (Fig. 70) (Badertscher *et al*., 2009). The couplings observed in the HSQC spectrum (Fig. 66) allowed to assign the signals resonating in the ^{13}C NMR spectrum (Fig. 65) at δ 84.7, 70.5, 29.2, 24.6, and 19.0 to the protonated carbons C-5, C-6, C-3, C-4, and Me-C-6, respectively (Breitmaier and Voelter, 1987). The couplings observed in the HMBC spectrum (Fig. 67) confirmed the assignment of the signal at the typical chemical shift value of δ 177.3 to the carbonyl group (C-1), as it coupled with H_2-3 and H-4a (Breitmaier and Voelter, 1987). Consequently, the chemical shifts of all protons and the corresponding carbons of lupinlactone (**16**) were assigned and reported in Table 7.

These results allowed to formulate lupinolactone (**16**) as 5-hydroxy-6-methyl-tetrahydro-pyran-2-one. The structure assigned to lupinlactone (**16**) was confirmed by all the other correlations observed in HMBC (Fig. 67) and by the

data of its HRESIMS spectrum (Fig. 69). This latter showed the sodiated $[2M+Na]^+$ and the protonated $[2M+H]^+$ dimer forms, the potassium $[M+K]^+$ and sodium $[M+Na]^+$ clusters, and the protonated molecular ion $[M+H]^+$ at *m/z* 283 and 261, 169 and 151, and 131.0709, respectively. Also, the ion generated from the protonated molecular ion by loss of H_2O $[M+H-H_2O]^+$ was recorded at *m/z* 113.

Table 7. ^{1}H and ^{13}C NMR data and HMBC correlations of lupinlactone (**16**) [a,b]

Position	δ_C[c]	δ_H (*J* in Hz)	HMBC
2	177.3 C		H_2-3, H-4A
3	29.2 CH_2	2.54 (1H) m 2.59 (1H) m	H_2-4
4	24.6 CH_2	2.26 (1H) m 2.04 (1H) m	H-6
5	84.7 CH	4.34 (1H) br dd (10.7, 6.8)	Me-C6
6	70.5 CH	3.78 (1H) d q (10.7, 6.8)	H-4B, Me-C6
Me-C6	19.0 CH_3	1.26 (3H) d (6.8)	H-6

[a]The chemical shifts are in δ values (ppm) from TMS. [b]2D ^{1}H, ^{1}H (COSY) ^{13}C, ^{1}H (HSQC) NMR experiments delineated the correlations of all the protons and the corresponding carbons. [c]Multiplicities were assigned by DEPT spectrum.

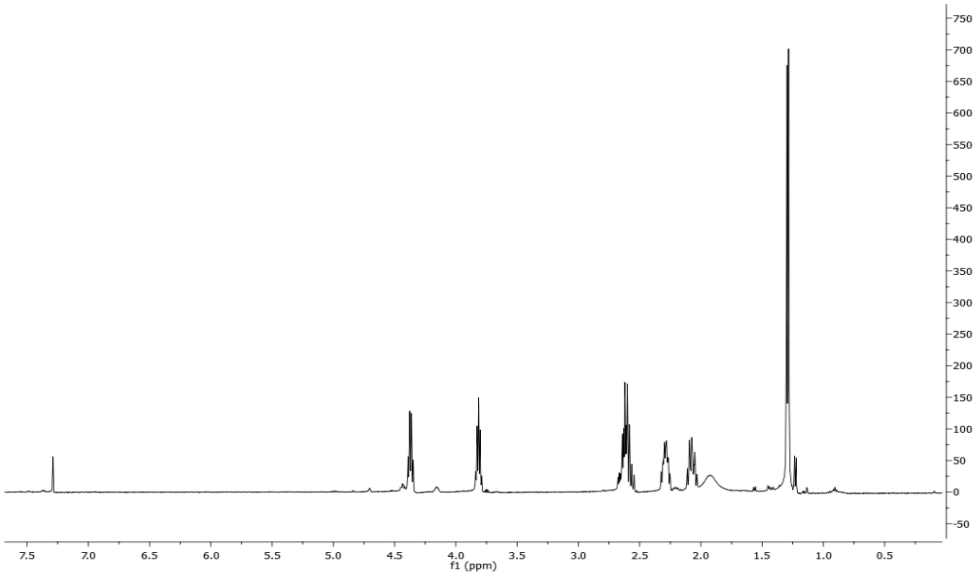

Figure 64. ^{1}H NMR spectrum of lupinlactone ($CDCl_3$, 500 MHz).

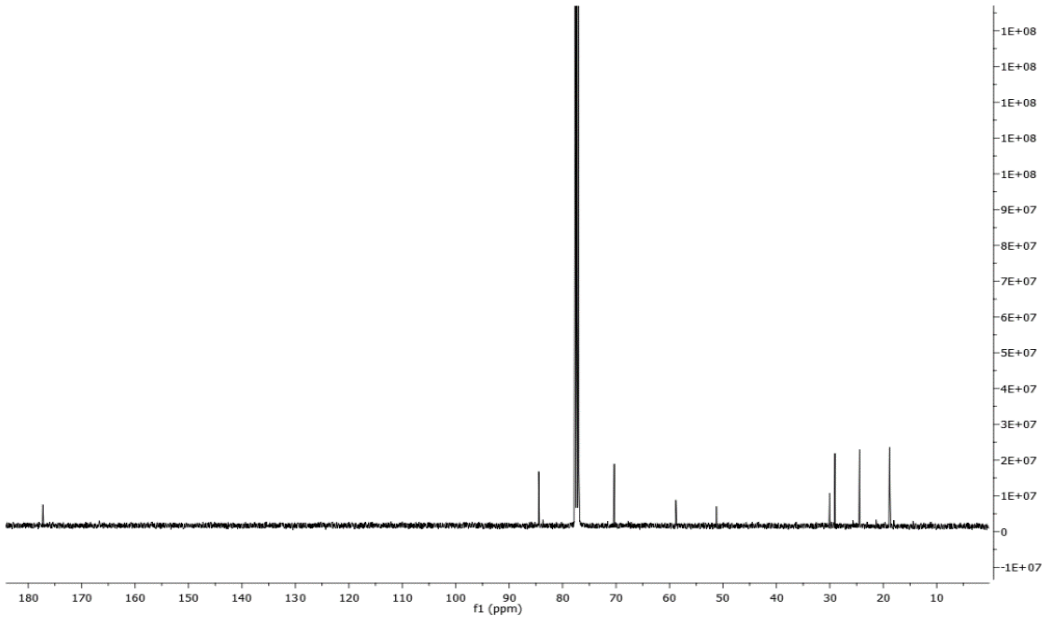

Figure 65. ^{13}C NMR spectrum of lupinlactone ($CDCl_3$, 500 MHz).

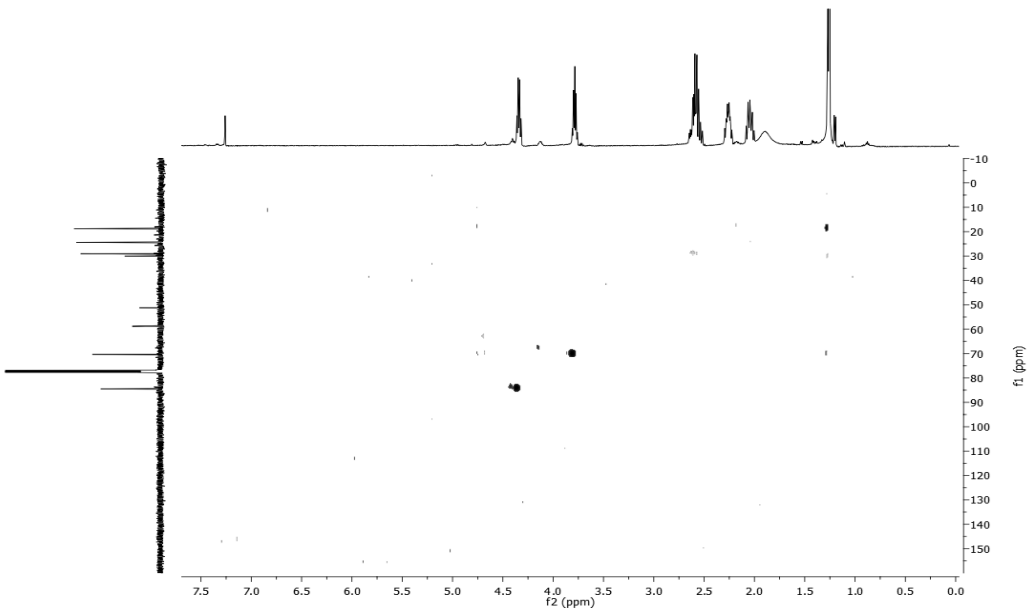

Figure 66. HSQC spectrum of lupinlactone ($CDCl_3$, 500 MHz).

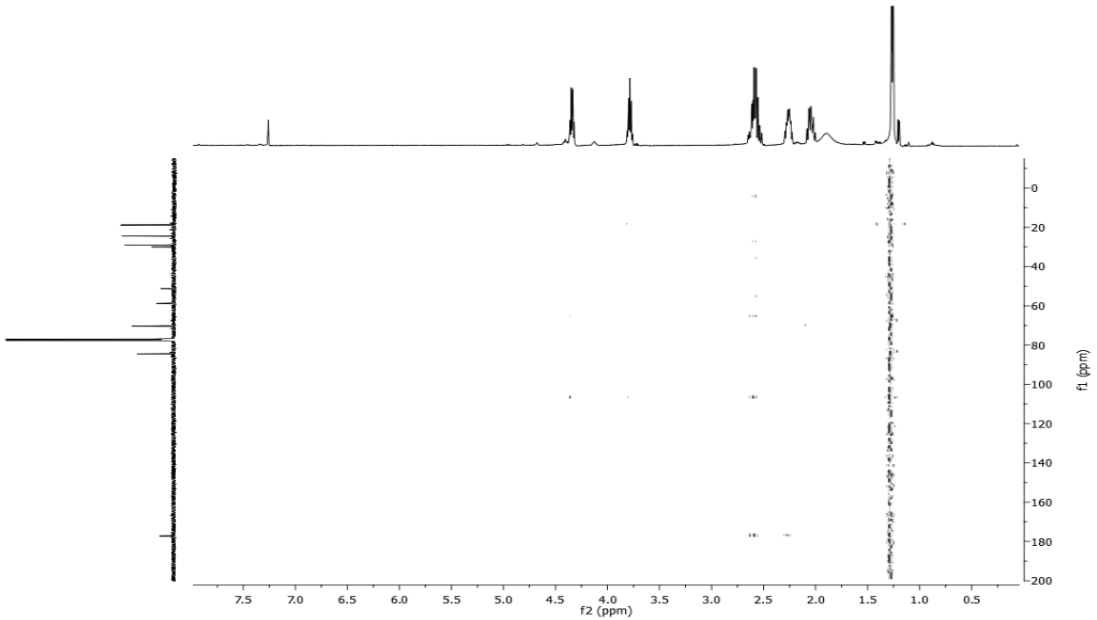

Figure 67. HMBC spectrum of lupinlactone ($CDCl_3$, 500 MHz).

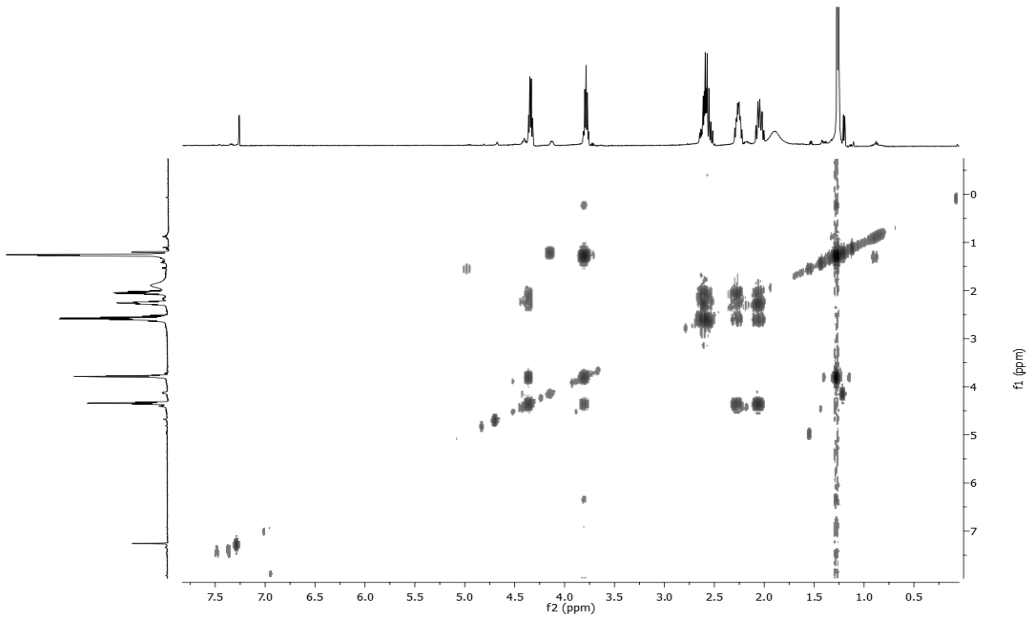

Figure 68. COSY spectrum of lupinlactone ($CDCl_3$, 500 MHz).

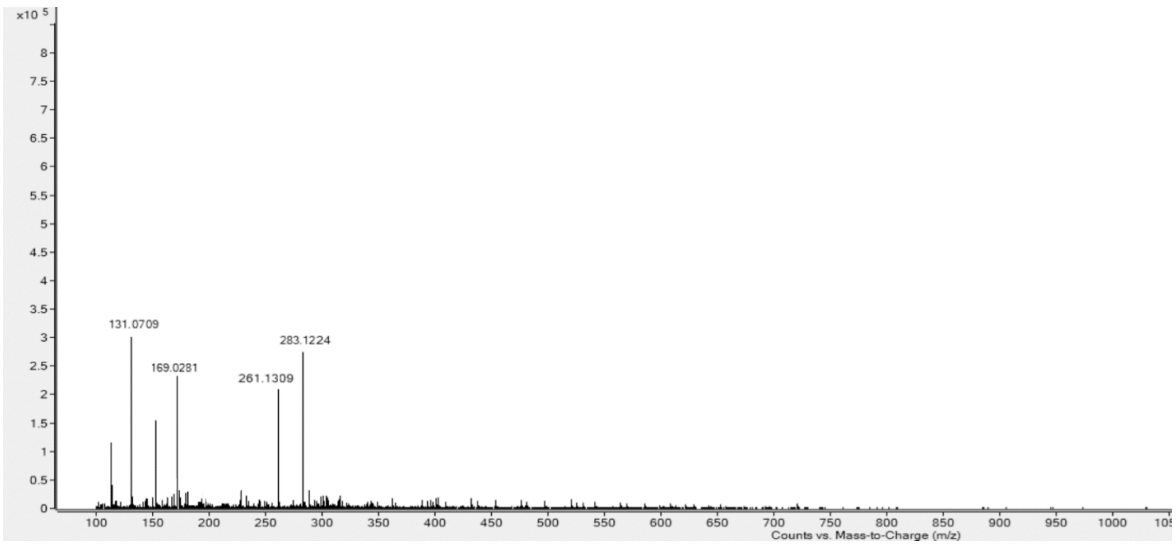

Figure 69. HRESIMS spectrum of lupinlactone.

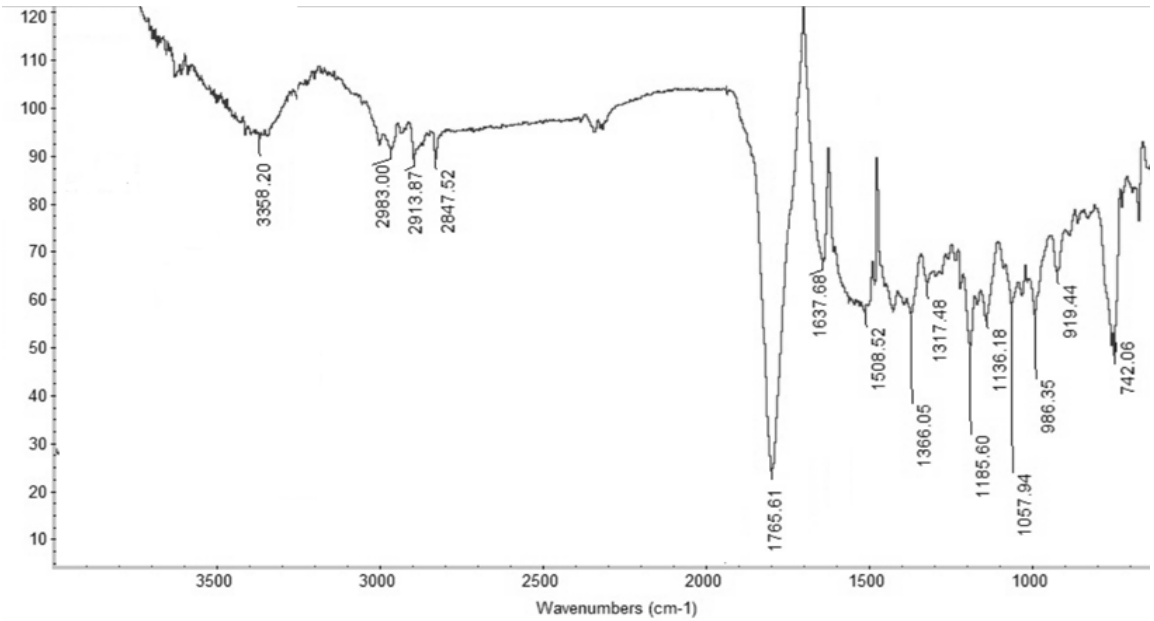

Figure 70. IR spectrum of lupinlactone.

5.3.3 Relative and absolute configuration of lupinlactone

The relative configuration of lupinlactone (**16**) was assigned by evaluation of the $^{3}J_{H,H}$ couplings constants measured in its ^{1}H NMR spectrum (Fig. 64) that allowed to locate both hydrogen at H-5 and H-6 *trans*-pseudodiaxal and consequently the hydroxyl and the methyl groups *trans*-pseudodiequatorial (Breitmaier and Voelter, 1987; Sternhell, 1969), assuming that the lactone ring has a chair-like conformation.

The absolute configuration of the secondary hydroxylated carbon (C-5) of lupinlactone (**16**) was determined by applying an advanced Mosher's method (Cimmino *et al*., 2017a).

Lupinlactone (**16**) was converted into the corresponding diastereomeric *S*-MTPA and *R*-MTPA monoesters (**19** and **20**) at C-5 by reaction with (*R*)-(-)-α-methoxy-α-trifluoromethylphenylacetyl (MTPA) and *S*-(+)-MTPA chlorides, whose spectroscopic data (Fig. 72 and 74) were consistent with the structure assigned to lupinlactone (**16**). Subtracting the chemical shift of the protons (Tab. 8) of the 5-*O*-(*R*)-MTPA (**20**) from that of 5-*O*-(*S*)-MTPA (**19**) esters, the Δδ values for all of the protons were determined as reported in Figure 71. The positive Δδ values were located on the right-hand side, and those with negative values on the left-hand side of the model A as reported in Figure 71 (Cimmino *et al*., 2017a). This model allowed the assignment of the *R* configuration at C-5 and consequently that of C-6 resulted to be *S*. Then lupinlactone (**16**) was formulated as (5*R*,6*S*)-5-hydroxy-6-methyl-tetrahydro-pyran-2-one.

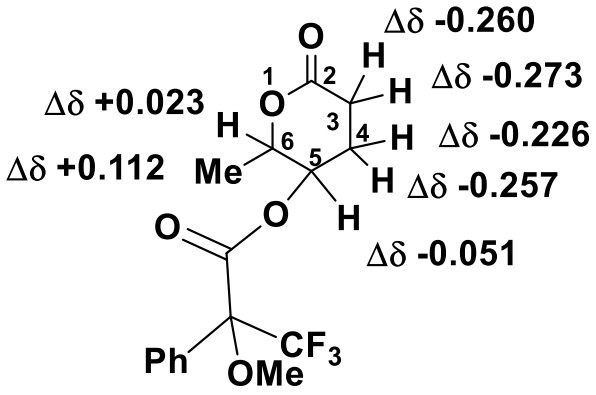

Figure 71. Structures of 5-*O*-*S*- and 5-*O*-*R*-MTPA esters of lupinlactone**.**

Table 8. ^{1}H NMR data of 5-*O*-(*S*)- and 5-*O*-(*R*)-MTPA esters of lupinlactone (**16**)[a]

	5-*O*-(*S*)- MTPA esters of lupinlactone (19)	**5-*O*-(*R*)-MTPA esters of lupinlactone (20)**
Position	**δ_H (*J* in Hz)**	**δ_H (*J* in Hz)**
2		
3	2.225 (1H) m 2.172 (1H) m	2.485 (1H) m 2.445 (1H) m
4	2.062 (1H) m 1.688 (1H) m	2.319(1H) m 1.914 (1H) m
5	5.127 (1H) br dd (10.7, 6.8)	5.178 (1H) br dd (10.7 6.8)
6	4.539 (1H) d q (10.7, 6.8)	4.516 (1H) d q (10.7, 6.8)
Me-C6	1.459 (3H) d (6.8)	1.347 (3H) d (6.8)
Ph	7.562-7.401 (5H) m	7.541-7.418 (5H) m

[a]The chemical shifts are in δ values (ppm) from TMS.

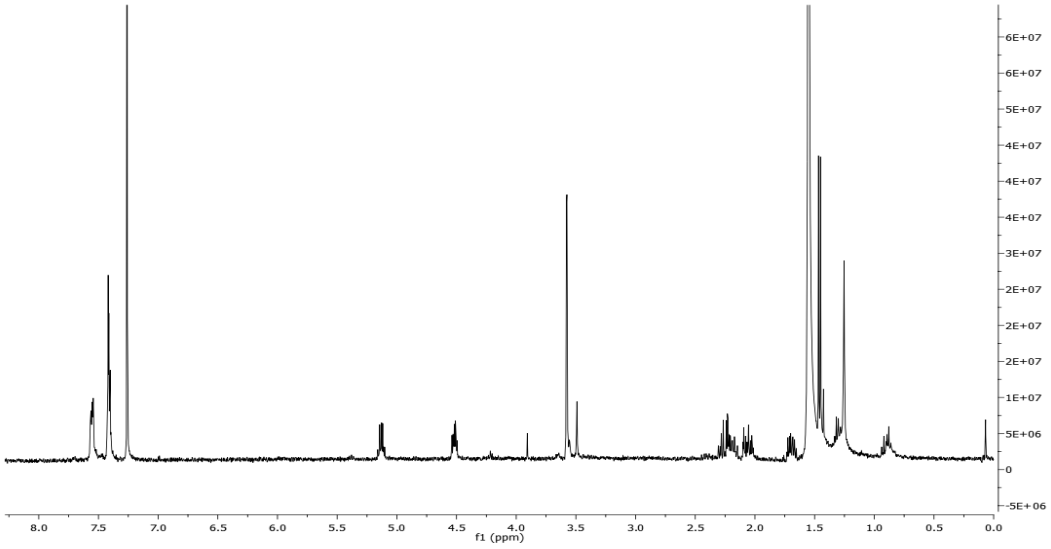

Figure 72. ^{1}H NMR spectrum of 5-*O*-(*S*)-α-methoxy-α-trifluoromethyl-α-phenylacetate (MTPA) ester of **16** ($CDCl_3$, 500 MHz).

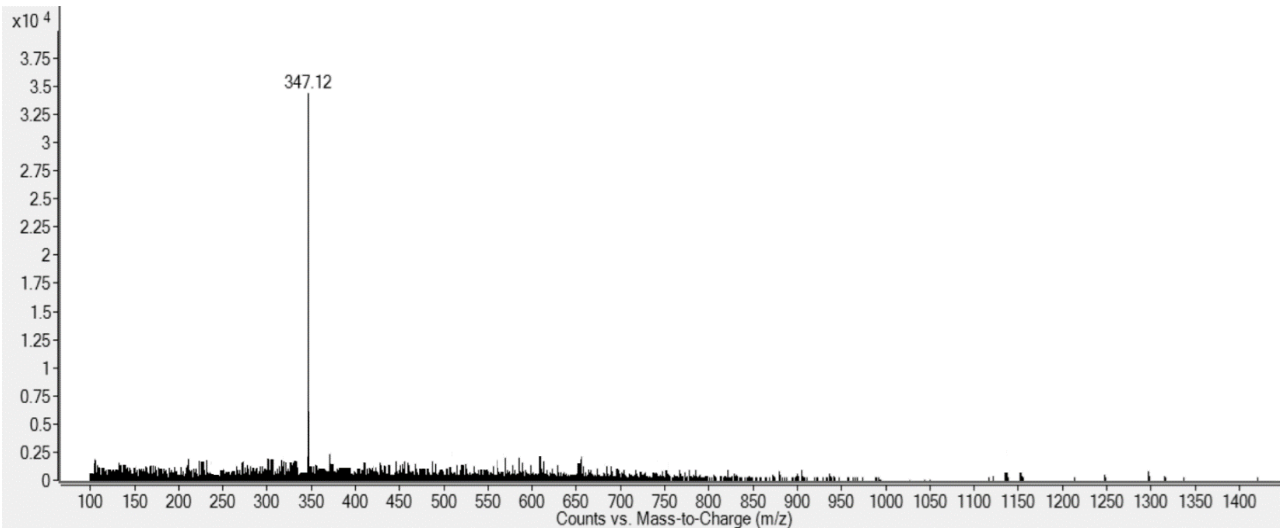

Figure 73. ESIMS spectrum of 5-*O*-(*S*)-α-methoxy-α-trifluoromethyl-α-phenylacetate (MTPA) ester of **16** ($CDCl_3$, 500 MHz).

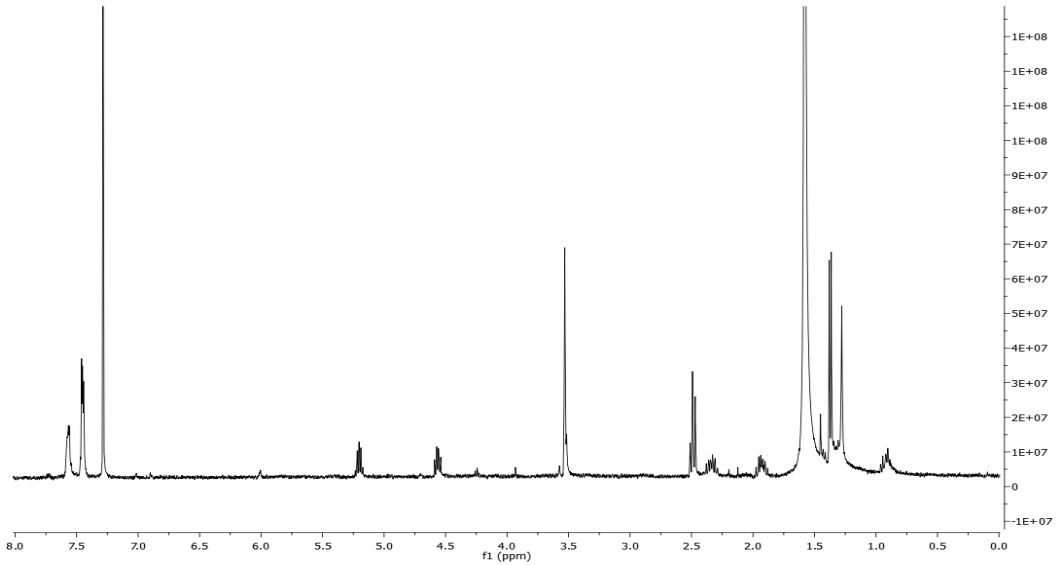

Figure 74. ^{1}H NMR spectrum of 5-*O*-(*R*)-α-methoxy-α-trifluoromethyl-α-phenylacetate (MTPA) ester of **16** ($CDCl_3$, 500 MHz).

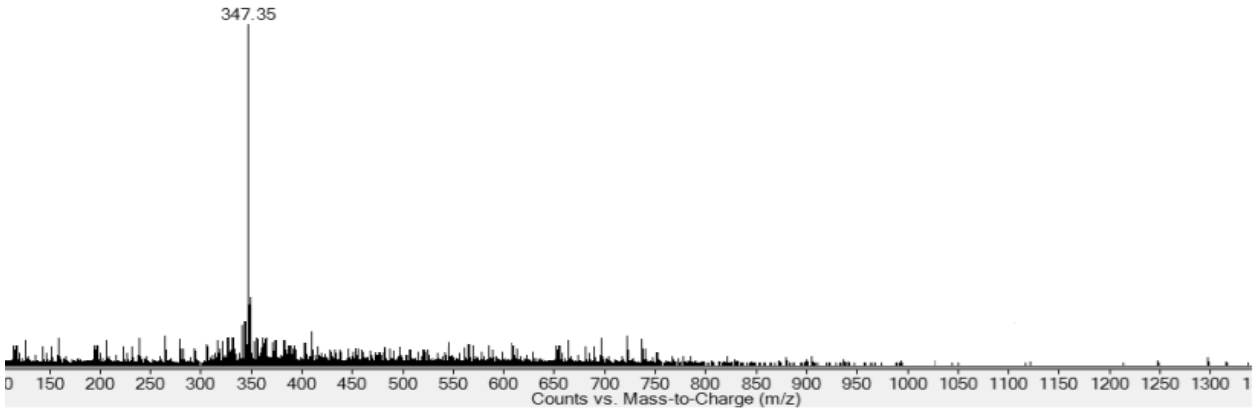

Figure 75. ESIMS spectrum of 5-*O*-(*R*)-α-methoxy-α-trifluoromethyl-α-phenylacetate (MTPA) ester of **16** ($CDCl_3$, 500 MHz).

5.3.4 Biological activities of secondary metabolites from *Colletotrichum lupini* culture filtrates.

5.3.4.1 Leaf puncture assay.

When assayed on lupin leaves, none of the pure compounds caused necrotic effects. Conversely, the culture filtrates, as well as the organic extracts and some of the fractions proved to be extremely active, causing the fast appearance of necrosis on the punctured leaves.

This probably means that the isolated compounds were not sufficiently active, when assayed individually, and thus a synergistic action could occur.

5.3.4.2 *Lemna minor* assay.

When assayed to *Lemna* fronds, all the metabolites caused an increased value in chlorophyll content (Tab. 9), which was almost double in case of tyrosol (**18**). This was partially confirmed in the assay on leaves. Indeed, in this latter assay both lupinlactone (**16**) and tyrosol (**18**) caused a retention of chlorophyll in the area of droplet application, becoming clearly evident when leaves started to turn yellow.

5.3.4.3 Assay on *Lepidium sativum* rootlet elongation.

On cress, the four metabolites tested (**15-18**) caused a reduction in root elongation around 30% (Tab. 9) regardless they type. Although not really active, this toxicity of the compounds can support the hypothesis of their synergistic activity.

5.3.4.4 Assay on seed germination of parasitic weed *Phelipanche ramosa*.

In the assay on germination of *P. ramosa* seeds, only lupindolinone (**15**) and (3*R*)-mevalolactone (**17**) caused an appreciable reduction in seed germination (32 and 42%, respectively, (Tab. 9).

Table 9. Phytotoxic effects in different biological systems[a]

Bioassay	**Cress**		**Lupin**	***Lemna minor***	***Phelipanche ramosa***
metabolite	**rootlet length (mm)**	**% reduction**	**leaf puncture**	**% chlorophyll degradation**	**% Seed germination**
Control	43.4	0	0	1.93	90
Lupindolinone (**15**)	31.4	28	0	3.16	32
Lupinlactone (**16**)	27.7	36	Green island	2.44	-
(3*R*)-Mevalonolactone (**17**)	32.1	26	0	2.49	42
Tyrosol (**18**)	29.9	31	Green island	4.70	-

[a]See materials and methods for detailed explanations

5.4 Structural identification of secondary metabolites from *Neofusicoccum batangarum* culture filtrates [4]

The organic extract of the culture filtrates of *N. batangarum* was purified, by combination of column chromatography and TLC, as detailed in Experimental section (Scheme 5) to yield five homogeneous metabolites. They were identified, by comparison of their spectroscopic and physical properties (essentially ^{1}H NMR and MS and specific optical rotation) with the data reported in literature, as (-)-(*R*)-mellein, (±)-botryosisocoumarin A, (-)-(3*R*,4*R*)- and (-)-(3*R*,4*S*)-4-hydroxymellein, (-)-terpestacin and (+)-3,4-dihydro-4,5,8-trihydroxy-3-methylisocoumarin, which was named neoisocoumarin (**21**-**26**; Fig. 76).

These data were very similar to those previously reported in literature for (-)-(*R*)-mellein (**21**) (Cole and Cox, 1981; Cabras *et al.*, 2006; Evidente *et al.*, 2010; Abou-Mansour *et al.*, 2015; Cimmino *et al*., 2017d), for (±)-botryosisocoumarin A (**22**), isolated in racemic mixture (Xu *et al*., 2012) for (-)-(3*R*,4*R*)- and (-)-(3*R*,4*S*)-4-hydroxymellein (**23** and **24**) (Cole and Cox, 1981; Devys *et al*., 1992; Cabras *et al.*, 2006; Djoukeng *et al.*, 2009; Evidente *et al.*, 2010; Abou-Mansour *et al.*, 2015) for (-)-terpestacin (**25**) (Oka *et al*., 1993; Trost, Dong and Vance, 2007; Cimmino *et al.*, 2016) and for neoisocoumarin (**26**) (Xiang Yang *et al*., 2011).

Furthermore, **21** and **23**-**25** were also identified by TLC analysis, carried out in different conditions, in comparison with the corresponding standard and by co-chromatography.

(-)-(*R*)-mellein (**21**) and its derivatives, including (-)-(3*R*,4*R*)- and (-)-(3*R*,4*S*)-4-hydroxymellein (**23** and **24**), belong to the class of isocoumarins and are widely distributed in the fungal kingdom (Krohn *et al.*, 1997; Djoukeng *et al.*, 2009; Rukachaisirikul *et al.*, 2009; Evidente *et al.*, 2010; Ramírez-Suero *et al.*, 2014; Abou-Mansour *et al.*, 2015; Cimmino *et al*., 2017d; Masi, Cimmino, *et al.*,

2018) and have also been found in other living organisms such as plants and insects (Bestmann *et al.*, 1992; Kern *et al.*, 1997; Manigaunha, Ganesh and Kharya, 2010; Herzner *et al.*, 2013). Furthermore, they are reported as phytotoxic metabolites of fungi pathogen of forest (Cimmino, Maddau, *et al.*, 2017; Masi, Maddau, *et al.*, 2018) and ornamental plants. In a recent perspective on fungal phytotoxins isolated from grapevine pathogens (Masi *et al*., 2018b), (-)-(*R*)-mellein, (3*R*,4*R*)- and (-)-(3*R*,4*S*)-4-hydroxymellein (**21**, **23** and **24**) have been reported as typical phytotoxins produced by Botryosphaeriaceae species involved in grapevine trunk disease. (-)-(*R*)-Mellein (**21**) has also been isolated from the infected grapevine wood (Abou-Mansour *et al*., 2015). These results further enhanced the idea to use them as biomarker for the development of a method to early recognize the disease (Masi *et al*., 2018b). However, the role of (-)-(*R*)-mellein, (-)-(3*R*,4*R*)- and (-)-(3*R*,4*S*)-4-hydroxymellein (**21**, **23** and **24**) in the pathogenic process is not yet clarified. In addition to phytotoxicity these compounds have been shown to exhibit a plethora of bioactivities including antiviral and antiparasitic activities (Krohn *et al.*, 1997; Höller, König and Wright, 1999; Dai *et al.*, 2001; Zhao *et al.*, 2012). From the view of potential application, some isocoumarin, as chenisocoumarin, have been evaluated for the control of noxious weeds (Cimmino *et al*., 2015b; Evidente *et al.*, 2015).

(±)-Botryoisocoumarin A (**22**) was isolated, together with two trisubstituted isochroman-1-ones from *Botryosphaeria* sp. F00741. (Xu *et al*., 2012). Then, it was also obtained together with other five metabolites from the mangrove Kandelia candel endophytic fungus *Botryopspheria* sp. KcF6 during a screening carried out to find new metabolites for drug development. (±)-Botryoisocoumarin A (**22**) showed COX-2 inhibitory activity (IC50 6.51 μM) but not any cytotoxic activity. However, the structure drawn did not correspond to that of **22** (Ju *et al*., 2015). Successively, **22** was isolated from the marine mangrove-derived fungus *Aspergillus ochraceus*, together with three new

metabolites and other eleven known ones. In this study some efforts were made to assign its absolute configuration (AC) at C-3 using X-ray methods but the results demonstrated the racemic nature of **22** that was then named (±)-botryoisocoumarin A (Liu *et al*., 2015). (±)-Botryoisocoumarin A (**22**), together with a new acetate derivative and four already known compounds were also isolated from *Aspergillus westerdijkiae* SCSIO 05233, a deep see fungus but **22** did not showed antibiotic and cytotoxic activities. (Fredimoses *et al*., 2015).

(-)-Terpestacin (**25**) together with its deacetyl analogue fusaproliferin, was recently isolated from a mangrove-derived endophytic fungus *F. proliferatum* MA-84 (Liu *et al*., 2013) and from the fimicolous fungi *Cleistothelebolus nipigonensis* and *Neogymnomyces virgineus* (Cimmino *et al*., 2016). Furthermore, some key hemisynthetic derivatives were prepared starting from terpestacin and fusaproliferin and their antifungal activity was tested against some *Ascomycetous* fungi. In particular, these metabolites and their derivatives reduced the growth of *Alternaria brassicicola*, *Botrytis cinerea* and *Fusarium graminearum*, demonstrating their allelopathic activity. (Cimmino *et al*., 2016). Recently, terpestacin was isolated, together with 9-*O*-methylfusarubin, 9-*O*-methylbostrycoidin, 5-*O*-methylnectriafurone, *trans*-methyl-*p*-coumarate, from the solid culture of this fungus *Rutstroemia capillus-albis* (*Rutstroemiaceae, Helotiales, Leotiomycetes*). This latter has been identified as the causal agent of 'bleach blonde syndrome' on the invasive annual grass weed *Bromus tectorum* (cheatgrass) in western North America (Masi *et al*., 2018c). When assayed on the host plant, 5- and 9-*O*-methylfusarubin showed high phytotoxicity at 10^{-4} M, thus they should have a role in pathogenesis on *B. tectorum* (Masi *et al*., 2018c).

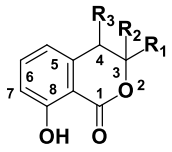

21, (-)-(*R*)-Mellein, R_1=βMe, R_2=R_3=H
22, (±)-Botryoisocoumarin, R_1=Me, R_2=OMe, R_3=H
23, (-)-(3*R*,4*R*)-4-Hydroxymellein, R_1=βMe, R_2=H, R_3=βOH
24, (-)-(3*R*,4*S*)-4-Hydroxymellein, R_1=βMe, R_2=H, R_3=αOH

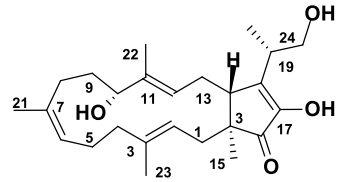

25, (-)-Terpestacin

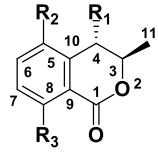

26, (+)-Neoisocoumarin, R_1=R_2=R_3=OH
27, 5,8-*O*,*O'*-dimethyl ether of neosicoumarin R_1=OH, R_2=R_3=OMe

Figure 76. *Neofusiccoccum batangarum* secondary metabolites.

5.4.1 Structural identification of (+)-neoisocoumarin

(+)-Neoisocoumarin (**26**) was previously isolated, together with two already known compounds, from the marine derived fungus *Phomopsis* sp. (No. ZH-111) during a screening aimed to found new metabolites from endophytic fungus of the South China Sea (Yang *et al*., 2011). When assayed on zebrafish, **26** significantly accelerates the growth of vessels but, it showed only weak cytotoxicity on the two cancer cell lines tested (Yang *et al*., 2011). However, the cited author, assigned only the relative configuration to **26** that, based on the correlation observed in the NOE spectrum (recorded in hexadeuterated acetone), between HO-4 and H-3 and HO-4 and Me-11 resulted to be 3R*,4S*. Recording the NOESY spectrum of **26** (Fig. 80) in the same conditions we observed the expected correlations between H-6 and H-7, H-3 and Me-11, and H-4 and Me-11 and thus **26** has the same relative configuration assigned by (Yang *et al*., 2011).

Thus, to assign the AC at C3 and C-4, **26** was firstly converted in the corresponding 5,8-*O*,*O*′-dimethyl ether derivative (**27**), whose spectroscopic data (^{1}H and ^{13}C NMR and ESIMS) are in full agreement with the structure of **26**. The ^{1}H NMR spectrum of **27** (Fig. 82) differed from that **26** essentially for the presence of the two methoxy groups at δ 3.90 and 3.88. Its ESIMS spectrum (Fig. 83) showed the dimer sodiated form $[2M+Na]^{+}$, the potassium $[M+K]^{+}$ and sodium $[M+Na]^{+}$ clusters and the protonated form $[M+H]^{+}$ at *m/z* 499, 277, 261 and 239, respectively. Furthermore, the protonated form by loss of H_2O generated the significant fragmentation ion $[M+H-H_2O]^{+}$ at *m/z* 221.

5,8-*O*,*O*'-dimethyl ether derivative of neoisocumarin (**27**) was converted into the corresponding diastereomeric *S*-MTPA and *R*-MTPA monoesters (**28** and **29**, Fig. 77) by reaction with *R*-(-)-α-methoxy-α-trifluoromethylphenylacetyl (MTPA) and *S*-(+)MTPA chlorides. Surprisingly, by investigation of ^{1}H NMR spectra of **28** and **29** (Fig. 84 and 96) compared to that of **27** we observed the

downfield shifts of H-3 (Δδ 0.48 and 0.47 in both **28** and **29**, respectively) instead of the expected downfield shift of H-4. The reaction mechanism that could explain this result is reported in Figure 77. However, the stereochemistry of C-3 and C-4 in the resulting benzofuranone did not change. The intermediate benzofuranone by reaction with with *R*-(-)-α-methoxy-α-trifluoromethylphenylacetyl (MTPA) and *S*-(+)MTPA chlorides afforded the corresponding diastereomeric *S*-MTPA and *R*-MTPA monoesters (**28** and **29**, respectively). Subtracting the chemical shifts of the protons of the 5-*O*-*R*-MTPA (**29**) from that of 5-*O*-*S*-MTPA (**28**) esters (Table 10), the Δδ (**28**–**29**) values for all the protons were determined as reported in Figure 78. The positive Δδ values were located on the right-hand side, and those with negative values on the left-hand side of the model A (Cimmino *et al*., 2017a). This model allowed the assignment of *R* configuration at C-3 and consequently, considering the relative configuration determined by NOESY and above reported, the *S* configuration at C-4. Then **26** was formulated as (+)-(3*R*,4*S*)-3,4 dihydro-4,5,8-trihydroxy-3-methylisocoumarin and named (+)-neoisocumarin.

Table 10. ^{1}H NMR data of 4-*O*-(*S*)- and 4-*O*-(*R*)-MTPA esters of 5,8-*O*,*O*'-dimetyl ether of neosisocoumarin

	4-*O*-(*S*)- MTPA esters of 5,8-*O*,*O*'-dimetyl ether of neosisocoumarin (28)	**4-*O*-(*R*)-MTPA esters of 5,8-*O*,*O*'-dimetyl ether of neosisocoumarin (29)**
Position	**δH (*J* in Hz)**	**δH (*J* in Hz)**
2		
3	5.960 (1H) dq (2.2, 6.6)	5.958 (1H) dq (2.2, 6.6)
4	5.694 (1H) d (1.9)	5.829 (1H) d (2.2)
6	7.361 (1H) d (8.9)	7.368 (1H) d (8.9)
7	7.129 (1H) dq (8.9)	7.141 (1H) d (8.8)
Me-C3	1.092 (3H) d (6.6)	0.982 (3H) d (6.6)
OMe[a]	3.950(3H) s	3.955 (3H) s
OMe[a]	3.888 (3H) s	3.896 (3H) s
OMe	3.574 (3H) s	3.626 (3H) s
Ph	7.585-7.485 (5H) m	7.584-7.481 (5H) m

[a]These two signals could be exchanged

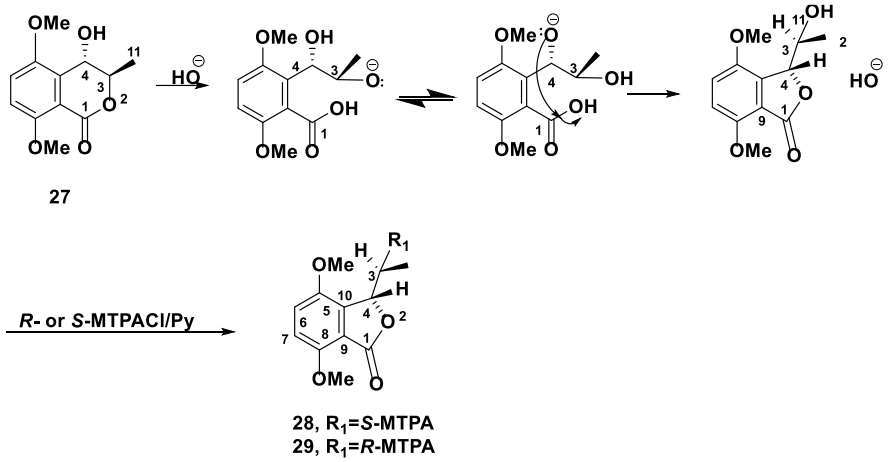

Figure 77. Mechanism of conversion of the dimethylether of neoisocoumarin (**27**) into the corresponding diastereomeric benzofuranones (**28** and **29**).

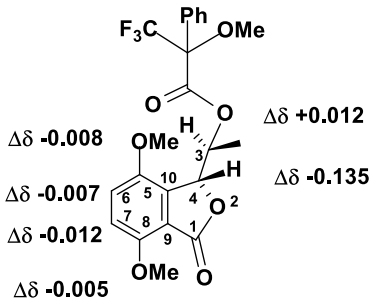

Figure 78. Structures of 4-*O*-*S*- and 4-*O*-*R*-MTPA esters of 5,8-O,O'-dimethyl ether of neosicoumarin.

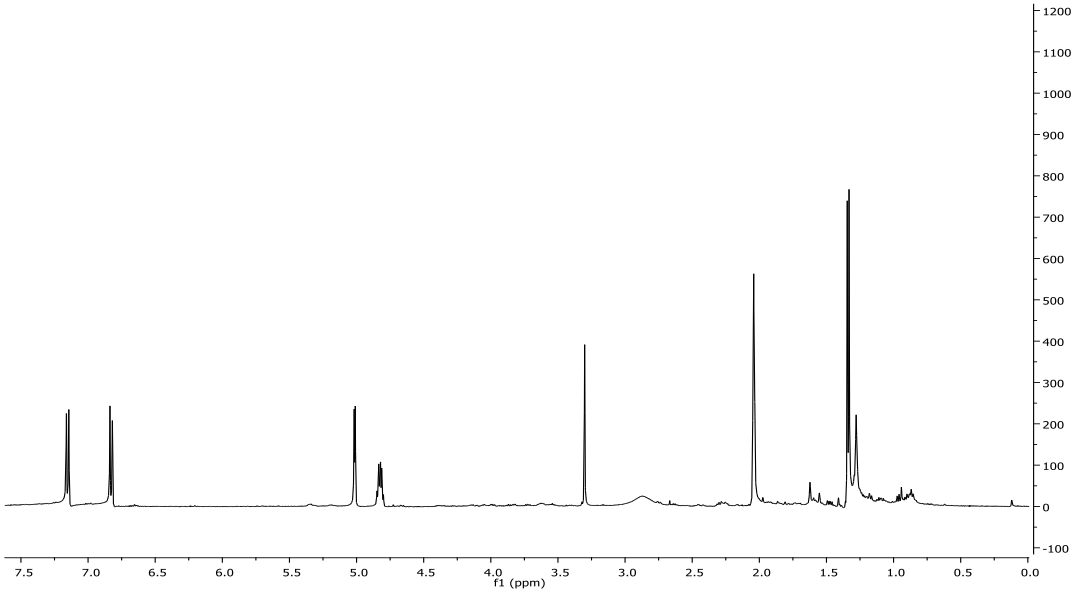

Figure 79. ^{1}H NMR spectrum of (+)-neoisocoumarin (Acetone-d_6, 500 MHz).

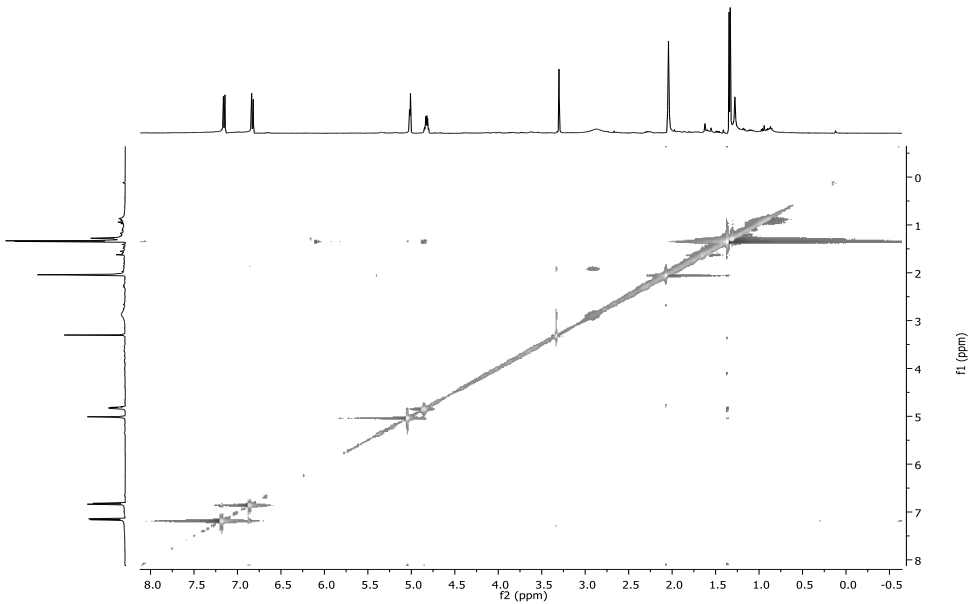

Figure 80. NOESY spectrum of neoisocoumarin (Acetone-d_6, 500 MHz).

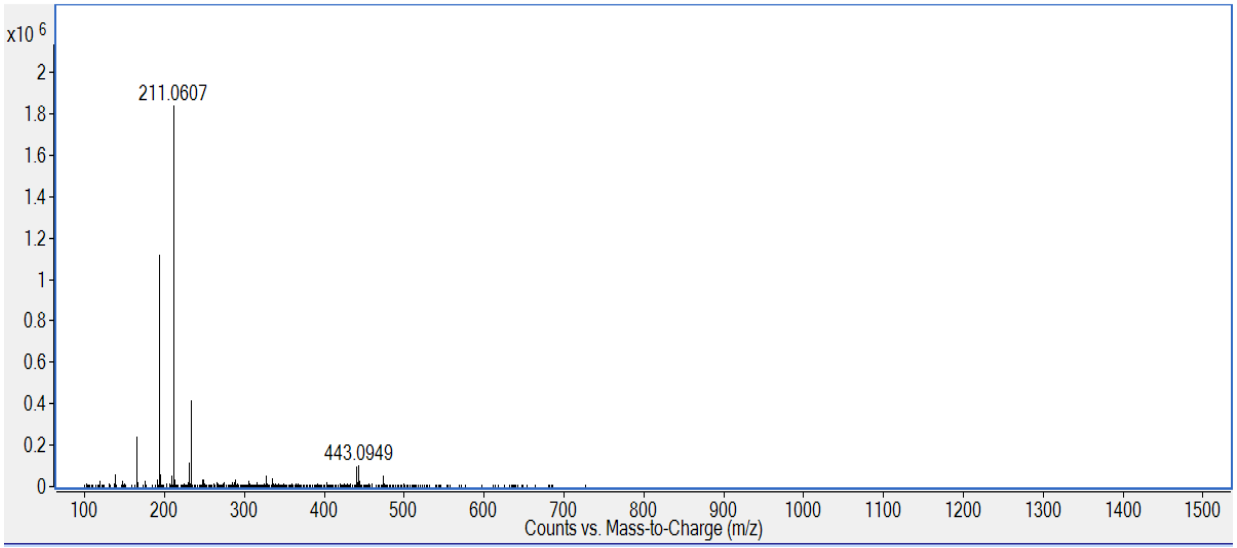

Figure 81. ESIMS spectrum of neoisocoumarin.

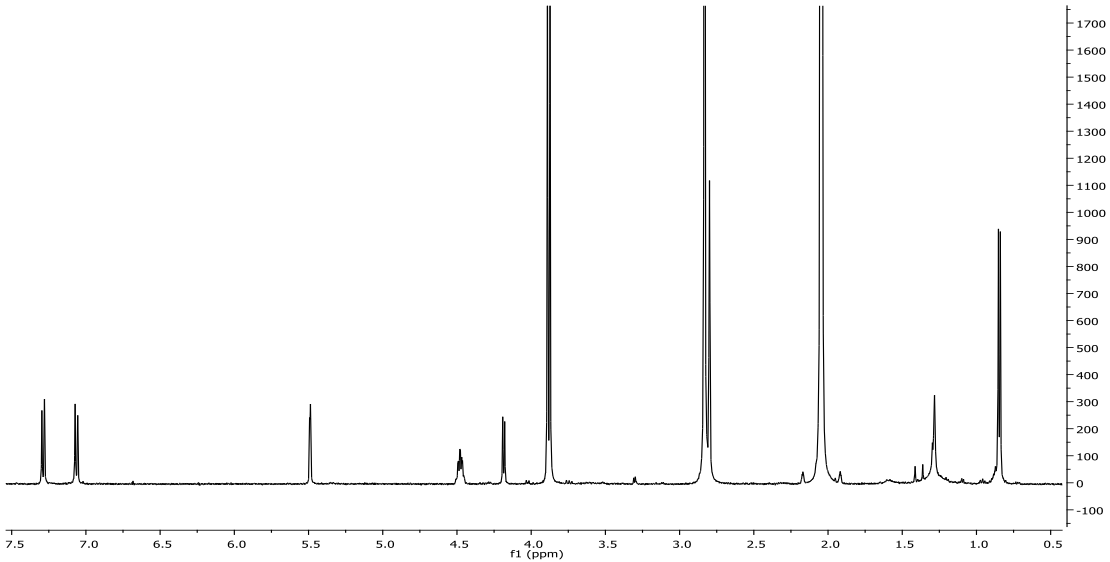

Figure 82. ^{1}H NMR spectrum of 5,8-*O*,*O*'-dimethyl ether of neoisocoumarin (Acetone-d_6, 500 MHz).

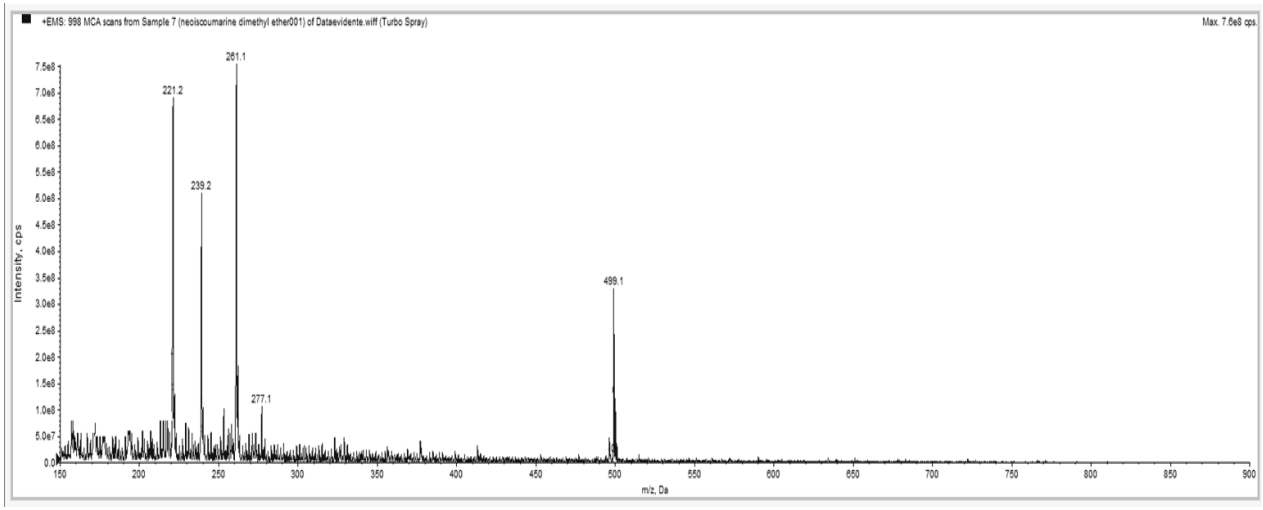

Figure 83. ESIMS spectrum of 5,8-*O*,*O*'-dimethyl ether of neoisocoumarin (Acetone-d_6, 500 MHz).

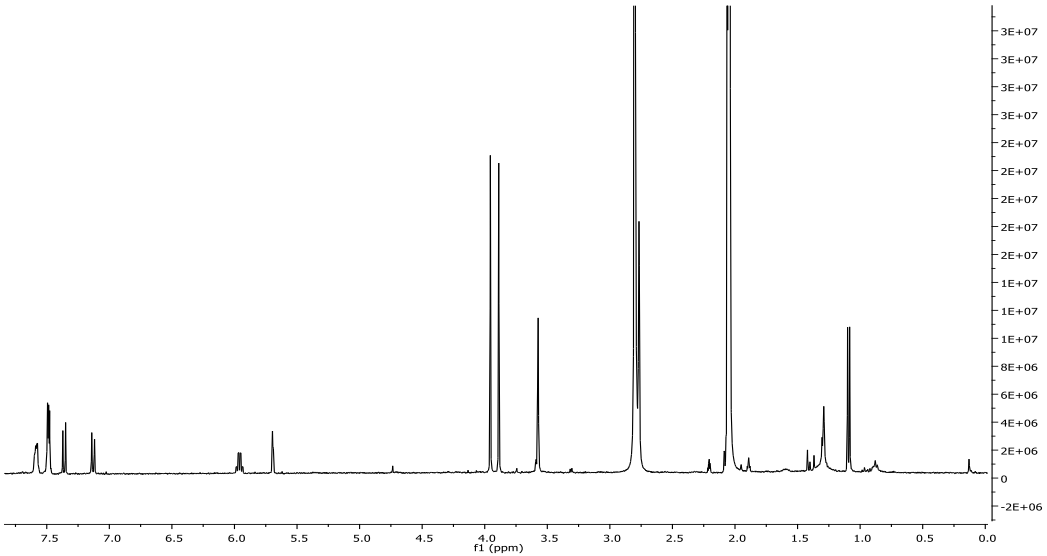

Figure 84. ^{1}H NMR spectrum of 4-*O*-(*S*)-MTPA ester of 5,8-*O*,*O*'-dimetyl ether of neoisocoumarin (Acetone-d_6, 500 MHz).

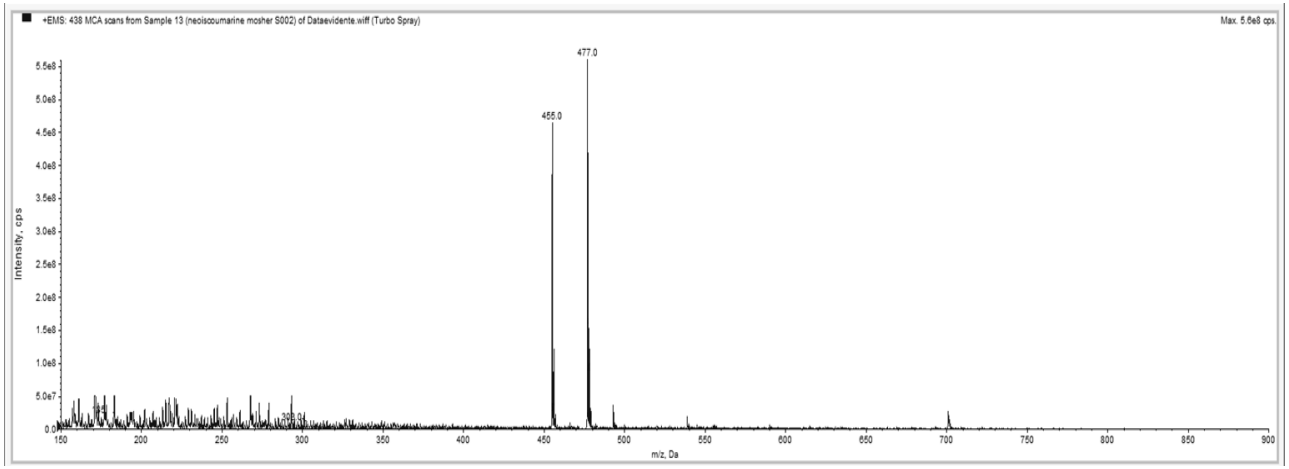

Figure 85. ESIMS spectrum of 4-*O*-(*S*)-MTPA ester of 5,8-*O*,*O*'-dimetyl ether of neoisocoumarin

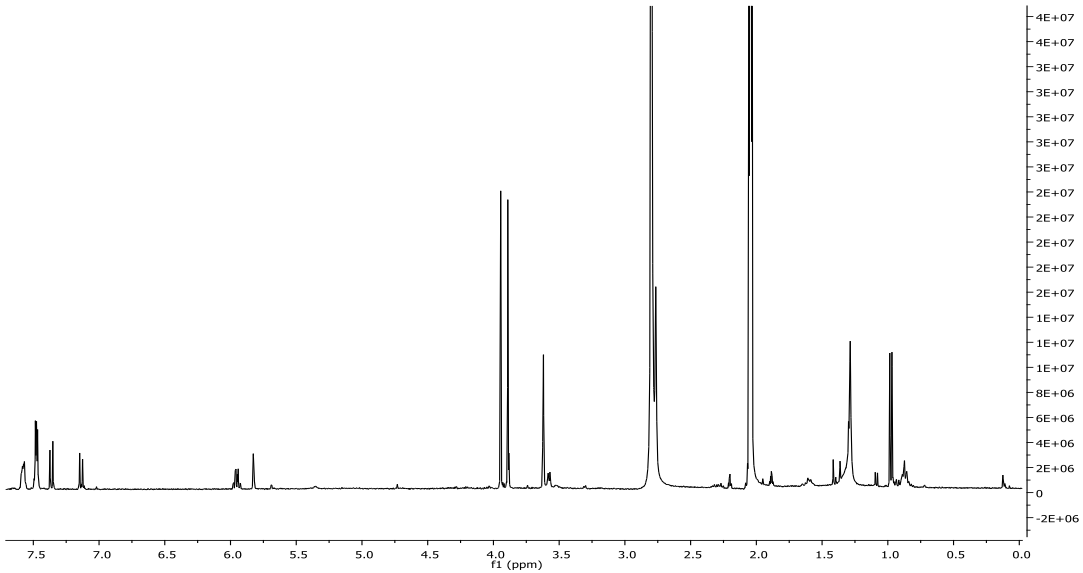

Figure 86. ^{1}H NMR spectrum of 4-*O*-(*R*)-MTPA ester of 5,8-*O*,*O*'-dimetyl ether of neoisocoumarin (Acetone-d_6, 500 MHz).

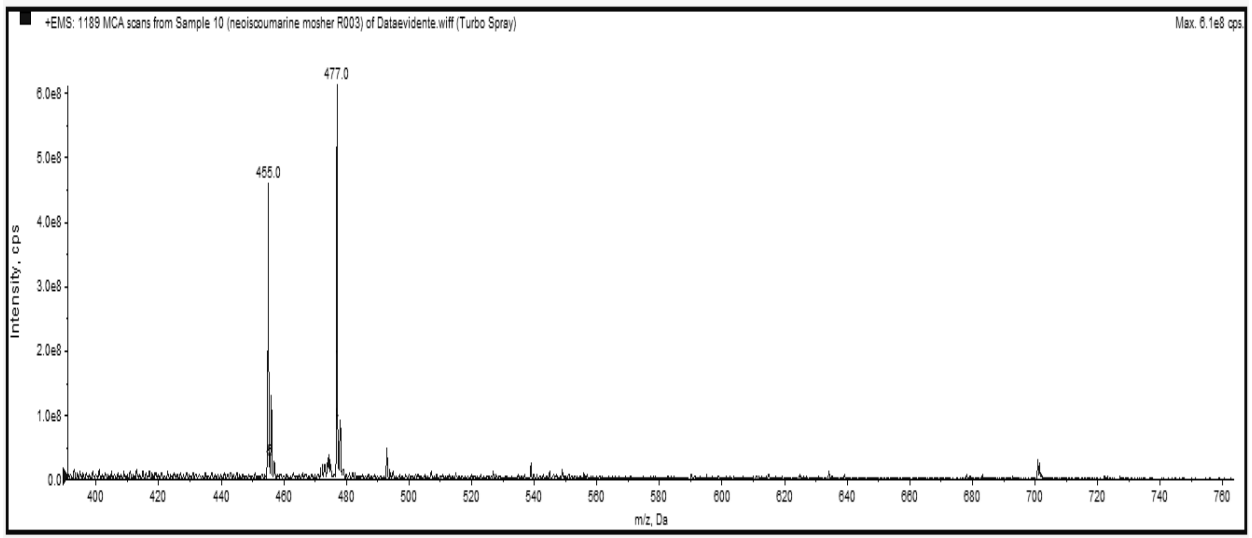

Figure 87. ESIMS spectrum of 4-*O*-(*R*)-MTPA ester of 5,8-*O*,*O*'-dimetyl ether of neoisocoumarin

5.4.2 Biological activities of fungal metabolites from *Neofusicoccum batangarum* culture filtrates

5.4.2.1 Leaf punctured assay

(-)-(*R*)-Mellein (**21**) and close (-)-(3*R*,4*R*)- and (-)-(3*R*,4*S*)- 4-hydroxymellein (**23** and **24**) were phytotoxic on both host, cactus pear, and non-host, tomato, plants (Table 10 and 11). (±)-Botryoisocoumarin A (**22**), (+)-neoisocoumarin (**26**) and (-)-terpestacin (**25**) showed phytotoxic activity both on tomato (non-host) and cactus pear (host) plants in biological assays (Table 10 and 11), even at the lowest concentration used ($2.4x10^{-4}$ M; 0.05 mg/mL). All phytotoxins (**21**-**26**) tested at the highest concentration induced necrosis around inoculation points after 7 days, on cladodes of cactus pear (Figure 89) as well on tomato leaves (Figure 88). In contrast, **21**, **23** and **24**, at the lowest concentrations used, were almost inactive to host and non-host plants. As compared to **22**, **25** and **26** proved to have almost the same spectrum of phytotoxic activity, but at a slightly lower intensity. In fact, at the same concentration **22**, **26** and **25** showed the same activity against host and non-host plants.

The results showed that (±)-botryoisocumarin A (**22**) and (+)-neoisocoumarin (**26**) were by far more phytotoxic than melleins (**21**, **23** and **24**) when tested on cladodes of cactus pear and tomato leaves. **22** and **26** were the most active at concentrations in a range from 10^{-3} M to 10^{-4} M inducing a necrosis area around inoculation points in both host and non-host plants, followed by **25**. The ability of **21**, **25** and **26** to induce large necrotic lesions on cactus pear cladodes suggests that these toxins may be involved in the scabby canker disease syndrome and the wide host spectrum of fungi in the Botryospaeriaceae family. These results could also indicate the fungi ability to produce phytotoxins active against not taxonomically related plants, such as cactus pear and tomato. Moreover, it can be hypothesized that the allelopatic activity of terpestacin enhances the ecological fitness of *N. batangarum* and might explain the ability

of this fungus to rapidly colonize the cactus pear cladode and sporulate on infected tissues before they are invaded by other saprophytes or opportunistic weak pathogens of the plant biosphere.

Table 10. Phytotoxicity on tomato of phytotoxins produced by *N. batangarum* (**21**-**26**)

Compound	Concentration (M)	Mean lesion area (mm^2) ± S.D.[a]	Compound	Concentration (M)	Mean lesion area (mm^2) ± S.D.[a]
21	5.6×10^{-3}	2.75 ± 0.68	**24**	5.2×10^{-3}	3.14 ± 0.00
	2.8×10^{-3}	2.36 ± 0.79		2.6×10^{-3}	2.75 ± 0.68
	1.4×10^{-3}	0.0 ± 0.00		1.3×10^{-3}	0.0 ± 0.00
	5.6×10^{-4}	0.0 ± 0.00		5.2×10^{-4}	0.0 ± 0.00
	2.8×10^{-4}	0.0 ± 0.00		2.6×10^{-4}	0.0 ± 0.00
22	4.8×10^{-3}	7.98 ± 1.28	**25**	2.5×10^{-3}	5.1 ± 1.29
	2.4×10^{-3}	7.46 ± 1.5		1.2×10^{-3}	5.5 ± 1.04
	1.2×10^{-3}	6.67 ± 1.5		6.2×10^{-4}	4.81 ± 1.17
	4.8×10^{-4}	6.8 ± 1.71		2.4×10^{-4}	4.81 ± 1.3
	2.4×10^{-4}	6.28 ± 1.03		1.2×10^{-4}	4.61 ± 1.6
23	5.2×10^{-3}	3.14 ± 0.00	**26**	4.8×10^{-3}	7.98 ± 1.28
	2.6×10^{-3}	2.36 ± 1.36		2.4×10^{-3}	7.07 ± 1.26
	1.3×10^{-3}	0.0 ± 0.00		1.2×10^{-3}	6.67 ± 0.81
	5.2×10^{-4}	0.0 ± 0.00		4.8×10^{-4}	4.97 ± 1.55
	2.6×10^{-4}	0.0 ± 0.00		2.4×10^{-4}	5.36 ± 1.65

[a]Mean of 12 replications (three plants and four leaves per plant)

Table 11. Phytotoxicity on Cactus Pear of phytotoxins produced by *N. batangarum* (**21**-**26**)

Compound	**Concentration (M)**	**Mean lesion area (mm^2) ± S.D.**[a]	**Compound**	**Concentration (M)**	**Mean lesion area (mm^2) ± S.D.**[a]
21	5.6×10^{-3}	3.14 ± 0.00	**24**	5.2×10^{-3}	6.28 ± 1.56
	2.8×10^{-3}	2.36 ± 0.79		2.6×10^{-3}	2.36 ± 0.79
	1.4×10^{-3}	2.75 ± 0.68		1.3×10^{-3}	3.14 ± 0.00
	5.6×10^{-4}	0.0 ± 0.00		5.2×10^{-4}	0.0 ± 0.00
	2.8×10^{-4}	0.0 ± 0.00		2.6×10^{-4}	0.0 ± 0.00
22	4.8×10^{-3}	11 ± 1.57	**25**	2.5×10^{-3}	11.58 ± 1.57
	2.4×10^{-3}	9.81 ± 1.75		1.2×10^{-3}	7.07 ± 1.67
	1.2×10^{-3}	11.78 ± 1.36		6.2×10^{-4}	6.28 ± 1.32
	4.8×10^{-4}	5.5 ± 0.79		2.4×10^{-4}	3.53 ± 0.68
	2.4×10^{-4}	7.07 ± 0.00		1.2×10^{-4}	2.94 ± 1.40
23	5.2×10^{-3}	3.14 ± 0.00	**26**	4.8×10^{-3}	11.78 ± 1.60
	2.6×10^{-3}	2.61 ± 0.93		2.4×10^{-3}	9.62 ± 1.55
	1.3×10^{-3}	3.14 ± 0.00		1.2×10^{-3}	9.62 ± 1.55
	5.2×10^{-4}	0.0 ± 0.00		4.8×10^{-4}	4.51 ± 1.61
	2.6×10^{-4}	0.0 ± 0.00		2.4×10^{-4}	3.5 ± 0.68

[a]Mean of eight replications (two cladodes from distinct plants and four punctures per each cladode).

Figure 88. Control cladode (MeOH 4%) (**a**), necrotic areas produced by (-)-(*R*)-mellein (**b**), (±)-botryoisocoumarin A (**c**), (-)-(3*R*,4*R*)-4-hydroxymellein (**d**), (-)-(3*R*,4*S*)-4-hydroxymellein (**e**), (-)-terpestacin (**f**) and (+)-neoisocoumarin (**g**) on cladodes of cactus pear.

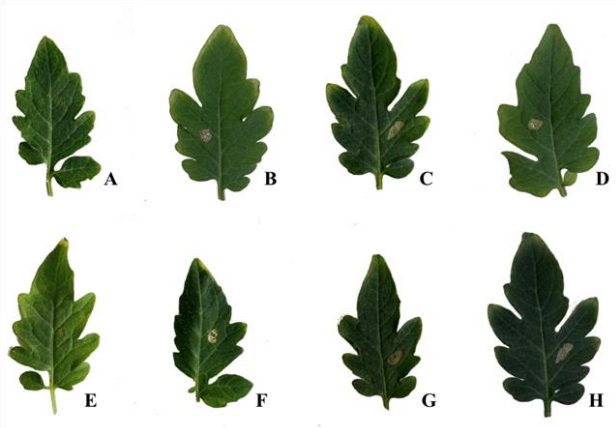

Figure 89. Control leafs with sterile distilled water (**A**) and MeOH (4%) (**E**); necrotic areas produced by (-)-(*R*)-mellein (**B**), (±)-botryoisocoumarin A (**C**), (-)-(3*R*,4*R*)-4-hydroxymellein (**D**), (-)-(3*R*,4*S*)-4-hydroxymellein (**F**), (-)-terpestacin (**G**) and (+)-neoisocoumarin (**H**) on tomato leaves.

6 CONCLUSIONS AND FUTURE PROSPECTIVE

In this thesis project, different phytotoxic metabolites (**1**-**5**, **7**-**18** and **21**-**26**) involved in heavy disease of some important agrarian crops have been identified, as below reported:

- *Ascochyta lentis* var. *lathyri* has recently been reported to be the causal agent of Ascochyta blight of grasspea (*Lathyrus sativus*), a disease characterized by the appearance of necrotic lesions of leaves and stems. From its culture filtrate two new phytotoxic metabolites have been isolated and named lathyroxins A and B (**1** and **2,** Fig. 6), which were characterized by spectroscopic methods as 4-(2-hydroxy-3,3-dimethoxypropyl)phenol (**1**) and 3-(4-hydroxyphenyl)propane-1,2-diol (**2**), respectively. The absolute configuration at C-2 of their 2-dimethoxy- and 2,3-diol-propyl side chain was assigned as *R*.

Moreover, other well-known fungal metabolites were isolated and identified as *p*-hydroxybenzaldehyde, *p*-methoxyphenol and tyrosol (**3**-**5**, Fig. 6).

Tested in different bioassays, lathyroxins A and B (**1** and **2**) showed interesting phytotoxic properties, being able to cause necrosis on leaves and to inhibit seed germination and rootlet elongation while they had no effects against some not target organisms.

- A strain of the pathogenic fungus *Ascochyta lentis*, the causal agent of Ascochyta blight of lentil (*Lens culinaris*) has been isolated and it was able to produce phytotoxic metabolites.

Three new anthraquinones derivatives, named lentiquinones A, B and C (**7**-**9**, Fig. 22), were isolated from its culture filtrates together with the well-known lentisone (**10**, Fig. 22). From its mycelium four already known analogues were identified as pachybasin, ω-hydroxypachybasin, 1,7-dihydroxy-3-methylanthracene-9,10-dione and phomarin (**11**-**14**, Fig. 22). Lentiquinones A-C (**7**-**9**) were characterized by spectroscopic methods as 3,4,6-tri-hydroxy-8-methyl-2*H*-benzo[γ]chromene-5,10-dione, 2,3,4,5,10-penta-hydroxy-7-methyl-

3,4,4a,10-tetrahydro-anthracen-9(2*H*)-one and its 2-epimer, respectively, and the relative configuration of the two latter compounds was deduced by X-ray analysis. Their absolute configuration was determined by electronic circular dichroism (ECD) in solution and solid state, and TDDFT calculations as 2*R*,3*S*,4*S*,4a*S* and 2*S*,3*S*,4*S*,4a*S*,10*R* (**8** and **9**), respectively.

When tested for the biological activity, using different bioassays, the novel compounds (**7**-**9**) showed interesting activities. In fact, when applied to punctured leaves, the three new compounds and lentisone (**7**-**9** and **10**) caused severe necrosis, and lentiquinone A (**7**) resulted to be the most active among the new metabolites. On cress, this latter compound (**7**) proved to be particularly active in inhibiting root elongation. On *Lemna minor* all the compounds (**7**-**14**) reduced the content of chlorophyll, with 1,7-dihyroxy-3-methylanthracene (**11**) that resulted to be the most active. Moreover, the new compounds, and lentisone (**7**-**9** and **10**) proved to have antibiotic properties.

- *Colletotrichum lupini*, the causal agent of anthracnose of lupin *(Lupinus albus* L.), a destructive seed-borne disease affecting stems and pods, has been grown *in vitro* to produce phytotoxic compounds. From its culture filtrates a 3-substituted indolinone, named lupindolinone (**15**, Fig. 55), and a 5,6-disubstituted tetrahydro-α-pyrone, named lupinlactone (**16**, Fig. 55), were isolated together with the known (3*R*)-mevalolactone and tyrosol (**17** and **18**, Fig 55). The absolute configuration of lupinlactone (**16**) at C-5 was determined applying the modified Mosher's method and considering its relative stereochemistry. Thus, the AC of lupinlactone was assigned as (5*R*, 6*S*).

Moreover, all the metabolites (**15**-**18**) were assayed using different biological tests and proved to have phytotoxic activities.

- *Neofusicoccum bagantarum*, the causal agent of cactus pear (*Opuntia ficus-indica* L.) canker, was isolated in a minor island in Sicily. The phytotoxic secondary metabolites isolated from its culture filtrates were identified as (-)-

(*R*)-mellein, (±)-botryosisocoumarin A, (-)-(3*R*,4*R*)- and (-)-(3*R*,4*S*)-4-hydroxymellein, (-)-terpestacin and (+)-3,4-dihydro-4,5,8-trihydroxy-3-methyl-isocoumarin, which was named neoisocoumarin (**21**-**26**; Fig. 76). They were identified, by comparison of their spectroscopic and physical properties (essentially ^{1}H NMR and MS and specific optical rotation) with the data reported in literature. The absolute configuration to neoisocoumarin (**26**) was assigned for the first time as (3*R*,4*S*) by applying the advanced Mosher's method.

Considering the phytotoxic activity on both host (cactus pear) and non-host (tomato leaves) test plants, it can be supposed that all the metabolites (**21**-**26**) are involved in the syndrome of scabby cankers disease of cactus pear and, like other Botryosphaeriaceae, *N. batangarum* has a wider host range than presently known.

In conclusion, the study of those compounds could be exploited to use them to:

- Understand their role in induction of disease symptoms;
- Develop a rapid and specific method for plant disease diagnosis;
- Develop method for their large-scale production by fermentation or total enantiomeric selective synthesis;
- Obtain variety of host plant resistant to the fungal disease;
- Prepare derivatives for structure-activity relationship and mode on action studies;
- Find bioactive metabolites with potential practical application in agriculture as biopesticides (natural safe herbicides, fungicides, insecticides etc.) and in medicine as pro-drug (anticancer, antibiotic, antimalaria, ant inflammatory etc.) with new mode of action.

7 BIBLIOGRAPHY

Abbas, H.K., and Duke, S.O. (1995). Phytotoxins from plant pathogens as potential herbicides. J. Toxicol. Toxin Rev *14*, 523–543.

Abou-Mansour, E., Débieux, J.-L., Ramírez-Suero, M., Bénard-Gellon, M., Magnin-Robert, M., Spagnolo, A., Chong, J., Farine, S., Bertsch, C., and L'Haridon, F. (2015). Phytotoxic metabolites from *Neofusicoccum parvum*, a pathogen of Botryosphaeria dieback of grapevine. Phytochemistry *115*, 207–215.

Affolter, C., Buhlmann, P., and Pretsch, E. (2000). Structure Determination of Organic Compounds: Tables of Spectral Data (Berlin Heidelberg: Springer).

Ahn, J.W., Lee, M.K., Choi, S.U., Lee, C.O., and Kim, B.S. (1998). Cytotoxic ophiobolins produced by Bipolaris sp. J. Microbiol. Biotechnol *8*, 406–408.

Alam, S.S., Bilton, J.N., Slawin, A.M.Z., Williams, D.J., Sheppard, R.N., and Strange, R.N. (1989). Chickpea blight: production of the phytotoxins solanapyrones A and C by *Ascochyta rabiei*. Phytochemistry *28*, 2627–2630.

Altomare, A., Burla, M.C., Camalli, M., Cascarano, G.L., Giacovazzo, C., Guagliardi, A., Moliterni, A.G., Polidori, G., and Spagna, R. (1999). SIR97: a new tool for crystal structure determination and refinement. J. Appl. Crystallogr *32*, 115–119.

Andolfi, A., Cimmino, A., Evidente, A., Iannaccone, M., Capparelli, R., Mugnai, L., and Surico, G. (2009). A new flow cytometry technique to identify *Phaeomoniella chlamydospora* exopolysaccharides and study mechanisms of esca grapevine foliar symptoms. Plant Dis *93*, 680–684.

Andolfi, A., Cimmino, A., Villegas-Fernández, A.M., Tuzi, A., Santini, A., Melck, D., Rubiales, D., and Evidente, A. (2013). Lentisone, a new phytotoxic anthraquinone produced by *Ascochyta lentis*, the causal agent of Ascochyta blight in *Lens culinaris*. J. Agric. Food Chem *61*, 7301–7308.

Araújo, S.S., Beebe, S., Crespi, M., Delbreil, B., González, E.M., Gruber, V., Lejeune-Henaut, I., Link, W., Monteros, M.J., Prats, E., et al. (2015). Abiotic stress responses in legumes: strategies used to cope with environmental challenges. Crit. Rev. Plant Sci *34*, 237–280.

Atkins, S.D., and Clark, I.M. (2004). Fungal molecular diagnostics: a mini review. J Appl Genet *45*, 3–15.

Au, T.K., Chick, W.S.H., and Leung, P.C. (2000). The biology of ophiobolins. Life Sci. *67*, 733–742.

Ayres, P.G. (1981). Effects of disease on the physiology of the growing plant (CUP Archive).

Aznar-Fernández, T., Cimmino, A., Masi, M., Rubiales, D., and Evidente, A. (2019). Antifeedant activity of long-chain alcohols, and fungal and plant metabolites against pea aphid (*Acyrthosiphon pisum*) as potential biocontrol strategy. Nat. Prod. Res *33*, 2471–2479.

Badertscher, M., Bühlmann, P., and Pretsch, E. (2009). Structure determination of organic compounds: Tables of spectral data (Berlin Heidelberg: Springer).

Bajsa, J., Singh, K., Nanayakkara, D., Duke, S.O., Rimando, A.M., Evidente, A., and Tekwani, B.L. (2007). A survey of synthetic and natural phytotoxic compounds and phytoalexins as potential antimalarial compounds. Biol. Pharm. Bull *30*, 1740–1744.

Balde, E.S., Andolfi, A., Bruyère, C., Cimmino, A., Lamoral-Theys, D., Vurro, M., Damme, M. Van, Altomare, C., Mathieu, V., and Kiss, R. (2010). Investigations of fungal secondary metabolites with potential anticancer activity. J. Nat. Prod *73*, 969–971.

Bani, M., Cimmino, A., Evidente, A., Rubiales, D., and Rispail, N. (2018). Pisatin involvement in the variation of inhibition of *Fusarium oxysporum* f. sp. *pisi* spore germination by root exudates of Pisum spp. germplasm. Plant Pathol *67*, 1046–1054.

Barilli, E., Cimmino, A., Masi, M., Evidente, M., Rubiales, D., and Evidente, A. (2017). Inhibition of early development stages of rust fungi by the two fungal metabolites cyclopaldic acid and *epi*-epoformin. Pest Manag. Sci *73*, 1161–1168.

Beaver, J.S., Rosas, J.C., Myers, J., Acosta, J., Kelly, J.D., Nchimbi-Msolla, S., Misangu, R., Bokosi, J., Temple, S., and Arnaud-Santana, E. (2003). Contributions of the Bean/Cowpea CRSP to cultivar and germplasm development in common bean. F. Crop. Res *82*, 87–102.

Bérdy, J. (1980). Handbook of antibiotic compounds (Florida: Crc Press).

Berestetskii, O.A., and Borovkov, A. V (1979). Phytotoxic metabolites of soil penicillia. Mikrobiol. Zh *41*, 291-302.

Berestetskii, O.A., and Borovkov, A. V (1981). Phytotoxic metabolites of soil Aspergillus species [Fungi]. Mikrobiol. Zh *43*, 515-530

Berestetskiy, A.O. (2008). A review of fungal phytotoxins: from basic studies to practical use. Appl. Biochem. Microbiol *44*, 453.

Berger, S., and Braun, S. (2004). 200 and more NMR experiments (Weinheim: Wiley-Vch).

Bestmann, H.J., Kern, F., Schäfer, D., and Witschel, M.C. (1992). 3,4-Dihydroisocoumarins, a new class of ant trail pheromones. Angew. Chemie Int. Ed. Engl *31*, 795–796.

Bhatnagar-Mathur, P., Palit, P., Kumar, C.S., Reddy, D.S., and Sharma, K.K. (2012). Grain legumes: biotechnological interventions in crop improvement for adverse environments. Improv. Crop Product. Sustain. Agric 16, 381–421.

Bick, I.R.C., and Rhee, C. (1966). Anthraquinone pigments from *Phoma foveata* Foister. Biochem. J *98*, 112-116.

Boari, A., and Vurro, M. (2004). Evaluation of Fusarium spp. and other fungi as biological control agents of broomrape (*Orobanche ramosa*). Biol. Control *30*, 212–219.

Bohlool, B.B., Ladha, J.K., Garrity, D.P., and George, T. (1992). Biological nitrogen fixation for sustainable agriculture: A perspective. Plant Soil *141*, 1–11.

Boote, K.J., Jones, J.W., Mishoe, J.W., and Berger, R.D. (1983). Coupling pests to crop growth simulators to predict yield reductions [Mathematical models]. Phytopathol *73*, 1581-1587.

Borges, W. de S., and Pupo, M.T. (2006). Novel anthraquinone derivatives produced by *Phoma sorghina*, an endophyte found in association with the medicinal plant *Tithonia diversifolia* (Asteraceae). J. Braz. Chem. Soc *17*, 929–934.

Bottalico, A., Capasso, R., Evidente, A., Randazzo, G., and Vurro, M. (1990). Cytochalasins: structure-activity relationships. Phytochemistry *29*, 93–96.

Brandwagt, B.F., Kneppers, T.J.A., Van der Weerden, G.M., Nijkamp, H.J.J., and Hille, J. (2001). Most AAL toxin-sensitive Nicotiana species are resistant to the tomato fungal pathogen *Alternaria alternata* f. sp. *lycopersici*. Mol. Plant-Microbe Interact *14*, 460–470.

Breitmaier, E., and Voelter, W. (1987). Carbon-13 NMR spectroscopy (Florida: VCH Publishers Inc).

Bruhn, T., Schaumlöffel, A., Hemberger, Y., and Bringmann, G. (2013). SpecDis: quantifying the comparison of calculated and experimental electronic circular dichroism spectra. Chirality *25*, 243–249.

Bruhn, T., Schaumlöffel, A., Hemberger, Y., and Pescitelli, G. (2019). SpecDis version 1.71; Berlin, Germany. 2017. Available Online Https/Specdis-Software. Jimdo. Com (Accessed 18 August 2018).

Bury, M., Girault, A., Megalizzi, V., Spiegl-Kreinecker, S., Mathieu, V., Berger, W., Evidente, A., Kornienko, A., Gailly, P., and Vandier, C. (2013). Ophiobolin A induces paraptosis-like cell death in human glioblastoma cells by decreasing BKCa channel activity. Cell Death Dis *4*, e561.

Butler, M.S. (2004). The role of natural product chemistry in drug discovery. J. Nat. Prod *67*, 2141–2153.

Cabras, A., Mannoni, M.A., Serra, S., Andolfi, A., Fiore, M., and Evidente, A. (2006). Occurrence, isolation and biological activity of phytotoxic metabolites produced in vitro by *Sphaeropsis sapinea*, pathogenic fungus of *Pinus radiata*. Eur. J. Plant Pathol *115*, 187-193.

Canonica, L., Fiecchi, A., Kienle, M.G., and Scala, A. (1966). The constitution of cochliobolin. Tetrahedron Lett *7*, 1211–1218.

Capasso, R., Cristinzio, G., Evidente, A., and Scognamiglio, F. (1992). Isolation, spectroscopy and selective phytotoxic effects of polyphenols from vegetable waste waters. Phytochemistry *31*, 4125–4128.

Chang, Y.-C., Deng, T.-S., Pang, K.-L., Hsiao, C.-J., Chen, Y.-Y., Tang, S.-J., and Lee, T.-H. (2013). Polyketides from the littoral plant associated fungus *Pseudallescheria boydii*. J. Nat. Prod *76*, 1796–1800.

Cimmino, A., Andolfi, A., Fondevilla, S., Abouzeid, M.A., Rubiales, D., and Evidente, A. (2012a). Pinolide, a new nonenolide produced by *Didymella pinodes*, the causal agent of ascochyta blight on *Pisum sativum*. J. Agric. Food Chem *60*, 5273–5278.

Cimmino, A., Andolfi, A., Zonno, M.C., Troise, C., Santini, A., Tuzi, A., Vurro, M., Ash, G., and Evidente, A. (2012b). Phomentrioloxin: a phytotoxic pentasubstituted geranylcyclohexentriol produced by Phomopsis sp., a potential mycoherbicide for *Carthamus lanatus* biocontrol. J. Nat. Prod *75*, 1130–1137.

Cimmino, A., Andolfi, A., Avolio, F., Ali, A., Tabanca, N., Khan, I.A., and Evidente, A. (2013). Cyclopaldic acid, seiridin, and sphaeropsidin A as fungal phytotoxins, and larvicidal and biting deterrents against *Aedes aegypti* (*Diptera*: *Culicidae*): structure-activity relationships. Chem. Biodivers *10*, 1239–1251.

Cimmino, A., Fernández-Aparicio, M., Andolfi, A., Basso, S., Rubiales, D., and Evidente, A. (2014). Effect of fungal and plant metabolites on broomrapes (Orobanche and Phelipanche spp.) seed germination and radicle growth. J. Agric. Food Chem *62*, 10485–10492.

Cimmino, A., Masi, M., Evidente, M., Superchi, S., and Evidente, A. (2015a). Fungal phytotoxins with potential herbicidal activity: chemical and biological characterization. Nat. Prod. Rep *32*, 1629–1653.

Cimmino, A., Masi, M., Evidente, M., and Evidente, A. (2015b). Fungal phytotoxins with potential herbicidal activity to control *Chenopodium album*. Nat. Prod. Commun. *10*, 1119-1126.

Cimmino, A., Evidente, M., Masi, M., Ali, A., Tabanca, N., Khan, I.A., and Evidente, A. (2015c). Papyracillic acid and its derivatives as biting deterrents against *Aedes aegypti* (*Diptera: Culicidae*): structure–activity relationships. Med. Chem. Res *24*, 3981–3989.

Cimmino, A., Sarrocco, S., Masi, M., Diquattro, S., Evidente, M., Vannacci, G., and Evidente, A. (2016). Fusaproliferin, terpestacin and their derivatives display variable allelopathic activity against some Ascomycetous fungi. Chem. Biodivers *13*, 1593–1600.

Cimmino, A., Masi, M., Evidente, M., Superchi, S., and Evidente, A. (2017a). Application of Mosher's method for absolute configuration assignment to bioactive plants and fungi metabolites. J. Pharm. Biomed. Anal *144*, 59–89.

Cimmino, A., Iannaccone, M., Petriccione, M., Masi, M., Evidente, M., Capparelli, R., Scortichini, M., and Evidente, A. (2017b). An ELISA method to identify the phytotoxic *Pseudomonas syringae* pv. *actinidiae* exopolysaccharides: A tool for rapid immunochemical detection of kiwifruit bacterial canker. Phytochem. Lett *19*, 136–140.

Cimmino, A., Cinelli, T., Masi, M., Reveglia, P., da Silva, M.A., Mugnai, L., Michereff, S.J., Surico, G., and Evidente, A. (2017c). Phytotoxic lipophilic metabolites produced by grapevine strains of Lasiodiplodia species in Brazil. J. Agric. Food Chem *65*, 1102–1107.

Cimmino, A., Maddau, L., Masi, M., Linaldeddu, B.T., Pescitelli, G., and Evidente, A. (2017d). Fraxitoxin, a new isochromanone isolated from *Diplodia fraxini*. Chem. Biodivers *14*, 1-6.

Cimmino, A., Nocera, P., Linaldeddu, B.T., Masi, M., Gorecki, M., Pescitelli, G., Montecchio, L., Maddau, L., and Evidente, A. (2018). Phytotoxic metabolites produced by *Diaporthella cryptica*, the causal agent of hazelnut branch canker. J. Agric. Food Chem *66*, 3435–3442.

Clark, A.M. (1996). Natural products as a resource for new drugs. Pharm. Res *13*, 1133–1141.

Clark, M.F., and Adams, A.N. (1977). Characteristics of the microplate method of enzyme-linked immunosorbent assay for the detection of plant viruses. J. Gen. Virol *34*, 475–483.

Cocks, P.S., and Bennett, S.J. (1999). Introduction: Role of pasture and forage legumes in Mediterranean farming systems. In Genetic resources of Mediterranean pasture and forage legumes, (Springer, Dordrecht), pp. 9–19.

Cole, R.J., and Cox, R.H. (1981). Handbook of toxic fungal metabolites (New York: Academic Press).

Colombo, L., Gennari, C., Scolastico, C., Aragozzini, F., and Merendi, C. (1979). Biosynthesis of ascochitine: incorporation studies with advanced precursors. J. Chem. Soc. Chem. Commun *11*, 492–493.

Coyne, D.P., Steadman, J.R., Godoy-Lutz, G., Gilbertson, R., Arnaud-Santana, E., Beaver, J.S., and Myers, J.R. (2003). Contributions of the bean/cowpea CRSP to management of bean diseases. F. Crop. Res *82*, 155–168.

Cutler, H.G. (1988). Perspectives on discovery of microbial phytotoxins with herbicidal activity. Weed Technol *2*, 525–532.

Cutler, H.G., Crumley, F.G., Cox, R.H., Davis, E.E., Harper, J.L., Cole, R.J., and Sumner, D.R. (1982). Prehelminthosporol and prehelminthosporol acetate: plant growth regulating properties. J. Agric. Food Chem *30*, 658–662.

Dai, J.-R., Carté, B.K., Sidebottom, P.J., Sek Yew, A.L., Ng, S.-B., Huang, Y., and Butler, M.S. (2001). Circumdatin G, a new alkaloid from the fungus *Aspergillus ochraceus*. J. Nat. Prod *64*, 125–126.

De Faria, S.M., Lewis, G.P., Sprent, J.I., and Sutherland, J.M. (1989). Occurrence of nodulation in the Leguminosae. New Phytol *111*, 607–619.

De Jonghe, K., De Dobbelaere, I., Sarrazyn, R., and Höfte, M. (2005). Control of *Phytophthora cryptogea* in the hydroponic forcing of witloof chicory with the rhamnolipid-based biosurfactant formulation PRO1. Plant Pathol *54*, 219–226.

De Napoli, L., Messere, A., Palomba, D., Piccialli, V., Evidente, A., and Piccialli, G. (2000). Studies toward the synthesis of pinolidoxin, a phytotoxic nonenolide from the fungus *Ascochyta pinodes*. Determination of the configuration at the C-7, C-8, and C-9 chiral centers and stereoselective synthesis of the C6-C18 fragment. J. Org. Chem *65*, 3432–3442.

De Stefano, S., and Nicoletti, R. (1999). Pachybasin and chrysophanol, two anthraquinones produced by the fungus *Trichoderma aureoviride*. Tab. *7*, 21–24.

Devys, M., Barbier, M., Bousquet, J.-F., and Kollmann, A. (1992). Isolation of the new (-)-(3*R*, 4*S*)-4-hydroxymellein from the fungus *Septoria nodorum* Berk. Zeitschrift Fuer Naturforsch. C *47*, 779–781.

Dewick, P.M. (2002). Medicinal natural products: A Biosynthetic approach (University of Nottingham: John Wiley & Sons).

Dita, M.A., Rispail, N., Prats, E., Rubiales, D., and Singh, K.B. (2006). Biotechnology approaches to overcome biotic and abiotic stress constraints in legumes. Euphytica *147*, 1–24.

Djoukeng, J.D., Polli, S., Larignon, P., and Abou-Mansour, E. (2009). Identification of phytotoxins from *Botryosphaeria obtusa*, a pathogen of black dead arm disease of grapevine. Eur. J. Plant Pathol *124*, 303–308.

Dubrulle, G., Pensec, F., Picot, A., Rigalma, K., Pawtowski, A., Nicolleau, S., Harzic, N., Nodet, P., Baroncelli, R., and Le Floch, G. (2019). Phylogenetic diversity and effect of temperature on pathogenicity of *Colletotrichum lupini*. Plant Dis, https://doi.org/10.1094/PDIS-02-19-0273-RE

Duke, J.A. (1992). Handbook of legumes of economic importance (New York: Plenum Press).

Duke, S.O. (1986). Microbially produced phytotoxins as herbicides: A perspective (London: Wiley).

Durbin, R.D. (1983). The biochemistry of fungal and bacterial toxins and their modes of action. Biochem. Plant Pathol *47*, 137–162.

Duvick, J. (2001). Prospects for reducing fumonisin contamination of maize through genetic modification. Environ. Health Perspect *109*, 337–342.

Escudero-Adán, E.C., Benet-Buchholz, J., and Ballester, P. (2014). The use of Mo Kα radiation in the assignment of the absolute configuration of light-atom molecules; the importance of high-resolution data. Acta Crystallogr. Sect. B Struct. Sci. Cryst. Eng. Mater *70*, 660–668.

Evidente, A., Capasso, R., Abouzeid, M.A., Lanzetta, R., Vurro, M., and Bottalico, A. (1993a). Three new toxic pinolidoxins from *Ascochyta pinodes*. J. Nat. Prod *56*, 1937–1943.

Evidente, A., Lanzetta, R., Capasso, R., Vurro, M., and Botralico, A. (1993b). Pinolidoxin, a phytotoxic nonenolide from *Ascochyta pinodes*. Phytochemistry *34*, 999–1003.

Evidente, A., Lanzetta, R., Capasso, R., Andolfi, A., Bottalico, A., Vurro, M., and Zonno, M.C. (1995). Putaminoxin, a phytotoxic nonenolide from *Phoma putaminum*. Phytochemistry *40*, 1637–1641.

Evidente, A., Andolfi, A., D'Apice, L., Iannelli, D., and Scala, F. (1997a). Identification by flow cytometry of seiridin, one of the main phytotoxins produced by three Seiridium species pathogenic to cypress. Nat. Toxins *5*, 14–19.

Evidente, A., Lanzetta, R., Capasso, R., Andolfi, A., Vurro, M., and Zonno, M.C. (1997b). Putaminoxins B and C from *Phoma putaminum*. Phytochemistry *44*, 1041–1045.

Evidente, A., Capasso, R., Andolfi, A., Vurro, M., and Zonno, M.C. (1998a). Structure–activity relationship studies of putaminoxins and pinolidoxins: phytotoxic nonenolides produced by phytopathogenic Phoma and Ascochyta species. Nat. Toxins *6*, 183–188.

Evidente, A., Capasso, R., Andolfi, A., Vurro, M., and Zonno, M.C. (1998b). Putaminoxins D and E from *Phoma putaminum*. Phytochemistry *48*, 941–945.

Evidente, A., Capasso, R., Cutignano, A., Taglialatela-Scafati, O., Vurro, M., Zonno, M.C., and Motta, A. (1998c). Ascaulitoxin, a phytotoxic bis-amino acid *N*-glucoside from *Ascochyta caulina*. Phytochemistry *48*, 1131–1137.

Evidente, A., and Motta, A. (2001). Phytotoxins from fungi, pathogenic for agrarian, forestal and weedy plants. Bioact. Compd. from Nat Sources *12*, 473-525.

Evidente, A., Maddau, L., Spanu, E., Franceschini, A., Lazzaroni, S., and Motta, A. (2003). Diplopyrone, a new phytotoxic tetrahydropyranpyran-2-one produced by *Diplodia mutila*, a fungus pathogen of cork oak. J. Nat. Prod *66*, 313–315.

Evidente, A., Andolfi, A., Cimmino, A., Vurro, M., Fracchiolla, M., and Charudattan, R. (2006a). Herbicidal potential of ophiobolins produced by *Drechslera gigantea*. J. Agric. Food Chem *54*, 1779–1783.

Evidente, A., Andolfi, A., Cimmino, A., Vurro, M., Fracchiolla, M., Charudattan, R., and Motta, A. (2006b). Ophiobolin E and 8-*epi*-ophiobolin J produced by *Drechslera gigantea*, a potential mycoherbicide of weedy grasses. Phytochemistry *67*, 2281–2287.

Evidente, A., Punzo, B., Andolfi, A., Cimmino, A., Melck, D., and Luque, J. (2010). Lipophilic phytotoxins produced by *Neofusicoccum parvum*, a grapevine canker agent. Phytopathol. Mediterr *49*, 74–79.

Evidente, A., Abouzeid, A.M., Andolfi, A., and Cimmino, A. (2011a). Recent achievements in the bio-control of Orobanche infesting important crops in the Mediterranean basin. J Agric Sci Technol A *1*, 461–483.

Evidente, A., Andolfi, A., and Cimmino, A. (2011b). Relationships between the stereochemistry and biological activity of fungal phytotoxins. Chirality *23*, 674–693.

Evidente, A., Kornienko, A., Cimmino, A., Andolfi, A., Lefranc, F., Mathieu, V., and Kiss, R. (2014). Fungal metabolites with anticancer activity. Nat. Prod. Rep *31*, 617–627.

Evidente, M., Cimmino, A., Zonno, M.C., Masi, M., Berestetskyi, A., Santoro, E., Superchi, S., Vurro, M., and Evidente, A. (2015). Phytotoxins produced by *Phoma chenopodiicola*, a fungal pathogen of *Chenopodium album*. Phytochemistry *117*, 482–488.

Evidente, A., Cimmino, A., and Masi, M. (2019). Phytotoxins produced by pathogenic fungi of agrarian plants. Phytochem. Rev *18*, 843–870.

FAO (2017). The future of food and agriculture–trends and challenges. Annu. Rep. www.fao.org/3/a-i6583e.pdf

Fernández-Aparicio, M., Cimmino, A., Evidente, A., and Rubiales, D. (2013). Inhibition of *Orobanche crenata* seed germination and radicle growth by allelochemicals identified in cereals. J. Agric. Food Chem *61*, 9797–9803.

Forseth, R.R., Amaike, S., Schwenk, D., Affeldt, K.J., Hoffmeister, D., Schroeder, F.C., and Keller, N.P. (2013). Homologous NRPS-like gene clusters mediate redundant small-molecule biosynthesis in *Aspergillus flavus*. Angew. Chemie Int. Ed *52*, 1590–1594.

Fred, E.B., Baldwin, I.L., and McCoy, E. (2002). Root nodule bacteria and Leguminous plants (UW-Madison: Libraries Parallel Press).

Fredimoses, M., Zhou, X., Ai, W., Tian, X., Yang, B., Lin, X., Xian, J.-Y., and Liu, Y. (2015). Westerdijkin A, a new hydroxyphenylacetic acid derivative from deep sea fungus *Aspergillus westerdijkiae* SCSIO 05233. Nat. Prod. Res *29*, 158–162.

Friesen, T.L., Faris, J.D., Solomon, P.S., and Oliver, R.P. (2008). Host-specific toxins: effectors of necrotrophic pathogenicity. Cell. Microbiol *10*, 1421–1428.

Frisch, M.J., Trucks, G.W., Schlegel, H.B., Scuseria, G.E., Robb, M.A., Cheeseman, J.R., Scalmani, G., Barone, V., Petersson, G.A., and Nakatsuji, H. Gaussian 16, Revision A. 03, Gaussian, Inc., Wallingford (CT, Technical Report, 2016 Search PubMed).

Fürstner, A., Radkowski, K., Wirtz, C., Goddard, R., Lehmann, C.W., and Mynott, R. (2002). Total syntheses of the phytotoxic lactones herbarumin I and II and a synthesis-based solution of the pinolidoxin puzzle. J. Am. Chem. Soc *124*, 7061–7069.

Gamboa-Angulo, M.M., García-Sosa, K., Alejos-González, F., Escalante-Erosa, F., Delgado-Lamas, G., and Peña-Rodríguez, L.M. (2001). Tagetolone and tagetenolone: two phytotoxic polyketides from *Alternaria tagetica*. J. Agric. Food Chem *49*, 1228–1232.

Ganassi, S., Grazioso, P., De Cristofaro, A., Fiorentini, F., Sabatini, M.A., Evidente, A., and Altomare, C. (2016). Long chain alcohols produced by *Trichoderma citrinoviride* have phagodeterrent activity against the bird cherry-oat aphid *Rhopalosiphum padi*. Front. Microbiol *7*, 297.

García, M., Marina, M., Laborda, F., and Torre, M. (1998). Chemical characterization of commercial soybean products. Food Chem *62*, 325–331.

García-Fortanet, J., Murga, J., Falomir, E., Carda, M., and Marco, J.A. (2005). Stereoselective total synthesis and absolute configuration of the natural decanolides (−)-microcarpalide and (+)-lethaloxin. Identity of (+)-lethaloxin and (+)-pinolidoxin. J. Org. Chem *70*, 9822–9827.

Gaugler, R. (1997). Alternative paradigms for commercializing biopesticides. Phytoparasitica *25*, 179–182.

Genta, H.D., Genta, M.L., Alvarez, N. V, and Santana, M.S. (2002). Production and acceptance of a soy candy. J. Food Eng *53*, 199–202.

Godfray, H.C.J., Beddington, J.R., Crute, I.R., Haddad, L., Lawrence, D., Muir, J.F., Pretty, J., Robinson, S., Thomas, S.M., and Toulmin, C. (2010). Food security: The challenge of feeding 9 billion people. Science *327*, 812-818.

Graham, P.H., and Vance, C.P. (2003). Legumes: importance and constraints to greater use. Plant Physiol *131*, 872–877.

Graniti, A. (1991). Phytotoxins and their involvement in plant diseases. Cell. Mol. Life Sci *47*, 751–755.

Greenspan, M.D., Yudkovitz, J.B., Lo, C.Y., Chen, J.S., Alberts, A.W., Hunt, V.M., Chang, M.N., Yang, S.S., Thompson, K.L., and Chiang, Y.C. (1987). Inhibition of hydroxymethylglutaryl-coenzyme A synthase by L-659,699. Proc. Natl. Acad. Sci *84*, 7488–7492.

Grigg, R., Whitney, S., Sridharan, V., Keep, A., and Derrick, A. (2009). Iridium catalysed C-3 alkylation of oxindole with alcohols under solvent free thermal or microwave conditions. Tetrahedron *65*, 4375–4383.

Hallock, Y.F., Lu, H.S.M., Clardy, J., Strobel, G.A., Sugawara, F., Samsoedin, R., and Yoshida, S. (1993). Triticones, spirocyclic lactams from the fungal plant pathogen *Drechslera tritici-repentis*. J. Nat. Prod *56*, 747–754.

Hawksworth, D.L. (2001). The magnitude of fungal diversity: the 1.5 million species estimate revisited. Mycol. Res *105*, 1422–1432.

Hawksworth, D.L., and Rossman, A.Y. (1997). Where are all the undescribed fungi? Phytopathology *87*, 888–891.

Hemtasin, C., Kanokmedhakul, S., Kanokmedhakul, K., Hahnvajanawong, C., Soytong, K., Prabpai, S., and Kongsaeree, P. (2011). Cytotoxic pentacyclic and tetracyclic aromatic sesquiterpenes from *Phomopsis archeri*. J. Nat. Prod *74*, 609–613.

Herzner, G., Schlecht, A., Dollhofer, V., Parzefall, C., Harrar, K., Kreuzer, A., Pilsl, L., and Ruther, J. (2013). Larvae of the parasitoid wasp *Ampulex compressa* sanitize their host, the American cockroach, with a blend of antimicrobials. Proc. Natl. Acad. Sci. *110*, 1369-1374.

Höhl, B., Weidemann, C., Höhl, U., and Barz, W. (1991). Isolation of solanapyrones A, B and C from culture filtrates and spore germination fluids of *Ascochyta rabiei* and aspects of phytotoxin action. J. Phytopathol *132*, 193–206.

Höller, U., König, G.M., and Wright, A.D. (1999). Three new metabolites from marine-derived fungi of the genera *Coniothyrium* and *Microsphaeropsis*. J. Nat. Prod *62*, 114–118.

Holm, L.G., Plucknett, D.L., Pancho, J. V, and Herberger, J.P. (1977). The world's worst weeds: Distribution and biology (Hawaii USA: University Press of Hawaii Honolulu).

Howell, C.R., and Stipanovic, R.D. (1984). Phytotoxicity to crop plants and herbicidal effects on weeds of viridiol produced by *Gliocladium virens*. Phytopathology *74*, 1346–1349.

Howieson, J.G., O'hara, G.W., and Carr, S.J. (2000). Changing roles for legumes in Mediterranean agriculture: developments from an Australian perspective. F. Crop. Res *65*, 107–122.

Hungria, M. (1997). Interactions among soil microorganisms and bean and maize grown in monoculture or intercropped. Pesq. Agropec. Bras *32*, 807–818.

Hymowitz, T. (1987). Taxonomy and speciation. Soybeans: improvement, production and uses. In Agronomy monograph nº 16 Wilcox J ed, (Madison, Wisconsin, USA: American Society of Agronomy, Inc.), pp. 23-48

Hynes, R.K., and Boyetchko, S.M. (2006). Research initiatives in the art and science of biopesticide formulations. Soil Biol. Biochem *38*, 845–849.

Imre, S., Sar, S., and Thomson, R.H. (1976). Anthraquinones in digitalis species. Phytochemistry *15* 317–320.

Infantino, A., Zaccardelli, M., Costa, C., Ozkilinc, H., Habibi, A., and Peever, T. (2016). A new disease of grasspea (*Lathyrus sativus*) caused by *Ascochyta lentis* var. *lathyri*. J. Plant Pathol *98*, 541–548.

Ijaz, M., Ali, Q., Ashraf, S., Kamran, M., and Rehman, A. (2019). Development of future bioformulations for sustainable agriculture. In Microbiome in Plant Health and Disease: Challenges and opportunities, (Singapore: Springer Singapore), pp. 421–446.

Iwai, I., and Mishima, H. (1965). Constitution of ascochitine. Chem. Ind *4*, 186-187.

John, J.E. (2009). Natural products-based drug discovery: some bottlenecks and considerations. Curr. Sci *96*, 753–754.

Ju, Z., Lin, X., Lu, X., Tu, Z., Wang, J., Kaliyaperumal, K., Liu, J., Tian, Y., Xu, S., and Liu, Y. (2015). Botryoisocoumarin A, a new COX-2 inhibitor from the mangrove Kandelia candel endophytic fungus Botryosphaeria sp. KcF6. J. Antibiot *68*, 653–656.

Kale, S., and Bennett, J.W. (1992). Strain instability in filamentous fungi. Handb. Appl. Mycol *5*, 311–332.

Kaplan, L., and Lynch, T.F. (1999). Phaseolus (Fabaceae) in archaeology: AMS. Econ. Bot *53*, 261–272.

Kelly, J.D., Gepts, P., Miklas, P.N., and Coyne, D.P. (2003). Tagging and mapping of genes and QTL and molecular marker-assisted selection for traits of economic importance in bean and cowpea. F. Crop. Res *82*, 135–154.

Kempenaar, C. (1995). Studies on biological control of *Chenopodium album* by *Ascochyta caulina* (Doctor of Philosophy).

Kennedy, A.R. (1995). The evidence for soybean products as cancer preventive agents. J. Nutr *125*, 733S-743S.

Kern, F., Klein, R.W., Janssen, E., Bestmann, H.-J., Attygalle, A.B., Schäfer, D., and Maschwitz, U. (1997). Mellein, a trail pheromone component of the ant *Lasius fuliginosus*. J. Chem. Ecol *23*, 779–792.

Khamthong, N., Rukachaisirikul, V., Phongpaichit, S., Preedanon, S., and Sakayaroj, J. (2014). An antibacterial cytochalasin derivative from the marine-derived fungus Diaporthaceae sp. PSU-SP2/4. Phytochem. Lett *10*, 5–9.

Khamthong, N., Rukachaisirikul, V., Tadpetch, K., Kaewpet, M., Phongpaichit, S., Preedanon, S., and Sakayaroj, J. (2012). Tetrahydroanthraquinone and xanthone derivatives from the marine-derived fungus *Trichoderma aureoviride* PSU-F95. Arch. Pharm. Res *35*, 461–468.

Kimura, Y., and Tamura, S. (1973). Isolation of l-β-phenyllactic acid and tyrosol as plant growth regulators from *Gloeosporium laeticolor*. Agric. Biol. Chem *37*, 2925.

Kindscher, K. (1992). Medicinal wild plants of the prairie. An ethnobotanical guide. (Lawrence, KS: University Press of Kansas.).

Kornienko, A., Mathieu, V., Rastogi, S.K., Lefranc, F., and Kiss, R. (2013). Therapeutic agents triggering nonapoptotic cancer cell death. J. Med. Chem *56*, 4823–4839.

Krohn, K., Bahramsari, R., Flörke, U., Ludewig, K., Kliche-Spory, C., Michel, A., Aust, H.-J., Draeger, S., Schulz, B., and Antus, S. (1997). Dihydroisocoumarins from fungi: Isolation, structure elucidation, circular dichroism and biological activity. Phytochemistry *45*, 313–320.

Kuo, S., Chen, P., Lee, S., and Chen, Z. (1995). Constituents of roots of *Rubia lanceolata Hayata*. J. Chinese Chem. Soc *42*, 869–871.

Lahlou, M. (2007). Screening of natural products for drug discovery. Expert Opin. Drug Discov *2*, 697–705.

Lee, S.B. (1990). Isolation of DNA from fungal mycelia and single spores. PCR Protoc. a Guid. to Methods Appl. 282–287.

Li, B., Park, Y., and Chang, S. (2014). Regiodivergent access to five-and six-membered benzo-fused lactams: Ru-catalyzed olefin hydrocarbamoylation. J. Am. Chem. Soc *136*, 1125–1131.

Liu, D., Li, X.-M., Li, C.-S., and Wang, B.-G. (2013). Sesterterpenes and 2*H*-pyran-2-ones (=α-Pyrones) from the mangrove-derived endophytic fungus *Fusarium proliferatum* MA-84. Helv. Chim. Acta *96*, 437–444.

Liu, W., and Ackermann, L. (2013). *Ortho*-and *para*-selective ruthenium-catalyzed C (sp^2)–H oxygenations of phenol derivatives. Org. Lett *15*, 3484–3486.

Liu, Y., Li, X.-M., Meng, L.-H., and Wang, B.-G. (2015). Polyketides from the marine mangrove-derived fungus *Aspergillus ochraceus* MA-15 and their activity against aquatic pathogenic bacteria. Phytochem. Lett *12*, 232–236.

Locato, V., Uzal, E.N., Cimini, S., Zonno, M.C., Evidente, A., Micera, A., Foyer, C.H., and De Gara, L. (2015). Low concentrations of the toxin ophiobolin A lead to an arrest of the cell cycle and alter the intracellular partitioning of glutathione between the nuclei and cytoplasm. J. Exp. Bot *66*, 2991–3000.

Magan, N., Hope, R., Colleate, A., and Baxter, E. (2002). Relationship between growth and mycotoxin production by fusarium species, biocides and environment. Eur. J. Plant Pathol *108*, 685–690.

Manet, I., Monti, S., Bortolus, P., Fagnoni, M., and Albini, A. (2005). The photochemistry of 4-chlorophenol in water revisited: the effect of cyclodextrins on cation and carbene reactions. Chem. Eur. J *11*, 4274–4282.

Manigaunha, A., Ganesh, N., and Kharya, M.D. (2010). Morning glory: a new thirst in-search of *de-novo* therapeutic approach. Int. J. Phytomedicine *2*, 18–21.

Marr, I.L., Suryana, N., Lukulay, P., and Marr, M.I. (1995). Determination of chlorophyll α and β by simultaneous multi-component spectrophotometry. Fresenius. J. Anal. Chem *352*, 456–460.

Marrone, P.G. (2019). Pesticidal natural products–status and future potential. Pest Manag. Sci *75*, 2325-2340

Martin, R.R., James, D., and Lévesque, C.A. (2000). Impacts of molecular diagnostic technologies on plant disease management. Annu. Rev. Phytopathol *38*, 207–239.

Masi, M., Cimmino, A., Boari, A., Zonno, M.C., Górecki, M., Pescitelli, G., Tuzi, A., Vurro, M., and Evidente, A. (2017). Colletopyrandione, a new phytotoxic tetrasubstituted indolylidenepyran-2, 4-dione, and colletochlorins G and H, new tetrasubstituted chroman-and isochroman-3,5-diols isolated from *Colletotrichum higginsianum*. Tetrahedron *73*, 6644–6650.

Masi, M., Maddau, L., Linaldeddu, B.T., Scanu, B., Evidente, A., and Cimmino, A. (2018). Bioactive metabolites from pathogenic and endophytic fungi of forest trees. Curr. Med. Chem *25*, 208–252.

Masi, M., Cimmino, A., Reveglia, P., Mugnai, L., Surico, G., and Evidente, A. (2018a). Advances on fungal phytotoxins and their role in grapevine trunk diseases. J. Agric. Food Chem *66*, 5948–5958.

Masi, M., Maddau, L., Linaldeddu, B.T., Scanu, B., Evidente, A., and Cimmino, A. (2018b). Bioactive metabolites from pathogenic and endophytic fungi of forest trees. Curr. Med. Chem *25*, 208–252.

Masi, M., Meyer, S., Górecki, M., Pescitelli, G., Clement, S., Cimmino, A., and Evidente, A. (2018c). Phytotoxic activity of metabolites isolated from Rutstroemia sp.n., the causal agent of bleach blonde syndrome on cheatgrass (*Bromus tectorum*). Molecules *23*, 1734

Mesbah, L.A., Van der Weerden, G.M., Nijkamp, H.J.J., and Hille, J. (2000). Sensitivity among species of Solanaceae to AAL toxins produced by *Alternaria alternata* f. sp. *lycopersici*. Plant Pathol *49*, 734–741.

Miller, S.A., and Martin, R.R. (1988). Molecular diagnosis of plant disease. Annu. Rev. Phytopathol *26*, 409–432.

Misaghi, I.J. (1982). The role of pathogen-produced toxins in pathogenesis. In Physiology and Biochemistry of plant-pathogen interactions, (Boston, MA: Springer), pp. 35–61.

Mitchell, R.E. (1984). The relevance of non-host-specific toxins in the expression of virulence by pathogens. Annu. Rev. Phytopathol *22*, 215–245.

Mitterbauer, R., and Adam, G. (2002). *Saccharomyces cerevisae* and *Arabidopsis thaliana*: Useful model systems for the identification of molecular mechanisms involved in resistance of plants to toxins. In Mycotoxins in Plant Disease, (Boston, MA: Springer), pp. 699–703.

Möbius, N., and Hertweck, C. (2009). Fungal phytotoxins as mediators of virulence. Curr. Opin. Plant Biol *12*, 390–398.

Molteni, A., Brizio-Molteni, L., and Persky, V. (1995). *In vitro* hormonal effects of soybean isoflavones. J. Nutr *125*, 751S-756S.

Montesinos, E. (2003). Development, registration and commercialization of microbial pesticides for plant protection. Int. Microbiol *6*, 245–252.

Morris, J.B. (1997). Special-purpose legume genetic resources conserved for agricultural, industrial, and pharmaceutical use. Econ. Bot *51*, 251–263.

Mudryj, A.N., Yu, N., and Aukema, H.M. (2014). Nutritional and health benefits of pulses. Appl. Physiol. Nutr. Metab *39*, 1197–1204.

Nakajima, M., Itoi, K., Takamatsu, Y., Sato, S., Furukawa, Y., Furuya, K., Honma, T., Kadotani, J., Kozasa, M., And Haneishi, T. (1991). Cornexistin: a new fungal metabolite with herbicidal activity. J. Antibiot *44*, 1065–1072.

Nakanishi, K. (1977). PH Solomon infrared absorption spectroscopy (San Francisco: Holden-Day Publisher).

Nozoe, S., Morisaki, M., Tsuda, K., Iitaka, Y., Takahashi, N., Tamura, S., Ishibashi, K., and Shirasaka, M. (1965). The structure of ophiobolin, a C25 terpenoid having a novel skeleton. J. Am. Chem. Soc *87*, 4968–4970.

Oerke, E.-C. (2006). Crop losses to pests. J. Agric. Sci *144*, 31–43.

Oikawa, H., Yokota, T., Sakano, C., Suzuki, Y., Naya, A., and Ichihara, A. (1998). Solanapyrones, phytotoxins produced by *Alternaria solani*: Biosynthesis and isolation of minor components. Biosci. Biotechnol. Biochem *62*, 2016–2022.

Oka, M., Iimura, S., Tenmyo, O., Sawada, Y., Sugawara, M., Ohkusa, N., Yamamoto, H., Kawano, K., Hu, S.-L., and Fukagawa, Y. (1993). Terpestacin, a new syncytium formation inhibitor from *Arthrinium* sp. J. Antibiot *46*, 367–373.

Oku, H., and Nakanishi, T. (1966). Mode of action of an antibiotic, ascochitine, with reference to selective toxicity. J. Phytopathol *55*, 1–14.

Oliver, R.P., and Solomon, P.S. (2008). Recent fungal diseases of crop plants: is lateral gene transfer a common theme? Mol. Plant-Microbe Interact *21*, 287–293.

Oliver, R.P., Dewey, F.M., and Schots, A. (1994). Modern assays for plant pathogenic fungi: Identification, detection and quantification (Oxford: Cab International).

Oppenheimer, S.J. (2001). Iron and its relation to immunity and infectious disease. J. Nutr *131*, 616S-635S.

Padula, D., Pietro, S. Di, Capozzi, M.A.M., Cardellicchio, C., and Pescitelli, G. (2014). Strong intermolecular exciton couplings in solid-state circular dichroism of aryl benzyl sulfoxides. Chirality *26*, 462–470.

Paetau, I., Chen, C.-Z., and Jane, J. (1994). Biodegradable plastic made from soybean products. 1. Effect of preparation and processing on mechanical properties and water absorption. Ind. Eng. Chem. Res *33*, 1821–1827.

Palombi, L., and Sessa, R. (2013). Climate-smart agriculture: Sourcebook (Rome: FAO).

Parsons, S. (2017). Determination of absolute configuration using X-ray diffraction. Tetrahedron: Asymmetry *28*, 1304–1313.

Parsons, S., Flack, H.D., and Wagner, T. (2013). Use of intensity quotients and differences in absolute structure refinement. Acta Crystallogr. Sect. B Struct. Sci. Cryst. Eng. Mater *69*, 249–259.

Patwardhan, B., Vaidya, A.D.B., and Chorghade, M. (2004). Ayurveda and natural products drug discovery. Curr. Sci. *86*, 789–799.

Peever, T.L., Canihos, Y., Olsen, L., Ibanez, A., Liu, Y.-C., and Timmer, L.W. (1999). Population genetic structure and host specificity of Alternaria spp. causing brown spot of *Minneola tangelo* and rough lemon in Florida. Phytopathology *89*, 851–860.

Pena-Rodriguez, L.M., and Chilton, W.S. (1989). 3-Anhydroophiobolin A and 3-anhydro-6-*epi*-ophiobolin A, phytotoxic metabolites of the Johnson grass pathogen *Bipolaris sorghicola*. J. Nat. Prod *52*, 1170–1172.

Pena-Rodriguez, L.M., Armingeon, N.A., and Chilton, W.S. (1988). Toxins from weed pathogens, I. Phytotoxins from a Bipolaris pathogen of Johnson grass. J. Nat. Prod *51*, 821–828.

Peoples, M.B., Herridge, D.F., and Ladha, J.K. (1995). Biological nitrogen fixation: an efficient source of nitrogen for sustainable agricultural production? In Management of biological nitrogen fixation for the development of more productive and sustainable agricultural systems, (Boston, MA: Springer), pp. 3–28.

Pescitelli, G., and Bruhn, T. (2016). Good computational practice in the assignment of absolute configurations by TDDFT calculations of ECD spectra. Chirality *28*, 466–474.

Pescitelli, G., Kurtan, T., Flörke, U., and Krohn, K. (2009). Absolute structural elucidation of natural products—A focus on quantum-mechanical calculations of solid-state CD spectra. Chirality Pharmacol. Biol. Chem. Consequences Mol. Asymmetry *21*, E181–E201.

Polhill, R.M. (1981). Evolution and systematics of the Leguminosae. Advences Legum. Syst *1*, 1–26.

Popenoe, H. (1989). Lost crops of the Incas: Little-known plants of the Andes with promise for worldwide cultivation. (Washington, DC: The National Academies Press).

Poppenberger, B., Berthiller, F., Lucyshyn, D., Sieberer, T., Schuhmacher, R., Krska, R., Kuchler, K., Glössl, J., Luschnig, C., and Adam, G. (2003). Detoxification of the *Fusarium* mycotoxin deoxynivalenol by a UDP-glucosyltransferase from *Arabidopsis thaliana*. J. Biol. Chem *278*, 47905–47914.

Puopolo, G., Cimmino, A., Palmieri, M.C., Giovannini, O., Evidente, A., and Pertot, I. (2014). *Lysobacter capsici* AZ78 produces cyclo (l-Pro-l-Tyr), a 2, 5-diketopiperazine with toxic activity against sporangia of *Phytophthora infestans* and *Plasmopara viticola*. J. Appl. Microbiol *117*, 1168–1180.

Ramírez-Suero, M., Bénard-Gellon, M., Chong, J., Laloue, H., Stempien, E., Abou-Mansour, E., Fontaine, F., Larignon, P., Mazet-Kieffer, F., Farine, S., et al. (2014). Extracellular compounds produced by fungi associated with *Botryosphaeria* dieback induce differential defence gene expression patterns and necrosis in *Vitis vinifera* cv. Chardonnay cells. Protoplasma *251*, 1417–1426.

Ren-Yi, G., Lei, X., Yi, K., Iii-Ming, C., Jian-Chun, Q., Li, L., Sheng-Xiang, Y., and Li-Chun, Z. (2015). Chaetominine,(+)-alantrypinone, questin, isorhodoptilometrin, and 4-hydroxybenzaldehyde produced by the endophytic fungus *Aspergillus* sp. YL-6 inhibit wheat (*Triticum aestivum*) and radish (*Raphanus sativus*) germination. J. Plant Interact *10*, 87–92.

Rimando, A.M., and Duke, S.O. (2006). Natural products for pest management. (Washington, DC: ACS Publications).

Roosevelt, A.C., Da Costa, M.L., Machado, C.L., Michab, M., Mercier, N., Valladas, H., Feathers, J., Barnett, W., Da Silveira, M.I., and Henderson, A. (1996). Paleoindian cave dwellers in the Amazon: the peopling of the Americas. Science *272*, 373–384.

Rosegrant, M.W., and Cline, S.A. (2003). Global food security: challenges and policies. Science *302*, 1917–1919.

Rossman, A.Y. (2008). The impact of invasive fungi on agricultural ecosystems in the United States. In Ecological Impacts of non-native invertebrates and fungi on terrestrial ecosystems, (Boston, MA: Springer), pp. 97–107.

Rubiales, D., and Mcphee, K. (2015). Perspectives (Córdoba: International Legume Society ILS).

Rukachaisirikul, V., Arunpanichlert, J., Sukpondma, Y., Phongpaichit, S., and Sakayaroj, J. (2009). Metabolites from the endophytic fungi *Botryosphaeria rhodina* PSU-M35 and PSU-M114. Tetrahedron *65*, 10590–10595.

Sarrocco, S., Diquattro, S., Avolio, F., Cimmino, A., Puntoni, G., Doveri, F., Evidente, A., and Vannacci, G. (2015). Bioactive metabolites from new or rare fimicolous fungi with antifungal activity against plant pathogenic fungi. Eur. J. Plant Pathol *142*, 61–71.

Saxena, S., and Pandey, A.K. (2001). Microbial metabolites as eco-friendly agrochemicals for the next millennium. Appl. Microbiol. Biotechnol *55*, 395–403.

Schrader, K.K., Andolfi, A., Cantrell, C.L., Cimmino, A., Duke, S.O., Osbrink, W., Wedge, D.E., and Evidente, A. (2010). A survey of phytotoxic microbial and plant metabolites as potential natural products for pest management. Chem. Biodivers *7*, 2261–2280.

Serra-Majem, L., and Medina, F.X. (2015). The Mediterranean diet as an intangible and sustainable food culture. In The Mediterranean diet, (London, UK: Academic Press-Elsevier), pp. 37–46.

Singh, A., Bhardwaj, R., and Singh, I.K. (2019). Biocontrol agents: Potential of biopesticides for integrated pest management. In Biofertilizers for sustainable agriculture and environment, (Cham: Springer International Publishing), pp. 413–433.

Sheldrick, G.M. (2008). A short history of SHELX. Acta Crystallogr. Sect. A Found. Crystallogr *64*, 112–122.

Socolow, R.H. (1999). Nitrogen management and the future of food: lessons from the management of energy and carbon. Proc. Natl. Acad. Sci *96*, 6001–6008.

Sorbo, G. Del, Evidente, A., and Scala, F. (1994). Production of polyclonal antibodies for cyclopaldic acid, a major phytotoxic metabolite produced by the plant pathogen *Seiridium cupressi*. Nat. Toxins *2*, 136–140.

Sperandio, S., de Belle, I., and Bredesen, D.E. (2000). An alternative, nonapoptotic form of programmed cell death. Proc. Natl. Acad. Sci *97*, 14376–14381.

Steele, J.A., Uchytil, T.F., Durbin, R.D., Bhatnagar, P., and Rich, D.H. (1976). Chloroplast coupling factor 1: A species-specific receptor for tentoxin. Proc. Natl. Acad. Sci *73*, 2245 LP–2248.

Sternhell, S. (1969). Correlation of interproton spin–spin coupling constants with structure. Q. Rev. Chem. Soc *23*, 236–270.

Strobel, G.A. (1974). Phytotoxins produced by plant parasites. Annu. Rev. Plant Physiol *25*, 541–566.

Strobel, G.A. (1982). Phytotoxins. Annu. Rev. Biochem *51*, 309–333.

Sugawara, F., and Strobel, G. (1986). Zinniol, a phytotoxin, is produced by *Phoma macdonaldii*. Plant Sci *43*, 19–23.

Sugawara, F., Takahashi, N., Strobel, G.A., Strobel, S.A., Lu, H.S.M., and Clardy, J. (1988). Triticones A and B, novel phytotoxins from the plant pathogenic fungus *Drechslera tritici-repentis*. J. Am. Chem. Soc *110*, 4086–4087.

Sun, P., Huo, J., Kurtán, T., Mándi, A., Antus, S., Tang, H., Draeger, S., Schulz, B., Hussain, H., and Krohn, K. (2013). Structural and stereochemical studies of hydroxyanthraquinone derivatives from the endophytic fungus Coniothyrium sp. Chirality *25*, 141–148.

Superchi, S., Scafato, P., Gorecki, M., and Pescitelli, G. (2018). Absolute configuration determination by quantum mechanical calculation of chiroptical spectra: basics and applications to fungal metabolites. Curr. Med. Chem *25*, 287–320.

Švábová, L., and Lebeda, A. (2005). *In vitro* selection for improved plant resistance to toxin-producing pathogens. J. Phytopathol *153*, 52–64.

Thuleau, P., Graziana, A., Rossignol, M., Kauss, H., Auriol, P., and Ranjeva, R. (1988). Binding of the phytotoxin zinniol stimulates the entry of calcium into plant protoplasts. Proc. Natl. Acad. Sci *85*, 5932LP–5935.

Tian, W., Deng, Z., and Hong, K. (2017). The biological activities of sesterterpenoid-type ophiobolins. Mar. Drugs *15*, 229.

Tilman, D., Balzer, C., Hill, J., and Befort, B.L. (2011). Global food demand and the sustainable intensification of agriculture. Proc. Natl. Acad. Sci *108*, 20260 LP–20264.

Tivoli, B., Baranger, A., Avila, C.M., Banniza, S., Barbetti, M., Chen, W., Davidson, J., Lindeck, K., Kharrat, M., and Rubiales, D. (2006). Screening techniques and sources of resistance to foliar diseases caused by major necrotrophic fungi in grain legumes. Euphytica *147*, 223–253.

Torrance, L. (1992). Techniques for the rapid detection of plant pathogens (Worcester: British Society of Plant Pathology).

Trost, B.M., Dong, G., and Vance, J.A. (2007). A diosphenol-based strategy for the total synthesis of (-)-terpestacin. J. Am. Chem. Soc *129*, 4540–4541.

Tscharntke, T., Clough, Y., Wanger, T.C., Jackson, L., Motzke, I., Perfecto, I., Vandermeer, J., and Whitbread, A. (2012). Global food security, biodiversity conservation and the future of agricultural intensification. Biol. Conserv *151*, 53–59.

Van Kammen, A. (1997). Biological nitrogen fixation for sustainable agriculture. In Biological fixation of nitrogen for ecology and sustainable agriculture, (Boston, MA: Springer), pp. 177–178.

Varejão, E.V.V., Demuner, A.J., Barbosa, L.C. de A., and Barreto, R.W. (2013). Phytotoxic effects of metabolites from *Alternaria euphorbiicola* against its host plant *Euphorbia heterophylla*. Quim. Nova *36*, 1004–1007.

Venkatasubbaiah, P., and Chilton, W.S. (1990). Phytotoxins of *Botryosphaeria obtusa*. J. Nat. Prod *53*, 1628–1630.

Vesonder, R.F., Labeda, D.P., and Peterson, R.E. (1992). Phytotoxic activity of selected water-soluble metabolites of Fusarium against *Lemna minor* L. (Duckweed). Mycopathologia *118*, 185–189.

Vurro, M., and Ellis, B.E. (1997). Effect of fungal toxins on induction of phenylalanine ammonia-lyase activity in elicited cultures of hybrid poplar. Plant Sci *126*, 29–38.

Vurro, M., Zonno, M.C., Evidente, A., Capasso, R., and Bottaiico, A. (1992). Isolation of cytochalasins A and B from *Ascochyta lathyri*. Mycotoxin Res *8*, 17–20.

Ward, E. (1994). Use of the polymerase chain reaction for identifying plant pathogens. In Ecology of Plant Pathogens, J. P. Blakeman, and B. Williamson, ed. (Wallingford, Oxon: CABI International), pp. 143–160.

Ward, E. (1995). Improved polymerase chain reaction (PCR) detection of *Gaeumannomyces graminis* including a safeguard against false negatives. Eur. J. Plant Pathol *101*, 561–566.

Ward, E., and Adams, M.J. (1998). Analysis of ribosomal DNA sequences of Polymyxa species and related fungi and the development of genus-and species-specific PCR primers. Mycol. Res *102*, 965–974.

Whipps, J.M., and Lumsden, R.D. (2001). Commercial use of fungi as plant disease biological control agents: status and prospects. Fungal Biocontrol Agents Progress, Probl. Potential 9–22.

Wigchert, S.C.M., Kuiper, E., Boelhouwer, G.J., Nefkens, G.H.L., Verkleij, J.A.C., and Zwanenburg, B. (1999). Dose-response of seeds of the parasitic weeds Striga and Orobanche toward the synthetic germination stimulants GR 24 and Nijmegen 1. J. Agric. Food Chem *47*, 1705–1710.

Wolf, C. (2007). Dynamic stereochemistry of chiral compounds: Principles and applications (Cambridge: Royal Society of Chemistry).

Xia, X., Huang, H., She, Z., Shao, C., Liu, F., Cai, X., Vrijmoed, L.L.P., and Lin, Y. (2007). ^{1}H and ^{13}C NMR assignments for five anthraquinones from the mangrove endophytic fungus Halorosellinia sp. (No. 1403). Magn. Reson. Chem *45*, 1006–1009.

Xiang Yang, J., Chen, Y., Huang, C., She, Z., and Lin, Y. (2011). A new isochroman derivative from the marine fungus Phomopsis sp. (No. ZH-111). Chem. Nat. Compd *47*, 13.

Xu, Y., Lu, C., and Zheng, Z. (2012). A new 3, 4-dihydroisocoumarin isolated from Botryosphaeria sp. F00741. Chem. Nat. Compd *48*, 205–207.

Yang, J.X., Chen, Y., Huang, C., She, Z., and Lin, Y. (2011). A new isochroman derivative from the marine fungus Phomopsis sp. (No. ZH-111). Chem. Nat. Compd *47*, 13.

Yang, T., Lu, Z., Meng, L., Wei, S., Hong, K., Zhu, W., and Huang, C. (2012). The novel agent ophiobolin O induces apoptosis and cell cycle arrest of MCF-7 cells through activation of MAPK signaling pathways. Bioorg. Med. Chem. Lett *22*, 579–585.

Yang, X.-W., Li, S.-M., Li, Y.-L., Feng, L., Shen, Y.-H., Lin, S., Tian, J.-M., Zeng, H.-W., Wang, N., and Steinmetz, A. (2014). Chemical constituents of *Abies delavayi*. Phytochemistry *105*, 164–170.

Zask, A., and Ellestad, G. (2018). Biomimetic syntheses of racemic natural products. Chirality *30*, 157–164.

Zeng, Q.L., Wang, H.Q., Liu, Z.R., Li, B.G., and Zhao, Y.F. (2007). Facile synthesis of optically pure (*S*)-3-*p*-hydroxyphenyllactic acid derivatives. Amino Acids *33*, 537–541.

Zhang, D., Fukuzawa, S., Satake, M., Li, X., Kuranaga, T., Niitsu, A., Yoshizawa, K., and Tachibana, K. (2012). Ophiobolin O and 6-*epi*-ophiobolin O, two new cytotoxic sesterterpenes from the marine derived fungus Aspergillus sp. Nat. Prod. Commun *7*, 1411-1414.

Zhao, J.H., Zhang, Y.L., Wang, L.W., Wang, J.Y., and Zhang, C.L. (2012). Bioactive secondary metabolites from Nigrospora sp. LLGLM003, an endophytic fungus of the medicinal plant *Moringa oleifera* Lam. World J. Microbiol. Biotechnol *28*, 2107–2112.